Dissertation zur Erlangung des Doktorgrades

der Fakultät für Chemie und Pharmazie

der Ludwig-Maximilians-Universität München

ENDOTHELIAL BARRIER PROTECTION

BY NATURAL COMPOUNDS

-

Crataegus extract WS® 1442 and atrial natriuretic peptide

inhibit endothelial hyperpermeability

Martin Friedrich Bubik

aus Pforzheim

2009

Erklärung:

Diese Dissertation wurde im Sinne von §13 Abs. 3 bzw. 4 der Promotionsordnung vom 29. Januar 1998 von Frau Prof. Dr. Angelika M. Vollmar betreut am Lehrstuhl für Pharmazeutische Biologie.

Ehrenwörtliche Versicherung:

Diese Dissertation wurde selbstständig, ohne unerlaubte Hilfe erarbeitet.

München, den 20.11.2009

Martin Bubik

Dissertation eingereicht am: 20.11. 2009

1. Gutachter: Prof. Dr. Angelika Vollmar

2. Gutachter: Prof. Dr. Christian Wahl-Schott

Mündliche Prüfung am: 18.12. 2009

meinen Eltern

CONTENTS

I INTRODUCTION

1 The endothelial barrier and inflammation

The barrier function is the central nature of the endothelium. The maintenance of a semi-permeable barrier by the endothelium is particularly important for controlling the passage of macromolecules and fluid between the blood and interstitial space and for establishing the formation of a transendothelial protein gradient (the colloid osmotic gradient) required for tissue fluid homeostasis. The endothelium controls the flux of fluid and solutes across the vessel wall by highly regulated transport pathways and allows the unimpeded transfer of dissolved gases and ions. The endothelium is restrictive to high-molecular-weight substances such as proteins because the tissue does usually not consume them rapidly, and there are important reasons to retain them in the circulation. And of cause the endothelium strictly regulates transmigration of cells into the tissue.[1-3]

In general, endothelial transport can be thought of as occurring *via* paracellular and transcellular pathways. In the resting endothelium the transport of proteins and liquids occurs *via* the transcellular pathway.[4] In contrast, the paracellular pathway plays a pivotal role in the context of inflammation. Intercellular gaps allow the passage of plasma proteins including albumin and liquids across the endothelial barrier in an unrestricted manner. The loss of barrier function results in tissue inflammation and is a hallmark of inflammation-induced diseases such as the acute respiratory distress syndrome. The inflammatory mediators thrombin, bradykinin, histamine, vascular endothelial growth factor (VEGF), and others disturb the organization of interendothelial junctions, and in concequence open the junctional barrier.

2 Inflammation activated endothelium

In recent years, cardiovascular diseases (CVD) like arteriosclerosis or chronic heart failure were classified as inflammatory diseases. Chronic inflammation-induced activation of the endothelium with its loss of barrier function is an important

parameter in the pathogenesis of these diseases (Figure 1).[5-11] There are two central markers of endothelial activation: The expression of endothelial cell adhesion molecules (CAMs) and endothelial hyperpermeability (EHP), are both hallmarks of endothelial inflammation and lead to the opening of the endothelial barrier for the passage of macromolecules and leukocytes. Thereby each of these mechanisms triggers the inflammatory response, so they enforce each other. The increase in EHP leads to edema formation, which can lead for example to hypoxic conditions in the surrounding tissue, as well as tissue damage by the activation of the complement cascade. This mechanism reinforce the inflammatory response and again leads to the progression of CVD.[12] The CAM expression at the cell surface of activated endothelial cells is vital for transmigration of the leukocytes through the endothelium into the underlying tissue. This again raises endothelial cell activation and is crucial for the pathogenesis of atherosclerosis. Vessel occlusion by the formation of atherosclerotic plaques triggers chronic inflammation by mechanical stress or areas of hypoxic conditions, leading again to the progression of CVD.

Great progress has been made in understanding these processes. To target this vicious cycle between endothelial activation and CVD progression is a great challenge in drug therapy and new therapeutic options are imperatively needed. CVD represent the main cause of death and morbidity in the Western world and is projected to be the number one global killer by 2020.[13]
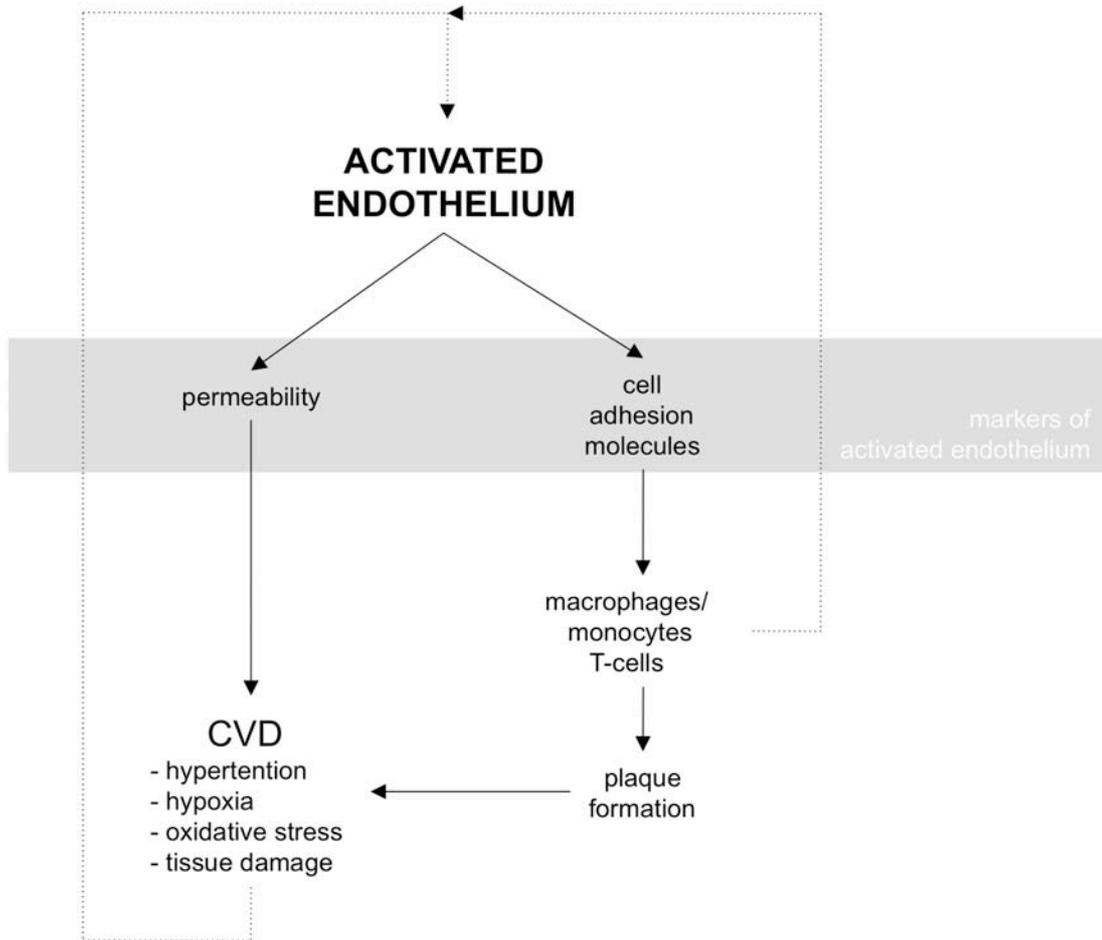
Figure 1: Vicious circle between endothelial activation and CVD progression. An activated
endothelium leads to increased vascular permeability or CAM expression, both hallmarks of
inflammation, which promote CVD. CVD itself leads to different responses that promote
inflammatory endothelial activation.

2.1 Signaling of endothelial activation: ICAM-expression

The expression of inter-cellular adhesion molecule-1 (ICAM-1), an inducible cell adhesion glycoprotein, is upregulated on the surface of EC after exposure to various inflammatory cytokines including tumor necrosis factor-α (TNFα). TNFα induces ICAM-1 promotor activities basically *via* the transcription factor nuclear factor κ-light-chain-enhancer of activated B cells (NFκB), *via* activator protein-1 (AP-1), as well as by signal transducers and activator of transcription protein-1 (STAT-1) (Figure 2).[11] ICAM-1 mediates the firm adhesion of leukocytes to the endothelium and therefore facilitates endothelial transmigration of leukocytes.
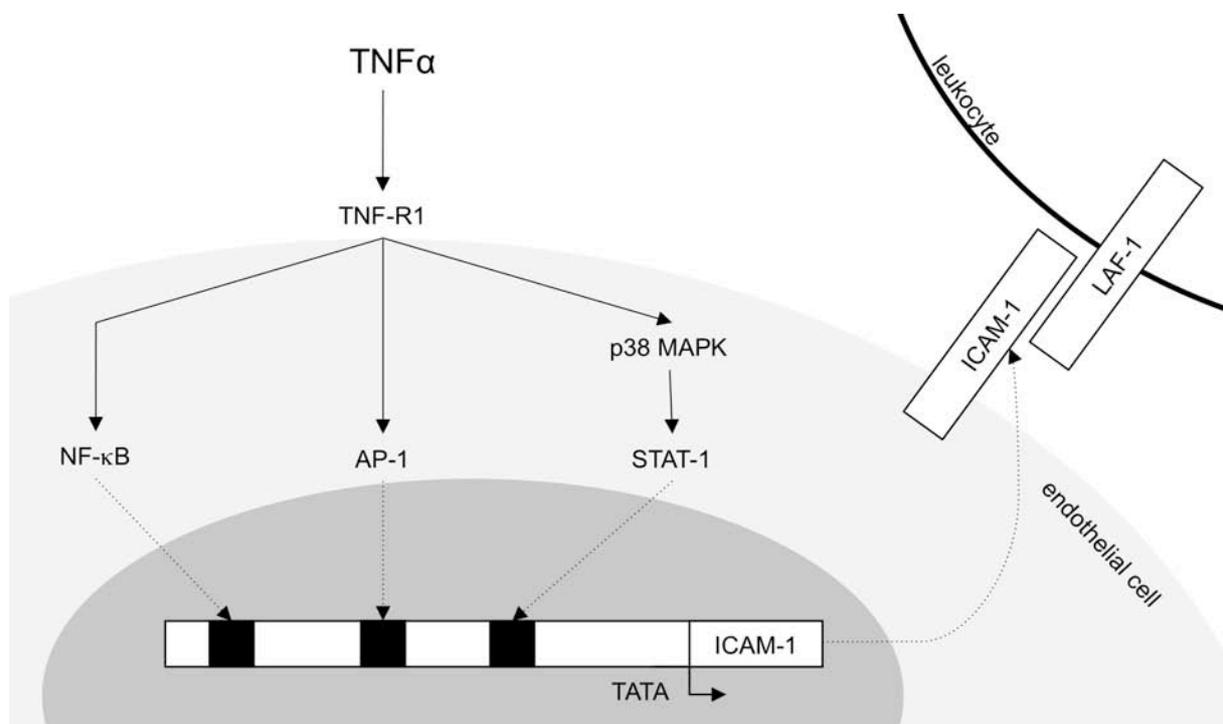
Figure 2: TNFα induces ICAM-1 promotor activity and therefore ICAM-1 expression by activating TNF receptor type 1. The crucial step in the underlying signaling cascades is the translocation of the transcription factors NFκB, AP-1, and STAT-1 to the nucleus. The upregulation of ICAM-1 on the cell surface mediates adhesion of leukocytes to the endothelium *via* Leukocyte function Associated Antigen-1 (LFA-1).[14]

2.2 Barrier-disturbing signaling: endothelial hyperpermeability

2.2.1 Signaling of endothelial activation: endothelial hyperpermeability

Inflammation-induced vascular leakage can be initiated by a great variety of stimuli, depending on the microenvironment and physiological state. Vascular leakage represents a characteristic process for inflammatory endothelial activation and is accompanied by reversible activation of the contractile cell machinery (induction of contractile forces) and adhesion junction (AJ) disruption (loss of adhesive forces), suggesting that the predominant transport pathway is a diffusive one (paracellular transport) and the compartimentation is abrogated.[15]

There are three key mechanisms in inflammatory conditions leading to endothelial barrier disruption (Figure 3). (I) The cytoskeletal proteins reorganization: the remodeling of cortical actin of resting EC into cell-spanning cytosolic stress fibers. (II) The activation of the contractile machinery by phosphorylation of myosin light chain2 (ppMLC2 $^{T18/S19}$). [16,17] (III) The disassembly of adhesion junctions induced by tyrosin phosphorylation of the adhesion protein vascular endothelial cadherin (pVEC^{Y731}). This leads to a dissociation of intracellular regulatory proteins (β-catenin, p120^{ctn}) from VEC, which results in its internalization or degradation.[18] All these factors together lead to the formation of interendothelial gaps, which disturb the endothelial barrier function (image in Figure 3).

Under inflammatory conditions, permeability-inducing factors such as histamine, TNFα, or thrombin are generated and released from platelets, mast cells, monocytes/ macrophages, and vascular cells. [19, 16] They activate specific receptors and increase the intracellular Ca^{2+} concentration ([Ca^{2+}]$_i$) (Figure 4). The [Ca^{2+}]$_i$-increase leads to activation of Ca^{2+}/calmodulin-dependent myosin light chain (MLC) kinase (MLCK), which phosphorylates MLC2 and therefore promotes the interaction of myosin2 with actin filaments, leading to cellular contraction. Activation of the small monomeric GTPase RhoA with its effector Rho kinase (ROCK) also contributes to MLC2 phosphorylation in endothelial cells by inhibition of myosin light chain phosphatase (MLCP). RhoA (*via* ROCK) is also known to be a central regulator of the actin cytoskeleton in terms of stress fibers formation, and thus is involved in the mechanism of cell retraction.

Additionally, RhoA as well as the activation of Ca^{2+}-dependent protein kinase C (PKC) isoform PKC-α, increases induction of endothelial permeability by disrupting the vascular endothelial cadherin (VEC) junctional complex. Therefore, the inflammation-induced Ca^{2+}-signaling affects all three key parameters of endothelial permeability.
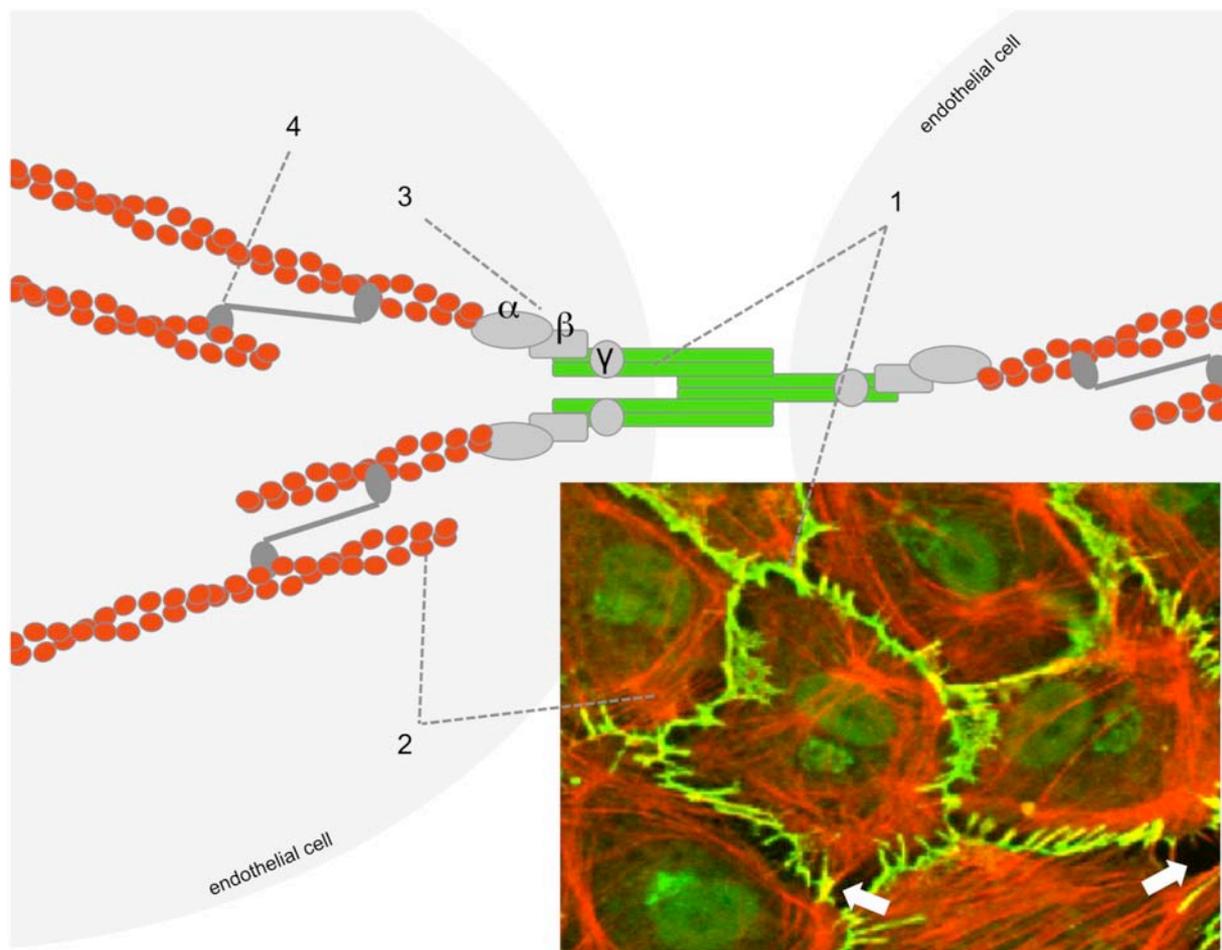
Figure 3: Structure of the key parameters of endothelial permeability. Adhesive junctions formed by VEC (1) and its regulatory proteins, the catenins (3), interconnect endothelial cells stabilizing the endothelial barrier. Contractile forces occure along the stress-fibers (2), *via* interaction with myosin (4). The loss of VEC connections between the cells and the induction of contractile forces lead to an opening of endothelial gaps (white arrows). The microscopic image shows a thrombin activated endothelial monolayer with the typical fringy, uncontinuous VEC seam (green) and stress-fibers (red).
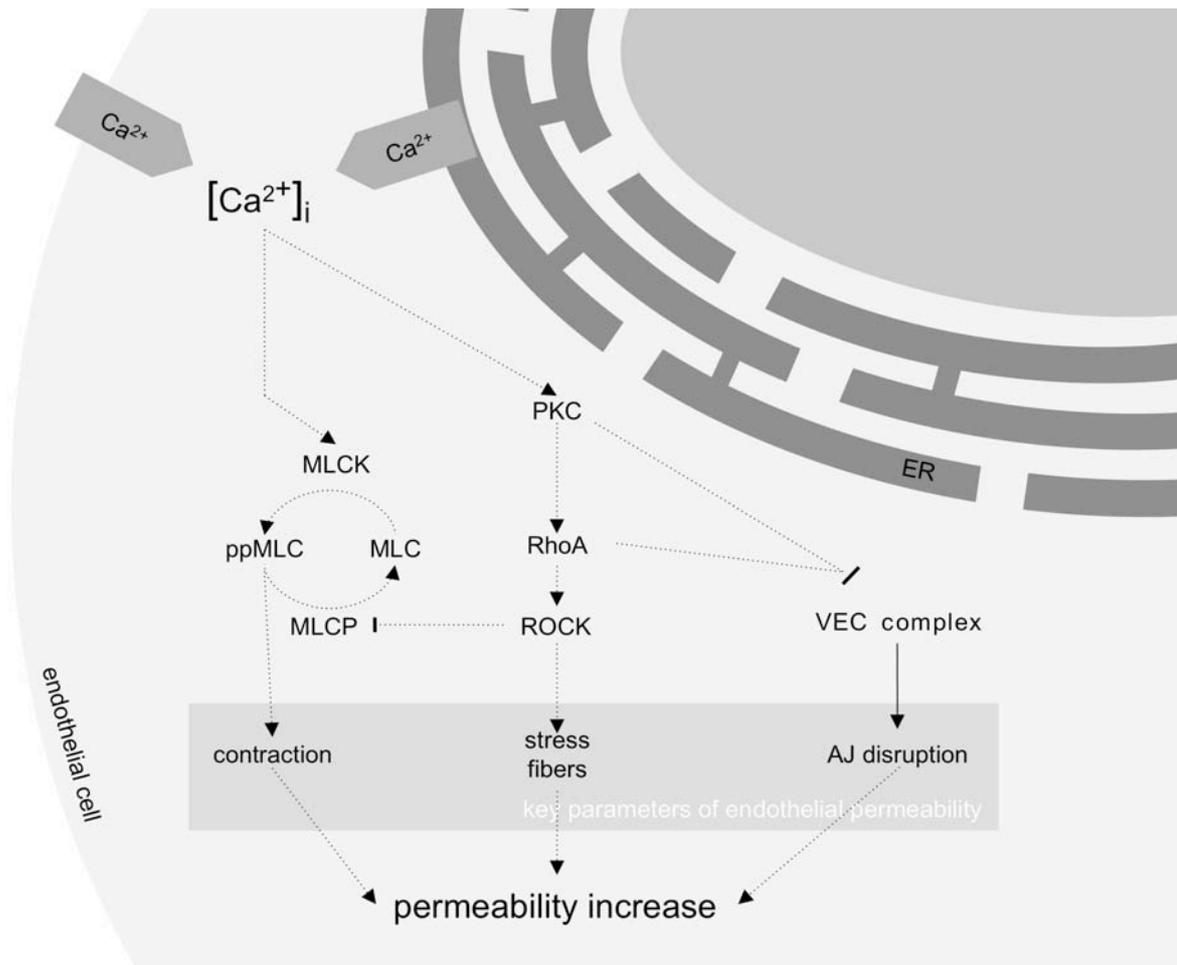
Figure 4: Inflammation-induced endothelial activation by mediators like TNFα, thrombin, or histamine, results in an increase of $[Ca^{2+}]_i$ levels. The subsequently induced downstream signaling of MLCK, RhoA and PKC affects the key parameters of endothelial permeability, which results in an increased in EHP.

2.2.2 Thrombin induced Ca^{2+} increase

Thrombin, a procoagulant serin protease, showed up to be the model substance for inflammation-induced endothelial permeability *in vitro*,[20-22] mediating its acute effects be raising intracellular Ca^{2+}.[4, 19, 23] An $[Ca^{2+}]_i$-response to thrombin is characterized by two distinct phases, including a transient rise corresponding to the release of Ca^{2+} from intracellular stores, and a more sustained increase due to an entry of Ca^{2+} across the plasmalemma.[23] Each phase can regulate discrete cellular functions. As an example, activation of endothelial cell phospholipase A2 depends on Ca^{2+} release, whereas inhibition of the adenylyl cyclase (AC) requires Ca^{2+} entry. [24-26]

$[Ca^{2+}]_i$ is induced by activation of the G protein-coupled protease-activated receptor-1 (PAR-1) (Figure 5). The $G\alpha_q$ protein activates phospholipase C (PLC), which catalyzes production of inositol triphosphat (IP_3) and diacylglycerol (DAG) from phosphatidylinositol 4,5-bisphosphate (PIP_2).[4] IP_3 in turn activates the IP_3 receptor in the endoplasmatic reticulum (ER) to cause the rapid release of sequestered Ca^{2+} into the cytosol, which forms the fast and strong first Ca^{2+}increase (first phase of the intracellular Ca^{2+} signal). This Ca^{2+}increase by ER-depletion activates the store-operated Ca^{2+} channels (SOCs) at the cell membrane, which elicits Ca^{2+} entry from the extracellular milieu leading to reduced, but sustained Ca^{2+}-influx (second phase of the intracellular Ca^{2+}-increase). Beside SOC, receptor-operated Ca^{2+} channels (ROCs) are activated by DAG induction. ROCs lead to a Ca^{2+}-influx from the extracellular space, and intensifies the Ca^{2+} increase in the first phase of Ca^{2+} signaling.[19]
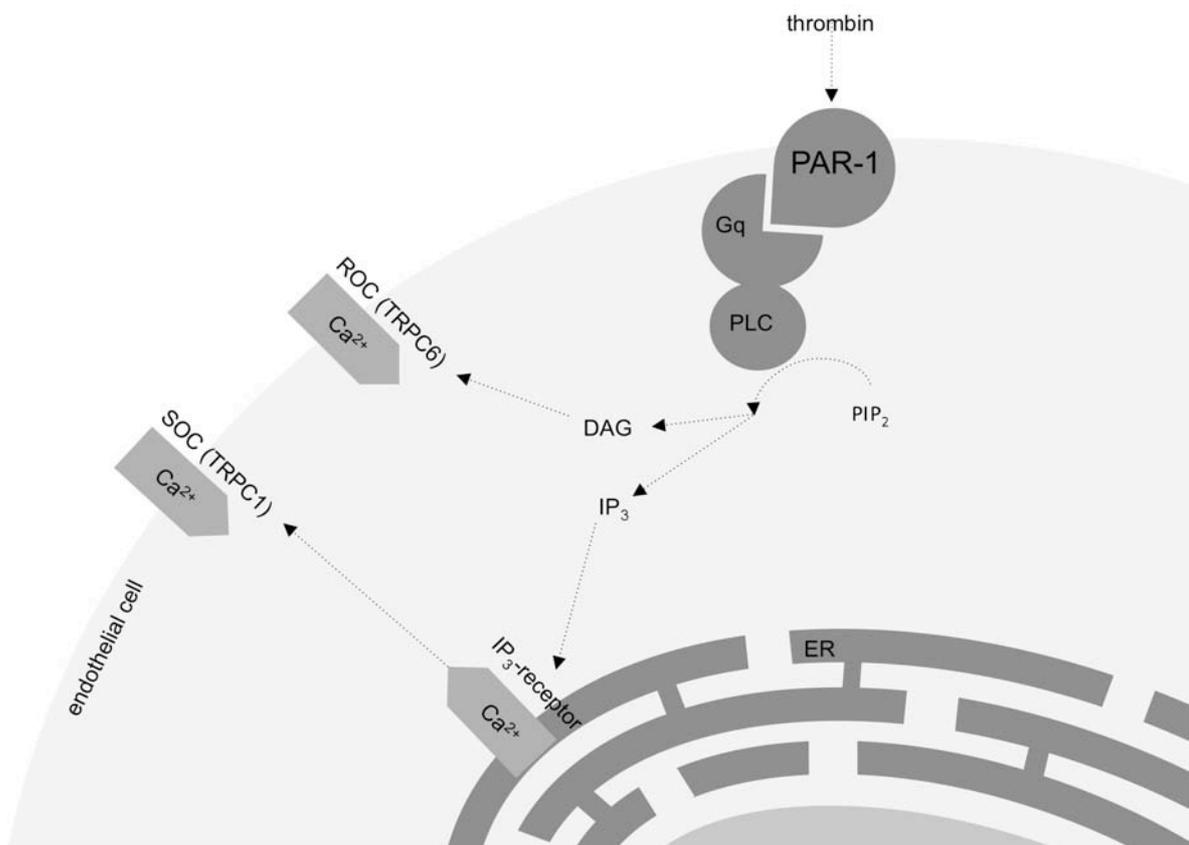
Figure 5: Pathway of thrombin-induced $[Ca^{2+}]_i$ increase.

3 Endothelial barrier protective cAMP- signaling

Cyclic adenosine 3´,5´-monophosphate (cAMP) is an universal second messenger, which is produced from ATP by adenylyl cyclase (AC) upon activation of G_s protein-coupled receptor (GPCR) and degraded to 5`AMP by phosphodiesterases (PDE) (Figure 6). In the vascular system, cAMP influences contraction and relaxation of vascular smooth muscle cells as well as their movement, and the permeability of vascular endothelial cells.[27] Elevation of cAMP in endothelial cells has been recognized to increase barrier function. cAMP-elevating drugs are known to reduce inflammation-induced permeability and edema formation.[28-31] A few years ago this inhibition was thought to be mediated by an activation of protein kinase A (PKA) and its effector vasodilator-stimulated phosphoprotein (VASP).[32] Recent work suggests that cAMP directly activates a new family named exchange proteins directly activated by cAMP (Epac), which seems to be the major regulator of endothelial barrier function.[33-35,36] They are guanine nucleotide exchange factors (GEFs) and activate Rap1, a small GTPases of the Ras family. This pathway represent a PKA independent and novel mechanism for governing signaling specificity within the cAMP cascade.[37, 38]

cAMP stabilizes the endothelial barrier by targeting all three key parameters of endothelial permeability. cAMP abrogates the RhoA-induced inhibition of MLCP and in consequence induces contractile forces that lead to cell rounding. The cAMP-dependent formation of cortical actin relies on an activation of cortactin and stabilizes the endothelial barrier function. The blocking of RhoA activity as well as the activation of cortactin is caused by cAMP-induced activation of Rac1. The increase of $[cAMP]_i$-levels also results in a stabilization of AJ by activating cortactin and stabilizing VEC-catenin binding *via* Rap1.[39, 40, 41]
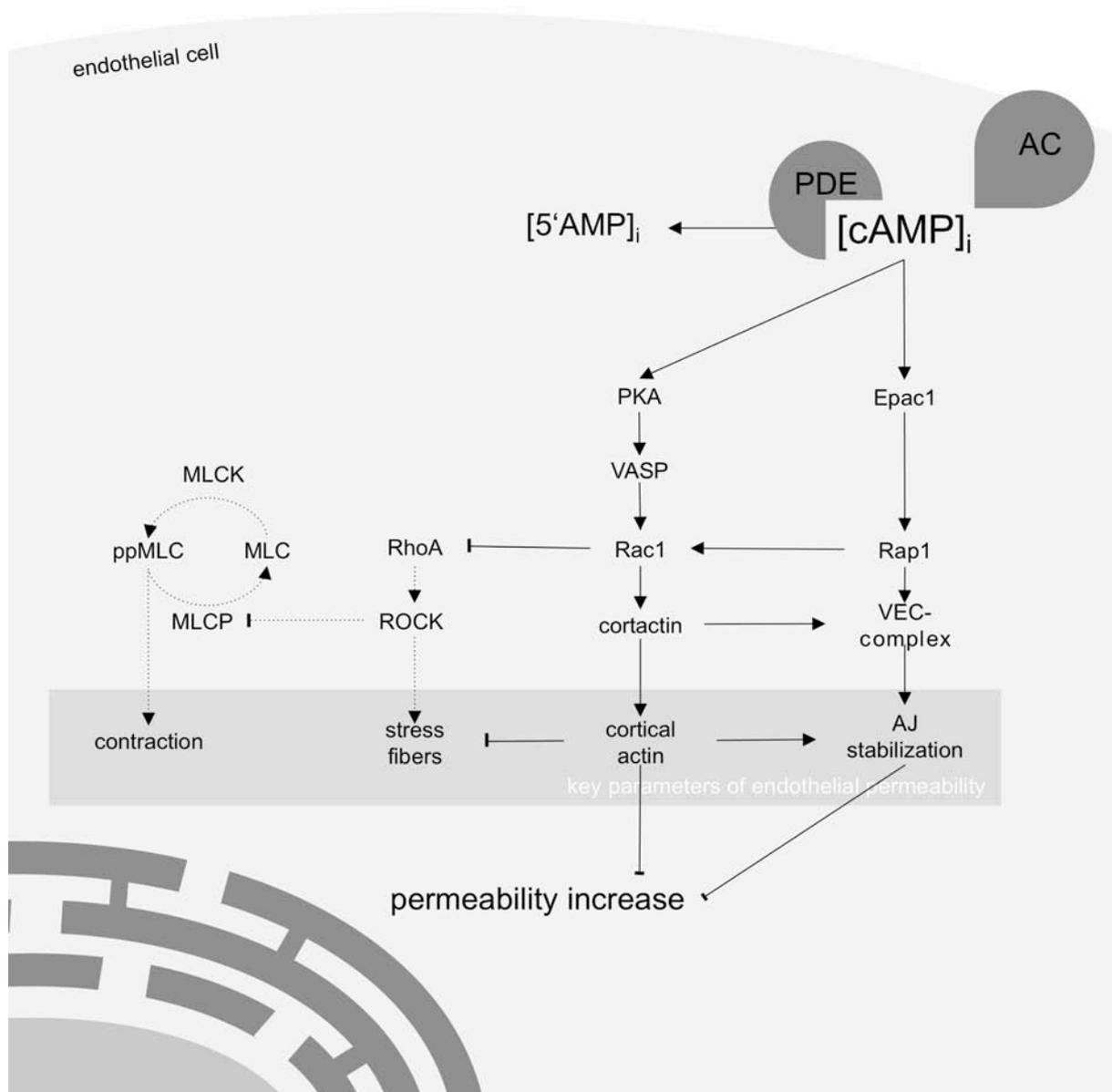
Figure 6: cAMP-dependent endothelial barrier protection due to targeting of the key parameters of endothelial permeability.

4 Hawthorn extract WS® 1442

Hawthorn extract is worldwide used as herbal remedy for the treatment of CVD, and especially in heart failure. WS® 1442 is the most used extract of the leaves and the flowers of *Crataegus monogyna* and *laevigata* (Figure 7). In contrast to several other Crataegus products, which are mostly available as nutraceuticals, it is registered as a phytopharmaceutical medicinal product for the treatment of early stages of congestive heart failure corresponding to stage II of the New York Heart Association (NYHA) classification. WS® 1442 is a dry extract from Crataegus leaves with flowers (4-6.6:1), extract solvent ethanol 45% (w/w), adjusted to a content of 17.3-20.1% of oligomeric procyanidines (OPC) (Figure 8). Besides OPC, WS® 1442 contains mainly flavonoids (flavones, flavonols), including hyperoside, rutin, and vitexin (Figure 9) as well as triterpenoids and phenol carboxylic acids. This standardized quality and different composition compared to other products is the requirement for the save and successful use, as a natural compound in drug therapy, or for scientific purposes.

Figure 7: leaves and flowers of Hawthorn
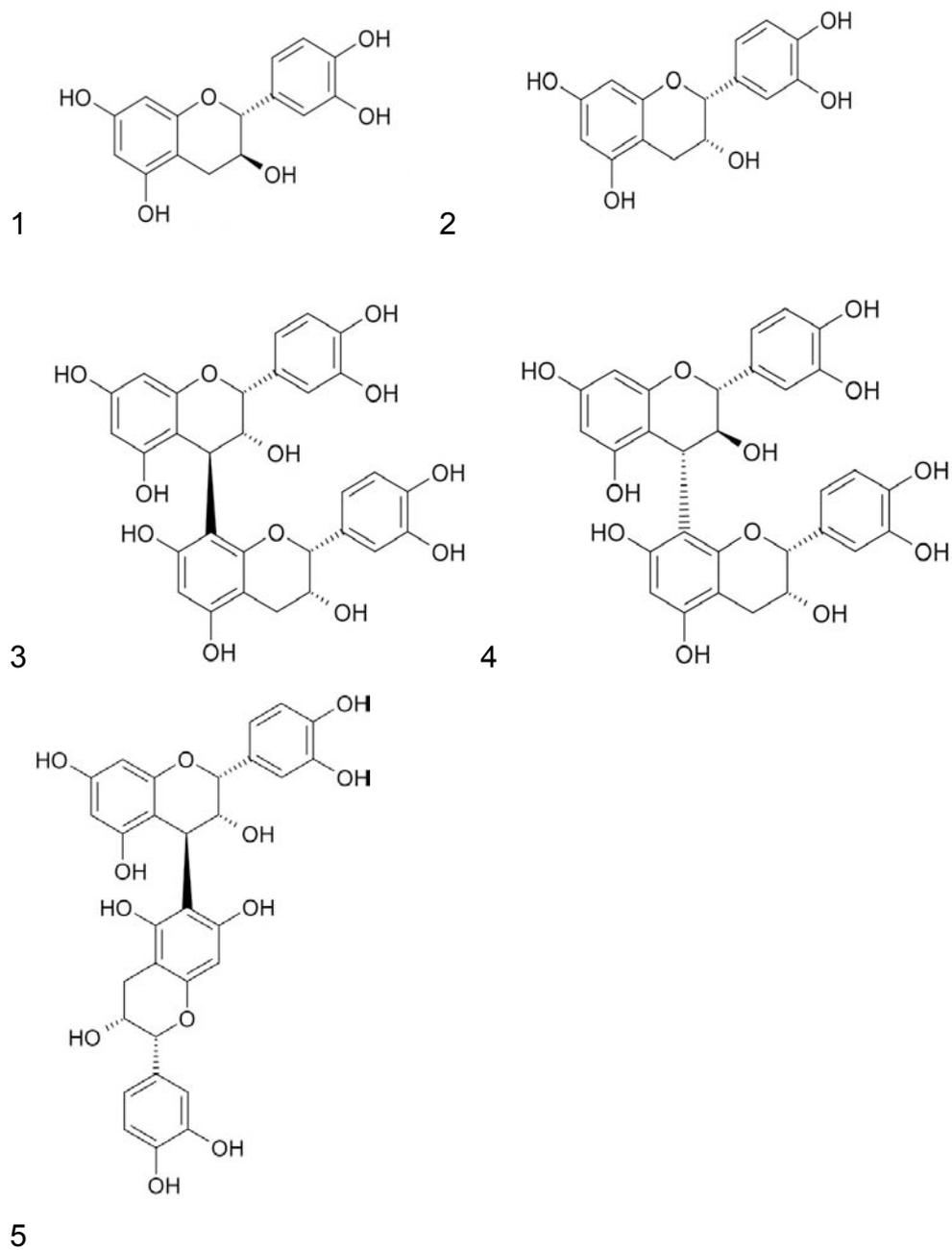
Figure 8: Structures of proanthocyanidines: (1) catechin, (2) Epicatechin, (3) procianidine B2, (4) procianidine B4, (5) procianidine B5.
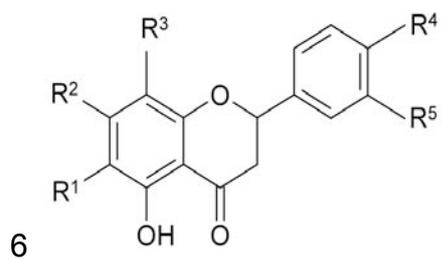
Figure 9:

R^1	R^2	R^3	R^4	R^5	
H	OH	β-D-Glu	H	OH	vitexin
O-β-D-Gal	OH	H	OH	OH	hyperoside
O-β-D-Glu-(6➔1)-α-L-Rha	OH	H	OH	OH	rutin

4.1 Pharmacology and clinical efficancy of WS® 1442

The hawthorn-extract WS® 1442 consists of a complex mixture of active constitutes, and affects a multitude of pharmacological targets. A positive inotropic effect is possibly mediated by a cAMP-independent inhibition of Na$^+$/K$^+$-ATPase. A concentration-dependent increase of myocardial contractility, accompanied by a transient raise in [Ca^{2+}]$_i$, was observed in *in vitro* experiments with human cardiac tissue.[42-44] In contrast to cardiac glycosides, WS® 1442 possesses pronounced anti-arrhythmic properties, by both prolonging the action potential and the refractory period.[45] Furthermore, a vasorelaxation by an endothelium-dependent NO-mediated mechanism was described recently.[46] In animal models of ischaemia and reperfusion, a significant reduction of ventricular fibrillation, tachycardia, area of infarction, and rate of mortality has been observed. An increased coronary blood flow as well as reduced endothelial dysfunction and inhibition of lipid oxidation properties may contribute to these cardio protective effects of WS® 1442.[47, 48]

In clinical trials, WS® 1442 showed an improvement of the exercise capacity, an increased ejection fraction, and decreased heart failure symptoms.[49, 50] The safety and efficiency of this herbal extract in congestive heart failure (CHF) during short and long term administration was also confirmed.[51] In 2008, Holubarsch et al. published the SPICE-trial (Survival and Prognosis: Investigation of Crataegus Extract WS®1442 in CHF)[52]. This randomized, double-blind, placebo-controlled multicenter study included adults suffering from CHF (NYHA class II or III) and reduced left ventricular ejection fraction, which received 900 mg/day WS® 1442 or placebo for 24 months as an add-on therapy. Primary endpoint was the period until the first cardiac event occurred. WS® 1442 as a positive inotropic active drug, showed no increase in

mortality,[53] and therefore confirmed its safety and standing as a valuable drug for symptoms control in CHF.

5 Aim of the Study

Inflammation-activated endothelial cells (EC) lose their barrier function leading to hyperpermeability[19]. As a result of the loss of barrier integrity, edema formation occurs and contributes to the pathogenesis of several disorders, including sepsis, heart failure, atherosclerosis, and asthma. [54-57, 12] These diseases represent some of the most important death-inducing factors, and endothelial hyperpermeability (EHP) poses a very important, highly intriguing central process of all these disorders. However, a specific pharmacological drug targeting remains widely lacking, and therefore no reliable standard therapy for inflammation induced vascular leakage is available. If one considers that EP is a hallmark of inflammation, which is involved in the progression of so many diseases, the search for a permeability-inhibiting compound seems to be an important today's unsolved task in modern medicine.

WS®️ 1442 is an approved drug for the treatment of congestive heart failure according to the New York Heart Association (NYHA) functional class II. The pharmacological properties of WS®️ 1442 have been predominantly investigated with regard to the direct effects on the heart: positive inotropic effects, anti-arrhythmic properties and enhanced coronary blood flow[44, 47, 58]. Although congestive heart failure is accompanied with edema formation[59], studies investigating potential beneficial effects of administered WS®️ 1442 on endothelial barrier dysfunction *in vitro* or *in vivo* are lacking.

Thus, we focused on the extra-cardiac actions of WS®️ 1442 extract concerning endothelial barrier protection in inflammatory conditions. The aims of our study were:

(I) to clarify the general potential of WS®️ 1442 to inhibit inflammatory endothelial activation*,* and to protecting against inflammation-induced endothelial hyper-permeability *in vitro* and *in vivo*,

(III) to decipher the mechanisms by which WS®️ 1442 influences the key regulators of endothelial permeability activation, and

(IV) to relate functions to classes of chemical compounds of the extract.

II MATERIALS AND METHODS

1 Materials

1.1 Crataegus extract WS$^®$ 1442

WS$^®$ 1442 is a well-defined extract of the leaves and the flowers of *Crataegus monogyna* and *laevigata* and was kindly provided by Dr. Willmar Schwabe GmbH & Co.KG (Karlsruhe, Germany).

For experiments, WS$^®$ 1442 was freshly dissolved in growth medium at a maximal concentration of 10,000 µg/ml. Tanning agents were separated by column chromatography with Sephadex LH20 and 75% EtOH (Separation was kindly performed by Dr. Guido Jürgenliemk Pharmaceutical Biology, University of Regensburg, Germany) and the tanning agent free extract was used for *in vivo* and *in vitro* experiments.

WS$^®$ 1442 fractions were used in the concentrations comparable to 100 µg/ml of the complete extract (separated by column chromatography with Sephadex LH20. Separation was kindly performed by Dr. Willmar Schwabe Pharmaceuticals).

WS$^®$ 1442 fraction #	eluate	mass [%] of complete extract	main compounds
30	H$_2$O	56.83	non-phenolic, aliphatic compounds
32	EtOH 95% / H$_2$O	17.00	flavanoids
34	MeOH	12.17	oligomeric proanthocyanidines
36	acetoniltrile 70% / H$_2$O	8.13	proanthocyanidines n>4

1.2 Biochemicals, Inhibitors and Dyes

8-Bromo-cAMP	Biotrend, Cologne, Germany
8-pCPT-2´-O-Me-cAMP	BIOLOG, Bremen, Germany
β-glycerophosphat	Calbiochem, Darmstadt, Germany
BSA (gamma globulin free)	Sigma Aldrich, Taufkirchen, Germany
cAMPS-Rp	Biotrend, Cologne, Germany
Complete^{TM}	Roche, Mannheim, Germany
FluorSave aqueous mounting medium	VWR, Darmstadt, Germany
FITC-Dextran 40 kDa	Sigma Aldrich, Taufkirchen, Germany
forskolin	Biotrend, Cologne, Germany
FURA-2, AM Ester	Biotrend, Cologne, Germany
histamine	Sigma Aldrich, Taufkirchen, Germany
L-NAME	Cayman Chemical Company, Michigan, USA
MTT	Sigma Aldrich, Taufkirchen, Germany
NaF	Merck, Darmstadt, Germany
Na_3VO_4	ICN Biomedicals, Aurora, Ohio, USA
PageRuler^{TM}	Fermentas, St. Leon-Rot, Germany
PMSF	Sigma Aldrich, Taufkirchen, Germany
thapsigargin	Sigma Aldrich, Taufkirchen, Germany
thrombin (human)	Sigma Aldrich, Taufkirchen, Germany
TNFα	Sigma Aldrich, Taufkirchen, Germany
Triton X-100	Sigma Aldrich, Taufkirchen, Germany

1.3 Technical equipment

Vi-CELL™ (Beckman Coulter)	Cell viability analyser
FACSCalibur (Becton Dickinson)	Flow cytometer
Axiovert 25 (Zeiss)	Inverted microscope
Axiovert 200 (Zeiss)	Inverted microscope
LSM 510 Meta (Zeiss)	Confocal laser scanning microscope
Sunrise™ (Tecan)	Plate-reading multifunction photometer
Curix 60 (Agfa)	Tabletop film processor
Thermoshake THO 500 (Gerhardt)	Incubator shaker
Nucleofector™ II (Amaxa)	Electroporation device
Cyclone Storage Phosphor System	Phosphorimager

2   Cell Culture

2.1 Solutions and reagents

The following solutions and reagents were used for the isolation as well as for the cultivation of endothelial cells.

PBS (pH 7.4)

NaCl	123.2	mM
Na_2HPO_4	10.4	mM
KH_2PO_4	3.2	mM
H_2O		

PBS^+ Ca^{2+}/Mg^{2+} (pH 7.4)

NaCl	137	mM
KCl	2.68	mM
Na_2HPO_4	8.10	mM
KH_2PO_4	1.47	mM

MgCl$_2$	0.25	mM
CaCl$_2$	0.5	mM
H$_2$O		

Trypsin/EDTA (T/E)

Trypsin	0.05	%
EDTA	0.20	%
PBS		

Growth medium

ECGM	500	ml
Supplement	23.5	ml
FCS	50	ml
Antibiotics	3.5	ml

Collagen A

Collagen A	10	%
PBS		

Freezing medium

FCS	50	%
DMSO	8	%
ECGM		

Stopping medium

M 199	500	ml
FCS	50	ml

Collagen G

Collagen G	0.001	%
PBS		

Cell culture reagents

Collagen A	BIOCHROM AG, Berlin, Germany
Collagen G	BIOCHROM AG, Berlin, Germany
Collagenase A	Roche, Mannheim, Germany
Culture flasks, plates, dishes	TPP, Trasadingen, Switzerland
ECGM containing supplement and antibiotics	Provitro, Berlin, Germany
FCS	PAA, Pasching, Austria
ibidi slides	ibidi GmbH, Munich, Germany
M199	PAN Biotech, Aidenbach, Germany

For heat inactivation, FCS was partially thawed for 30 min at room temperature. Subsequently, it was totally thawed at 37°C using a water bath. Finally, FCS was inactivated at 56°C for 30 min. Thereafter, 50 ml aliquots of heat inactivated FCS were stored at -20°C.

2.2 HMEC-1 – human microvascular endothelial cells

The cell line CDC/EU.HMEC-1 was kindly provided by the Centers for Disease Control and Prevention (Atlanta, GA, USA). The immortalized HMEC-1 cell line was created by transfection of human dermal microvascular endothelial cells with a plasmid coding for the transforming SV40 large T-antigen. HMEC-1 were shown to retain endothelial morphologic, phenotypic, and functional characteristics.[60, 61]

2.3 HUVEC – human umbilical vein endothelial cells

Human umbilical cords were kindly provided by hospitals from the Munich area. After childbirth, umbilical cords were stored in PBS+Ca^{2+}/Mg^{2+} containing Penicillin (100 U/ml) and Streptomycin (100 µg/ml), 4°C. Cells were isolated within one week. The umbilical vein was washed with PBS+Ca^{2+}/Mg^{2+}, filled with 0.1 g/l collagenase A, and incubated for 45 min at 37°C. To isolate endothelial cells, the vein was flushed with stopping medium and the eluate was centrifuged (1000 rpm; 5 min). Afterwards, cells were replaced in growth medium and plated in a 25 cm^2 flask. After reaching confluency, cells were trypsinized and plated in a 75 cm^2 flask. Experiments were

performed using cells at passage 3, when they were at least two days in a confluent state.

2.4 Passaging

After reaching confluency, cells were either sub-cultured 1:3 in 75 cm^2 culture flasks or seeded either in multiwall plates or dishes for experiments. For passaging, medium was removed and cells were washed twice with PBS before incubation with trypsin/ethylene diamine tetraacetic acid (EDTA) (T/E) for 1-2 min at 37°C. Thereafter, cells were gradually detached and the digestion was stopped using stopping medium. After centrifugation (1,000 rpm, 5 min, 20°C), the pellet was resuspended in growth medium and cells were plated.

2.5 Long-time storage

For freezing, confluent HMECs from a 75 cm² flask were trypsinized, centrifuged (1,000 rpm, 5 min, 20°C), and resuspended in 3 ml ice-cold freezing medium. 1.5 ml aliquots were frozen in cryovials. After storage at -80°C for 24 h, aliquots were moved to liquid nitrogen for long-time storage.

For thawing, a cryovial was warmed to 37°C and the content was immediately dissolved in prewarmed growth medium. In order to remove DMSO, cells were centrifuged, resuspended in growth medium, and transferred to a 75 cm² culture flask.

3 Protein sample preparation

3.1 Total cell lysate

Endothelial cells were treated as indicated, washed once with ice-cold PBS and subsequently lysed in Ripa lysis buffer. Immediately, cells were frozen at -85°C. Afterwards, cells were scraped off and transferred to Eppendorf tubes (Peske, Aindling-Arnhofen, Germany) before centrifugation (14,000 rpm, 10 min, 4°C). Protein concentration was determined using the BCA or the Bradford assay. Laemmli sample buffer (3x) was added and samples were heated at 95°C for 5 min. The reducing agent β-mercaptoethanol cleaves disulfide bonds and boiling leads to complete denaturation of the proteins. SDS is an anionic detergent that attaches to hydrophobic parts of the proteins, resulting in permanent negatively charged proteins. Samples were kept at -20°C until Western blot analysis.

For the protection of phosphorylated proteins the cells were washed with modified PBS containing activated Na_2VO_3 and H_2O_2 (s. modified cell washing solution), and the Ripa lysis buffer additionally contained H_2O_2, β-glycerophosphate and pyrophosphate (s. modified Ripa lysis buffer).

**Modified cell washing
solution**

activated Na_2VO_4	600	µM
H_2O_2	600	µM
PBS		

Modified Ripa lysis buffer

NaCl	150	mM
Tris	50	mM
Nonidet P-40	1	%
Deoxycholate	0.25	%
SDS	0.10	%
β-glycerophosphate	3	mM
pyrophosphate	10	mM

H$_2$O

add before use:		
Complete^{TM}	4	mM
PMSF	1	mM
NaF	1	mM
activated Na$_2$VO$_3$	1	mM
H$_2$O$_2$	600	µM

Laemmli sample buffer (3x)

Tris-HCl	187.5	mM
SDS	6	%
Glycerol	30	%
Bromphenolblue	0.025	%
H$_2$O		
add before use:		
β-mercaptoethanol	12.5	%

3.2 Membrane fractionation

HUVEC lysates were separated into a soluble (cytosolic) and a particulate (membranous) fraction, as described previously by Li H *et al.*[62] HUVECs were treated as indicated, washed twice with ice-cold PBS, and homogenized in lysis buffer. Lysates were centrifuged at 100,000 g for 1 hour. The supernatant (cytosolic fraction) was collected, the pellet was washed in lysis buffer containing 1.0 M NaCl, and centrifuged at 100,000 g for 30 minutes. The supernatant was discarded and the pellet was solubilized with lysis buffer containing 20 mM CHAPS at 4°C for 30 minutes. After centrifugation at 100,000 g for 1 hour, the supernatant was kept as membranous fraction. Both fractions were used for Western blotting.

Membrane lysing buffer

Tris-HCl pH 7.5	0.05	M
EDTA	0.5	mM
EGTA	0.5	mM

Glutathione	7.0	mM
Glycerol	10	%
H_2O		

add before use:		
PMSF	1.0	mM
Complete®	4	mM

3.3 Extraction of nuclear protein

HUVEC were grown in 6-well plates until reaching confluency and were treated as indicated in the respective figures. Nuclear extracts were prepared according to the method of Schreiber et al.[63] as follows: after treatment, cells were washed twice with ice-cold PBS, scraped off in PBS with a rubber cell scraper, centrifuged, and resuspended in an ice-cold cytosol lysing buffer. Cells were incubated on ice for 15 min. Nonidet P-40 was added to the cells and after vigorous vortexing the homogenate was centrifuged. The nuclear pellet was resuspended by vigorous rocking for 15 min at 4°C in nucleus lysing buffer containing HEPES pH 7.9 20 mM, NaCl 400 mM, EDTA 1 mM, EGTA 0.5 mM, glycerol 25 %, DTT 1 mM, PMSF 1 mM, and Complete® 2 %. The nuclear extract was centrifuged and the supernatant containing nuclear proteins was frozen at -80°C. The protein concentrations were determined by the method of Bradford.[64]

Cytosol lysing buffer

HEPES pH 7.9	10	mM
KCL	10	mM
EDTA	0.1	mM
EGTA	0.1	mM
DTT	1	mM
H_2O		

add before use:		
PMSF	0.5	mM
Complete®	1	%

Nucleus lysing buffer

HEPES pH 7.9	20	mM
NaCl	400	mM
EDTA	1	mM
EGTA	0.5	mM
Glycerol	25	%
DTT	1	mM
H_2O		

add before use:

PMSF	1	mM
Complete®	2	%

4   Protein Quantification

4.1 Bicinchoninic protein assay (BCA)

Bicinchoninic (BCA) Protein Assay (BC Assay reagents, Interdim, Montlucon, France) was performed as described previously.[65] 10 µl protein samples were incubated with 200 µl BC Assay reagent for 30 min at 37°C. Absorbance of the blue complex was measured photometrically at 550 nm (Tecan Sunrise Absorbance reader, TECAN, Crailsheim, Germany). Protein standards were obtained by diluting a stock solution of Bovine Serum Albumin (BSA, 2 mg/ml). Linear regression was used to determine the actual protein concentration of each sample.

4.2 Bradford assay

Bradford Assay (Bradford solution, Bio-Rad, Munich, Germany) was performed as described previously.[64] It employes Coomassie Brillant Blue as a dye, which binds to proteins. 10 µl protein samples were incubated with 190 µl Bradford solution (1:5 dilution in water) for 5 min. Thereafter, absorbance was measured photometrically at 592 nm (Tecan Sunrise Absorbance reader, TECAN, Crailsheim, Germany). Protein standards were achieved as described above (BCA Assay).

5 Western blot transfer

In order to employ equal amounts of proteins in all samples for Western blot analysis, protein concentrations were determined using the Bicinchoninic Protein Assay (BCA). After measurement, protein concentration was adjusted by adding Laemmli sample buffer (1x).

5.1 SDS-PAGE

Proteins were separated by discontinuous SDS-polyacrylamid gel electrophoresis (SDS-PAGE) according to Laemmli.[66] Equal amounts of protein were loaded on gels and separated using the Mini-PROTEAN 3 electrophoresis module (Bio-Rad, Munich, Germany). Discontinuous polyacrylamide gels were used consisting of a separation and stacking gel. The concentration of Rotiphorese^{TM} Gel 30 (acrylamide) in the separating gel was adjusted for an optimal separation of the proteins depending on their molecular weights (**Table 1**). Electrophoresis was carried out at 100 V for 21 min for protein stacking and 200 V for 45 min for protein separation. The molecular weight of proteins was determined by comparison with the prestained protein ladder PageRuler^{TM}.

Table 1: Acrylamide concentration in the separation gel:

Protein	acrylamide concentration	
phos. MLC, pp38, RhoA, Rac1, Rap1, βActin, phos. VASP	15	%
VEC, phos. VEC, p120^{ctn}, β-catenin, phos. PKC(pan), phos. PKC-Sub., cortactin, phos cortactin,	10	%

Separation gel 10/15 %

Rotiphorese^{TM} Gel 30	33.3/50	%
Tris (pH 8.8)	375	mM
SDS	0.1	%

TEMED	0.1	%
APS	0.05	%
H_2O		

Stacking gel

Rotiphorese[TM] Gel 30	40	%
Tris (pH 6.8)	125	mM
SDS	0.1	%
TEMED	0.2	%
APS	0.1	%
H_2O		

Electrophoresis buffer

Tris	4.9	mM
Glycine	38	mM
SDS	0.1	%
H_2O		

5.2 Tank-electroblotting

After protein separation, proteins were transferred onto a nitrocellulose membrane (Hybond-ECL[TM], Amersham Bioscience, Freiburg, Germany) by electro tank blotting. Electroblotting, also denoted as Western blotting, is the most commonly used method to transfer proteins from a gel to a membrane.[67] A blotting sandwich was prepared in a box filled with 1x Tank Buffer to avoid bubbles as follows: cathode – pad – blotting paper – separating gel (from SDS-PAGE) – nitrocellulose membrane – blotting paper – pad – anode. Pads, papers, and membrane were equilibrated with 1x Tank buffer 15 minutes prior to running the tank blot. Sandwiches were mounted in the Mini Trans-Blot® system (Bio-Rad, Munich, Germany), ice-cold 1x Tank buffer filled the chamber and a cooling pack was inserted to avoid excessive heat. Transfers were carried out at 4°C, either at 100 V for 90 minutes or at 24 V overnight (especially for high-molecular weight proteins).

5x Tank buffer

Tris base	15.2	g
Glycine	72.9	g
H_2O	ad 1.0	l

1x Tank buffer

5x Tank buffer	200	ml
Methanol	200	ml
H_2O	ad 1.0	l

5.3 Protein detection

Prior to the immunological detection of the relevant proteins, unspecific protein binding sites were blocked. Therefore, the membrane was incubated in Blotto 5% or BSA 5% for 2 h at room temperature. Afterwards, detection of the proteins was performed by incubating the membrane with the respective primary antibody at 4°C overnight. After three washing steps with PBS containing 0.1% Tween (PBS-T), the membrane was incubated with the secondary antibody, followed by 3 additional washing steps. All steps regarding the incubation of the membrane were performed under gentle agitation. In order to visualize the proteins, two different methods have been used depending on the labels of secondary antibodies.

5.4 Enhanced chemiluminescence

Membranes were incubated for 2 h with HRP-conjugated secondary antibodies. For detection, luminol was used as a substrate. The membrane was incubated with ECL (enhanced chemoluminescence) solution for 1 minute (ECL Plus Western Blotting Detection Reagent RPN 2132, GE Healthcare, Munich, Germany). The appearing luminescence was detected by exposure of the membrane to an X-ray film (Super RX, Fuji, Düsseldorf, Germany) and subsequently developed with a Curix 60 Developing system (Agfa-Gevaert AG, Cologne, Germany).

5.5 Infrared Imaging

Secondary antibodies coupled to IRDye^{TM} 800 and Alexa Fluor$^®$ 680 with emission at 800 and 700 nm, respectively, were used (**Table 3**). Membranes were incubated for 1 h. Protein bands of interest were detected using the Odyssey imaging system (Li-Cor Biosciences, Lincoln, NE). After scanning the membrane with two-color detection, bands could be quantified using the Odyssey software. Primary antibodies used for protein detection are listed in **Table 2**.

Table 2: Primary antibodies

Antigen	Source	Dilution	in		Provider
actin	mouse monoclonal	1:10,000	Blotto	1 %	Chemicon
β-catenin	rabbit polyclonal	1:10,000	Blotto	1 %	Santa Cruz
VEC	mouse monoclonal	1:10,000	Blotto	1 %	Santa Cruz
phos.VEC ^{Y731}	rabbit polyclonal	1:5,000	Blotto	1 %	Biosource
p120ctn	rabbit polyclonal	1:10,000	Blotto	1 %	Santa Cruz
phos. cortactin^{Y421}	rabbit polyclonal	1:1,000	BSA	5 %	Cell Signaling
phos. MLC $^{T18/S19}$	rabbit polyclonal	1:1,000	BSA	1 %	Biosource
phos. PKA-sub.	rabbit monoclonal	1:1,000	Blotto	5 %	Cell Signaling
phos. PKC-sub.	rabbit polyclonal	1:1,000	BSA	5 %	Cell Signaling
phos. PKC(pan)^{T514}	rabbit polyclonal	1:1,000	BSA	5 %	Cell Signaling
phos. p38$^{T180/Y182}$	mouse monoclonal	1:5,000	Blotto	5 %	Cell Signaling
phos.VASP^{S157}	rabbit polyclonal	1:1,000	BSA	1 %	Cell Signaling
Rac1	mouse monoclonal	1:1,000	Blotto	3 %	UPSTATE
Rap1	rabbit polyclonal	1:1,000	BSA	3 %	PIERCE
RhoA	mous monoclonal	1:500	BSA	3 %	PIRECE

Table 3: Secondary antibodies

Antibody	Dilution	in	Provider
Goat anti-mouse IgG1: HRP	1:1,000	Blotto 1%	Biozol
Goat anti mouse IgG2b: HRP	1:1,000	Blotto 1%	Southern Biotech.
Goat anti-rabbit: HRP	1:1,000	Blotto 1%	Dianova
Alexa Fluor® 680 goat anti-mouse IgG	1:10,000	Blotto 1%	Molecular Probes
Alexa Fluor® 680 goat anti-rabbit IgG	1:10,000	Blotto 1%	Molecular Probes
IRDye™ 800 goat anti-rabbit IgG	1:10,000	Blotto 1%	Rockland

5.6 Stripping and reprobing

In order to remove primary and secondary antibodies from the membrane ("stripping"), blots were incubated twice in stripping buffer for 15 min at room temperature. After extensive washing, stripping efficiency was confirmed by scanning/detecting the membrane to see if signals have been removed. Subsequently, the blot was re-blocked with Blotto 5% for 2 h and incubated with antibodies.

Stripping buffer (pH 2.0)

Glycine	25	mM
SDS	0.1	%
H_2O		

6   Electrophoretic mobility shift assay (EMSA)

6.1 Radioactive labeling of consensus oligonucleotides

Double-stranded oligonucleotide probes containing the consensus sequence either for AP-1 (5'-CGCTTGATGAGTCAGCCGGAA-3') or for NF-κB (5'-AGTTGAGGG GACTTTCCCAGGC-3') (both from Promega, Mannheim, Germany) were 5'-end-labeled with adenosine 5'-[γ-^{32}P] triphosphate (3,000 Ci/mmol) (Amersham, Freiburg, Germany) by using the T4 polynucleotide kinase (PNK) (USB, Cleveland, USA),

which catalyzes the transfer of the terminal phosphate of ATP to the 5'-hydroxyl-termini of DNA. The oligonucleotides were incubated with T4 PNK for 10 min at 37°C and the reaction was stopped by adding EDTA solution (0.5 M). The radiolabeled DNA was separated from unlabeled remnants by using NucTrap probe purification columns (Stratagene, La Jolla, USA). Radiolabeled DNA was eluated from the column by STE buffer pH 7.5 and frozen at -20°C.

STE buffer pH 7.5

Tris-HCl	10	mM
NaCl	100	mM
EDTA	1	mM
H_2O		

6.2 Binding reaction and electrophoretic separation

Equal amounts of nuclear protein (approx. 2 µg) were incubated for 5 min at room temperature in a total volume of 14 µl containing poly(dIdC) 2 µg and reaction buffer 3 µl. Subsequently, 1 µl of the radiolabeled oligonucleotide probe (approx. 300,000 cpm) was added. After incubation for 30 min at room temperature, the nucleoprotein-oligonucleotide complexes were resolved by electrophoresis (Mini-Protean 3, Bio-Rad, Munich, Germany) on non-denaturating polyacrylamide gels (4.5 %). TBE was used as electrophoresis buffer. Bands were visualized by applying the gels to Cyclone Storage Phosphor Screens (Canberra-Packard, Dreieich, Germany) and analysis by a phosphorimager (Cyclone Storage Phosphor System, Canberra-Packard, Dreieich, Germany).

Non-denaturating polyacrylamide gels 4.5%

10x TBE	5.3	%	
Rotiphorese^{TM} Gel 30		15.8	%
Glycerol	2.6	%	
TEMED	0.05	%	
APS	0.08	%	
H_2O			

10x TBE pH 8.3

Tris	0.89	M
Boric acid	0.89	M
EDTA	0.02	M
H_2O		

5x Binding buffer pH 7.5

Glycerol	20	%
$MgCl_2$	5	mM
EDTA	2.5	mM
NaCl	250	mM
Tris-HCl	50	mM
H_2O		

Gel loading buffer pH 7.5

Tris-HCl	250	mM
Bromphenol blue	0.2	%
Glycerol	40	%
H_2O		

Reaktion buffer

DTT	2.6	mM
5x binding buffer	90	%
gel loading buffer	10	%

7   Transfection of cells

HUVECs were transiently transfected with plasmids for pEGFP-C1-actin, which was kindly provided by S. Linder (Inst f. Prophylaxe und Epidemiologie der Kreislauferkrankungen). For electroporation the Nucleofector® II device in combination with the HUVEC Nucleofector® Kit (both from Amaxa, Cologne, Germany) was used. Plasmids were amplified in the *E. coli* strain DH5α and purificated by using the EndoFree Plasmid Maxi Kit (Qiagen GmbH, Hilden, Germany). Expression procedures were done according to the provided protocol. For each transfection, $1x10^6$ HUVECs were suspended in 100 µl HUVEC Nucleofector Solution including 5 µg of the respective plasmid. Electroporation was performed according to Amaxa protocols (program A-034). After transfection, cells were seeded into ibidi µ-slides (8-well ibiTreat, ibidi GmbH, Munich, Germany, 300,000 cells per well). Experiments were performed 48 h after transfection.

8   Rac, Rho and Rap pull-down assay

In a pull-down assay, the activation state of GTPases can be analyzed. The assay is based on the principle that only the active form of the GTPase interacts with its specific downstream effectors. The GTPase-binding domains from these downstream effectors are expressed as recombinant glutathione S-transferase (GST) fusion proteins immobilized on glutathione resin and can be used for affinity precipitation (pull-down) of the active GTPase from cell lysates. Pulled-down active GTPases are eluted from the resin and detected by immunoblotting with a specific antibody.

Pull-down assays were performed using the RhoA Activation Assay Kit 89854, Rap1 Activation Assay Kit 89872 (both from PIERCE, Rockford, IL, USA) and Rac1/Cdc42 Activation Assay Kit 17-441 (from Millipore, Billerica, MA, USA). HUVECs were seeded into 100 mm^2 dishes and grown 3 days (long confluence). Procedures were done according to the provided protocol. For adjustment of protein contents of the respective samples, protein concentration was determined using the Bradford-assay. Proteins were detected by Western Blot analysis.

9 Macromolecular permeability assay

HMECs (0.125×10^6 cells/well) were seeded on collagen G-coated 12-well Transwell® plate inserts (pore size 0.4 µm, polyester membrane; Corning, New York, USA) and cultured for 48 h. FITC-dextran (40 kDa; 1 mg/ml; Sigma-Aldrich) was given to the upper compartment at t = 0 min. Cells were treated as indicated. Samples were taken from the lower compartment at t = 0/5/10/15/30 min. The fluorescence increase (ex 485/em 535) of the samples was detected with a fluorescence plate reader (SpectraFluor Plus, Tecan Deutschland GmbH). The mean fluorescence of untreated cells at t = 30 was set as 100%. The data are expressed as the percent increase of fluorescence versus the control.
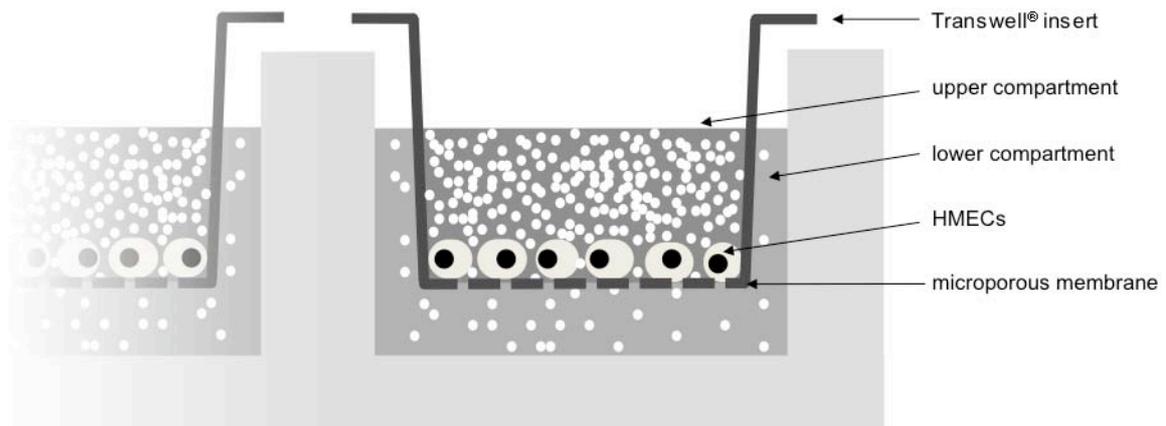
Figure 10: Close up of a Transwell® insert with a HMEC monolayer

10 Ca²⁺-measurement

Changes in intracellular calcium levels can be analyzed by ion sensitive indicators, whose light emission reflects the local concentration of the ion. Fura-2 is a calcium indicator often used in the esterified form Fura-2 acetoxymethyl ester (Fura-2-AM). The acetoxymethyl ester group increases the uptake of the dye and is hydrolyzed by cytoplasmic esterases to regenerate and trap the dye in the cytosol. Fura-2 free of Ca^{2+} emits fluorescence upon excitation at 380 nm but after binding to Ca^{2+}

experiences a shift to 340 nm in its excitation wavelength. Therefore, the ratio of fluorescence intensity obtained by excitation at 340 nm to the intensity obtained by excitation at 380 nm provides an accurate measurement of the free Ca^{2+} concentration.

Hepes buffer, pH 7.40

NaCl	125	mM
KCl	3	mM
$NaH_2PO_4 \times H_2O$	1.25	mM
$CaCl_2 \times 2H_2O$	2.5	mM
$MgCl_2 \times 6H_2O$	1.5	mM
Glucose	10	mM
HEPES	10	mM

Variations in cytosolic calcium were studied in HUVECs. For this purpose, HUVECs were seeded in 60 mm^2 dishes and grown three days to long confluence. Afterwards, cells were washed twice with Hepes buffer (37°C). Fura-2-AM was added in Hepes buffer containing 0.1% BSA to a final concentration of 1 µM and the cell suspension was incubated for 30 min at 37°C. After two washing steps with Hepes buffer-0.1% BSA, the dish with new Hepes buffer 0.1% BSA was placed on the stage of a Zeiss Axiovert 200 inverted microscope (Zeiss, Oberkochen, Germany) equipped with a Polychrome V monochromator and an IMAGO-QE camera (TILL Photonics GmbH, Gräfelfing, Germany). Chamber temperature was maintained at 37°C by placing the coverslip holder on a heating insert P (Zeiss, Oberkochen, Germany) for additional 10 min. Cells were stimulated as indicated. Excitation wavelengths were alternately selected at 340 nm and 380 nm and fluorescence filtered at 510 nm (LP filter) was recorded. Images were acquired every 10 sec and analysed using the TILLvisION Software 4.0.1.2 (TILL Photonics GmbH, Gräfelfing, Germany). Areas of interest corresponding to the whole field of vision were selected, the background was subtracted and the average intensity of each area over the course of the experiment was recorded. Changes in ratio of fluorescence emitted by excitation at 340 and 380 nm represent changes in the intracellular Ca^{2+} content. For measurement in Ca^{2+}-free conditions, 0.1% BSA-containing Hepes buffer without Ca^{2+} was used.

11   cAMP Enzyme-Linked Immunosorbent Assay (ELISA)

The cAMP assay was performed in two steps: we performed the accumulation of cAMP in intact cells, and the determination of cAMP was studied by an enzyme-linked immunosorbant assay (ELISA) kindly performed by Prof. Dr. Hermann Ammer (Professor of Clinical Pharmacology, Department of Veterinary Sciences, University of Munich).

Accumulation of cAMP in intact HUVECs was determined as follows: HUVECs were seeded in 24-well plates and grown until long confluence (3 days). Immediately before stimulation, cells were washed three times with 1 ml/well pre-warmed DMEM containing 10 mM HEPES (pH 7.4) and 0.01% BSA. Subsequently, cells were stimulated in a total volume of 250 µl. Accumulation of cAMP was allowed for 15 min at 37°C and was terminated by the addition of 750 µl ice-cold HCl 50 mM. The amount of cAMP generated was determined in the supernatants by enzyme-linked immunosorbant assay after acetylation of the samples.

12   Confocal microscopy

A Zeiss LSM 510 META confocal microscope (Zeiss, Oberkochen, Germany) equipped with a heating stage from EMBL (Heidelberg, Germany) was used for obtaining images of fixed cells as well as for life cell imaging experiments.

12.1 Microscopy with fixed cells

HUVECs were cultured in ibidi µ-slides (8-well ibiTreat, ibidi GmbH, Munich, Germany) until reaching long confluency (3 days). Afterwards, cells were treated as indicated, washed with PBS and fixed with 4% parafomaldehyde in PBS at room temperature (10 min), followed by permeabilization *via* incubation with 0.2% Triton X-100 (Sigma, Taufkirchen, Germany) in PBS (2 min). Cells were washed and unspecific binding was blocked with 0.2% BSA in PBS for 30 min. Afterwards, cells were incubated with the respective primary antibody for 1 h at room temperature (**Table 4**).

Table 4: Primary antibodies used for confocal microscopy

Antigen	Isotype	Dilution	in	Provider
VEC	mouse monoclonal	1:400	BSA 0.2 %	Santa Cruz
cortactin	rabbit polyclonal	1:400	BSA 0.2 %	Cell Signaling
phos.cortactin^{Y421}	rabbit polyclonal	1:400	BSA 0.2 %	Cell Signaling
phos. MLC $^{T18/S19}$	rabbit polyclonal	1:400	BSA 0.2 %	Biosource
phos. PKA-sub.	rabbit monoclonal	1:400	BSA 0.2 %	Cell Signaling
phos. VASP^{S157}	rabbit polyclonal	1:400	BSA 0.2 %	Cell Signaling
p65	rabbit polyclonal	1:400	BSA 0.2 %	Santa Cruz

Following three washing steps with PBS, cells were incubated with the respective secondary antibodies or with rhodamin/phalloidin for staining of F-actin, respectively, for 45 min at room temperature (**Table 5**).

Table 5: Secondary antibodies/dye used for confocal microscopy

Antibody/Dye	Dilution	in	Provider
AlexaFluor® 488 goat-anti-mouse	1:400	BSA 0.2 %	Molecular Probes
AlexaFluor® 488 goat-anti-rabbit	1:400	BSA 0.2 %	Molecular Probes
AlexaFluor® 647 chicken-anti-rabbit	1:400	BSA 0.2 %	Molecular Probes
AlexaFluor® 633 goat-anti-mouse	1:400	BSA 0.2 %	Molecular Probes
Rhodamin/phalloidine	1:400	BSA 0.2 %	Molecular Probes

Finally, preparates were again washed three times with PBS (5 min) and embedded in FluorSave aqueous mounting medium (VWR, Darmstadt, Germany).

12.2 Live cell imaging

Live cell imaging was performed to visualize the dynamics of single cells during cytoskeleton rearrangement. HUVECs were transfected with 5 µg of the indicated plasmid. After transfection, HUVECs were seeded into ibidi µ-slides (8-well ibiTreat, 300,000 cells per well). A time series was collected by taking images every 30 sec

(10 min ahead and 30 min after stimulation). LSM Image Browser (Zeiss) was used for analysis of images.

13   Flow cytrometry

Flow cytometry (FACS) allows counting, sorting, and analysis of various parameters of single cells or particles suspended in a fluid. Each cell passes a focused laser beam and scatters the illuminating light. If particles have previously been stained with a fluorescent dye, fluorescence emission occurs and can be detected.

Flow cytometry has been used for the analysis of intercellular adhesion molecule-1 (ICAM-1) expression. All measurements were performed on a FACSCalibur (Becton Dickinson, Heidelberg, Germany). Cells were illuminated by a blue argon laser (488 nm).

Cells were seeded in 12-well plates and grown to confluence and either left untreated or preincubated with WS$^®$ 1442 for 24h. After stimulation with TNFα (10 ng/ml) for 24h, cells were harvested with T/E, washed with PBS, and fixed in PBS/4% formalin on ice for 10 min. Afterwards, cells were washed two times with PBS and 0.5 µg FITC-labeld ICAM-1 antibody (Biozol, Eching, Germany) was added for 45 min at 21°C. Cells were washed three times and 10,000 cells were measured by flow cytometry to detect the membrane expression of ICAM-1 as evidenced by a median shift in fluorescence intensity (FL1: 509 nm) (Figure 11).
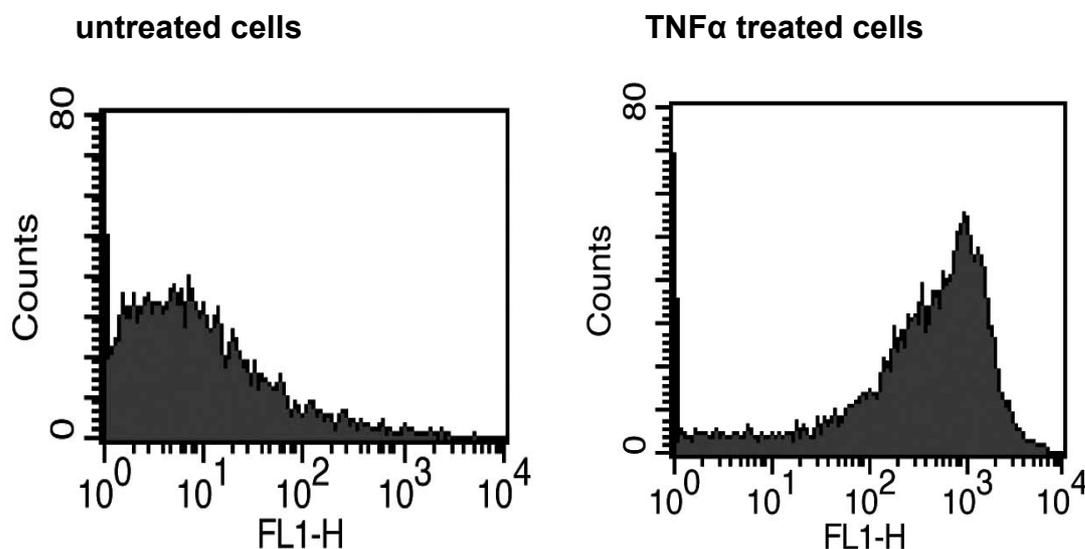
Figure 11: Median shift of fluorescence intensity (indicates ICAM-1 cell surface expression).

FACS buffer (pH 7.4)

NaCl	138.95	mM
K_2HPO_4	1.91	mM
NaH_2PO_4	16.55	mM
KCl	3.76	mM
LiCl	10.14	mM
NaN_3	3.08	mM
Na_2EDTA	0.97	mM
H_2O		

14 F-actin Quantification

HUVECs were cultured to long confluence in collagen G-coated 100 mm dishes, treated for the indicated times, and subsequently stained with rhodamine-phalloidin (Molecular Probes/Invitrogen, Karlsruhe, Germany) according to the protocol of chapter 12.1 . Cells were washed and the bound dye was extracted from the cells with methanol (30 min; 4°C). The fluorescence intensity (ex: 542 nm/em: 565 nm) of the methanolic dye solution was measured in a fluorescence plate reader (SpectraFluor Plus, Tecan Deutschland GmbH). The mean fluorescence intensity of untreated cells was set as 100%. The data are expressed as percent increase of fluorescence versus the control.

15 Measurement of Vascular Permeability in the Mouse Cremaster Muscle *in Vivo*

Male C57BL/6NCrl mice (Charles River Laboratories, Sulzfeld, Germany) weighting 23 to 25 g were used. All experiments were performed according to the German legislation for the protection of animal. Surgery and measurement of vascular permeability has been described previously. In brief, mice were anesthetized i.p. using a ketamine (Pfizer, Karlsruhe, Germany)/xylazine (Bayer, Leverkusen, Germany) mixture. Fluorescein isothiocyanate-dextran (150 kDa; Sigma-Aldrich), Ringer solution (control), and Crataegus special extract WS® 1442 (tanning agents-free, bolus sufficient to reach 100 µg/ml plasma concentration), was applied into the

left femoral artery. 30 min after WS$^{®}$ 1442 application, the cremaster was superfused with histamine (30 µM; Sigma-Aldrich) for 10 min. Postcapillary venules with diameters of 18 to 30 µm were analyzed. 10 regions of interest (50 x 50 µm^2) in the interstitial tissue (approximately 50 µm distance from the venule) were randomly selected. Intravital microscopy images were recorded with an IMAGO charge-coupled device camera (TILL Photonics, Gräfelfing, Germany) and subjected to digital image analysis (TILLvisION 4.0; TILL Photonics). These experiments were kindly performed by the working group of Prof. Dr. F. Krombach at the Walter-Brendel-Center for Experimental Medicine in Munich.

16 Statistical analysis

All experiments were performed at least three times unless otherwise indicated in the respective figure legend. Data are expressed as mean ± standard error of the mean. Statistical analysis was performed with SigmaStat software version 3.1 (Aspire Software International). Statistical tests are indicated in the figure legend. Statistical significance is assumed if p≤0.05.

III RESULTS

1   Anti-inflammatory potential of WS[®] 1442 on the endothelium

1.1 WS[®] 1442 reduces TNFα induced ICAM-1 surface expression

To clarify whether WS[®] 1442 has an anti-inflammatory potential on the endothelium, we measured the ability of WS[®] 1442 to reduce the cell surface expression of the intercellular adhesion molecule-1 (ICAM-1), an important marker of inflammation-activated endothelial cells, which can be induced by the pro-inflammatory cytokine TNFα. Pretreatment with WS[®] 1442 led to a 25 % reduction of TNFα-induced ICAM-1 expression, suggesting a protective effect of WS[®]1442 on the TNFα-induced activated endothelium (Figure 12).
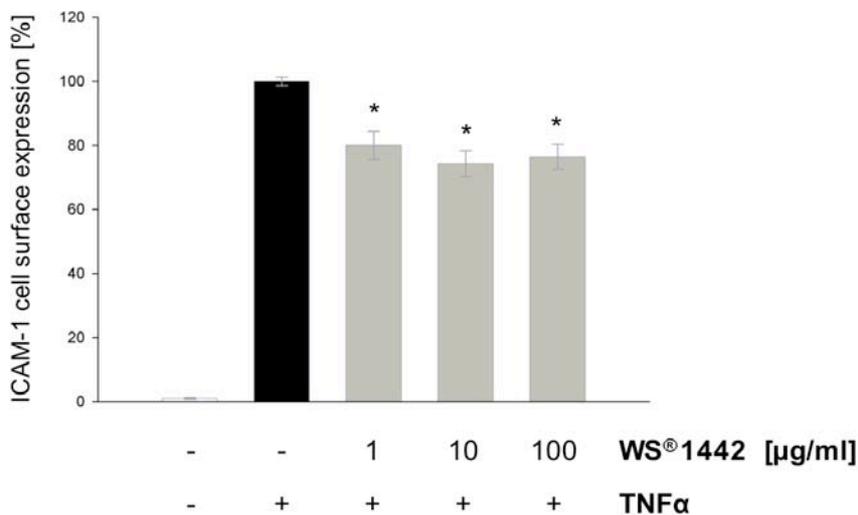
Figure 12: Effect of WS[®]1442 on the TNFα-induced ICAM-1 cell-surface expression. HUVECs were grown to confluence, pretreated with WS[®] 1442 (24 h; 10 µg/ml) in the indicated concentrations, followed by the treatment with TNFα (10 ng/ml; 24h). ICAM-1 cell surface expression was determined by FACS analysis as described in section II 13.

1.2 WS® 1442 does not affect NF-κB activity.

The transcription factor NF-κB plays a key role in the upregulation of ICAM-1 cell surface expression upon TNFα signaling. In our system, TNFα-activated NF-κB is not influenced by the Crataegus extract WS® 1442. Figure 13 shows that WS® 1442 neither alters the TNFα-induced increase of NF-κB DNA-binding activity (Figure 13A), nor the TNFα-induced p65 translocation to the nucleus (Figure 13B). This suggests that WS®1442 does not mediate its effect on the ICAM-1 expression *via* inhibition of NF-κB activity.
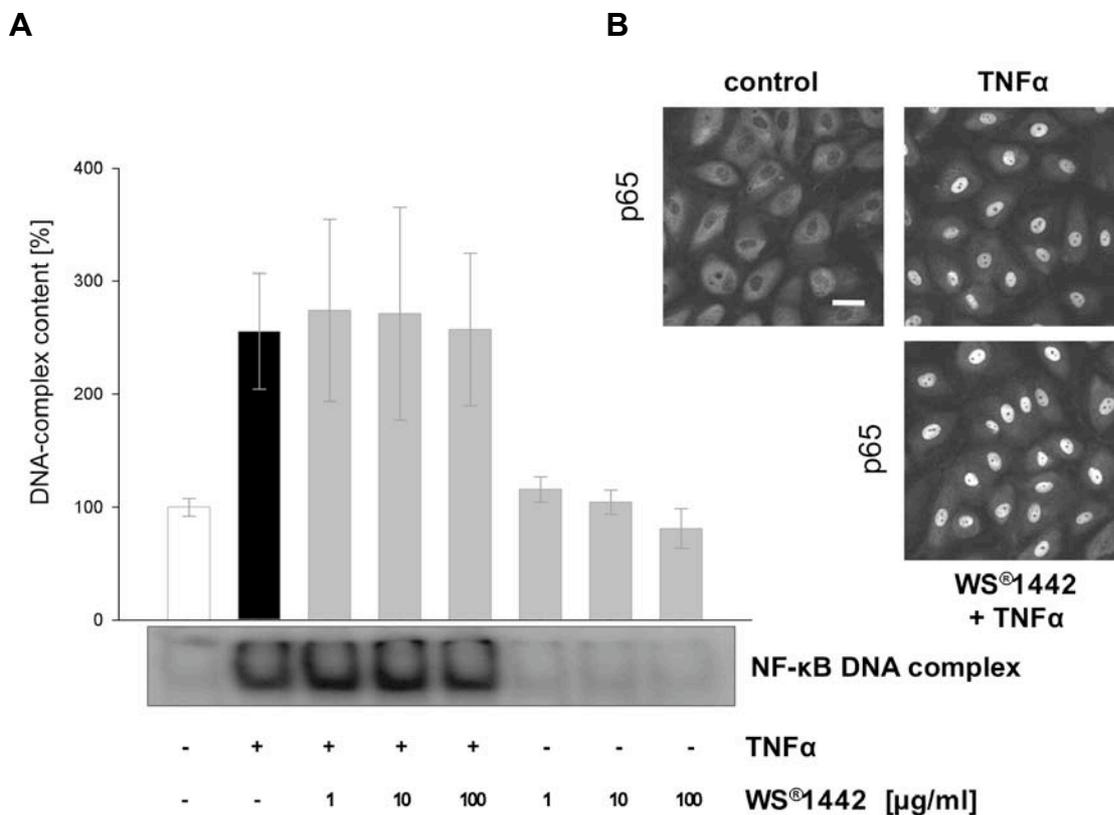
Figure 13: Influence of WS® 1442 on TNFα induced NF-κB-signaling activation. **A** HUVECs were either left untreated, treated with TNFα (10 ng/ml; 24 h), or with TNFα after preincubation with WS® 1442 (24 h) at indicated concentrations. NF-κB DNA-binding activity was analyzed by EMSA as described in section II 6. **B** HUVECs were left untreated (control), treated for 30 min with TNFα (10 ng/ml), or with TNFα after preincubation with WS® 1442 (100 μg/ml; 24 h) (n=2; white bar = 10 μm). Immunocytochemistry of p65 and confocal microscopy were performed as described in section II 12.1 .

1.3 WS$^{®}$ 1442 does not affect p38 MAPK activity.

Since we found that NF-κB is not influenced by WS$^{®}$ 1442, we analyzed the activity of the mitogen-activated protein kinase p38, which upregulates ICAM-1 cell-surface expression in response to cytokines as well.[11] Treatment with WS$^{®}$ 1442 for 24 h did not change the degree in phosphorylation and therefore the activity state of MAPK p38, caused by TNFα (10 min). Thus, WS$^{®}$ 1442 does not mediate the reduction of ICAM-1 cell surface expression *via* inhibition of p38 MAPK activity (Figure 14).
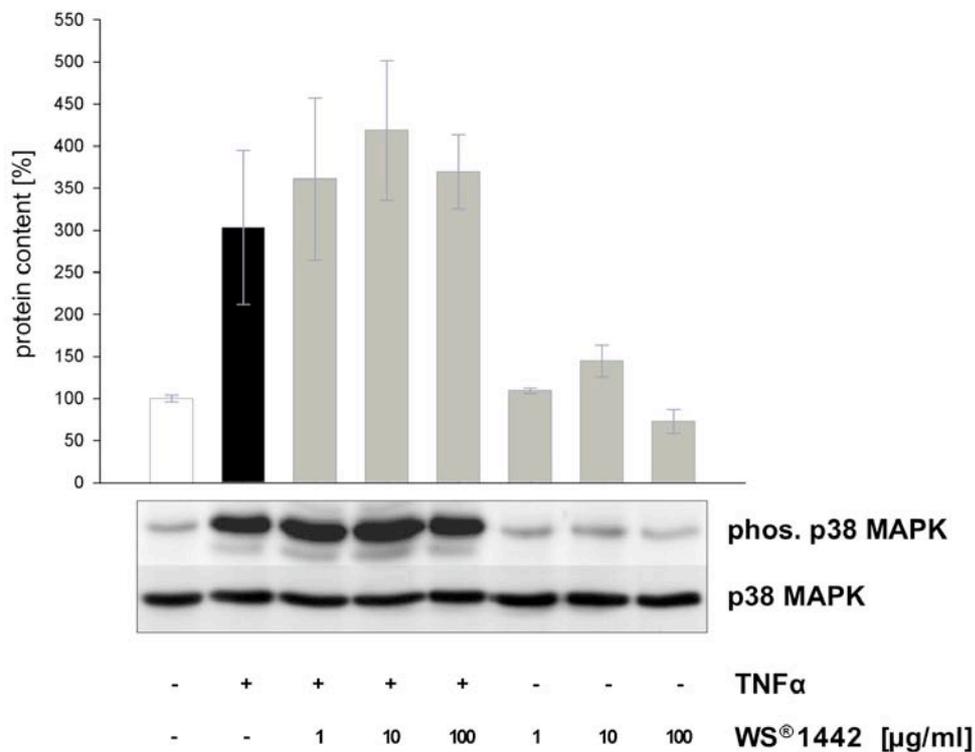
Figure 14: WS$^{®}$ 1442 does not influence TNFα induced p38 MAPK activity. HUVECs were left untreated, treated with TNFα (10 ng/ml; 10 min), or with TNFα after preincubation with WS$^{®}$ 1442 (24 h) at indicated concentrations. p38 MAPK phosphorylation was analyzed by Western blot analysis as described in section II 5.

1.4 WS®1442 does not affect AP-1 activity.

In analogy to NF-κB, we analyzed DNA-binding activity of the third major player in cytokine induced ICAM-1 upregulation, the transcription factor activator protein 1 (AP-1). Likewise, WS®1442 showed no significant reduction of the TNFα induced DNA binding activity of AP-1 (Figure 15). These data suggested that WS®1442 does not affect the TNFα-mediated AP-1 activity, and therefore, does not reduce ICAM-1 upregulation *via* targeting AP-1.
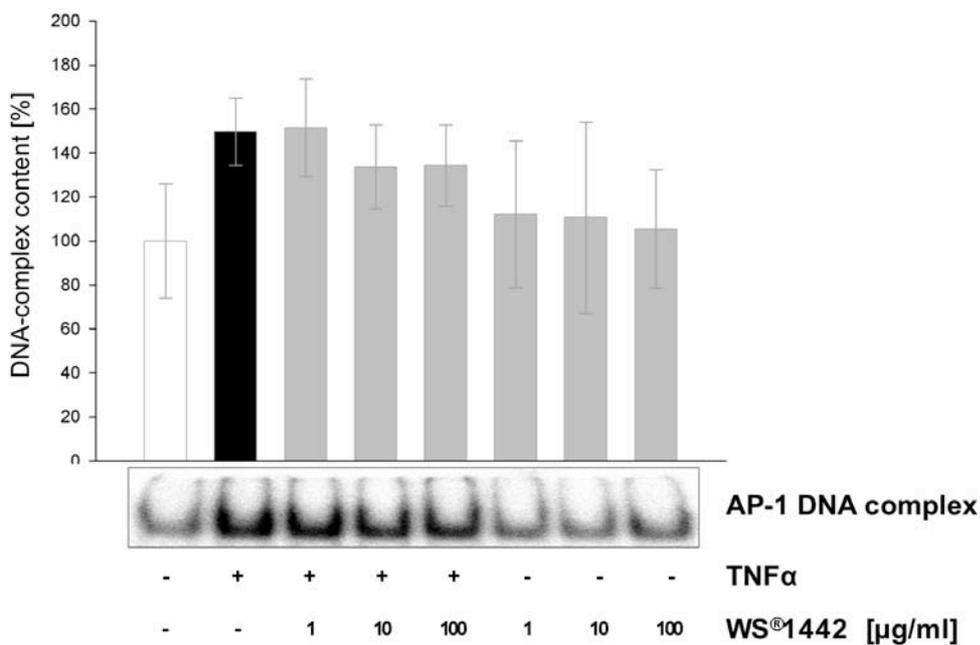
Figure 15: Influence of WS® 1442 on TNFα-induced AP-1 activity. HUVECs were left untreated, treated with TNFα (10 ng/ml; 24 h) or with TNFα after preincubation with WS® 1442 (24 h) in the indicated concentrations. AP-1 DNA-binding activity was analyzed by EMSA as described in section II 6.

2   Effects of WS®1442 on endothelial hyperpermeability

2.1 Inhibition of inflammation-induced endothelial hyperpermeability *in vitro*

Besides the upregulation of ICAM-1, hyperpermeability is a clear indicator of inflammatory activation of the endothelium. In order to test if WS®1442 has a protective potential, we treated HMECs with thrombin, a well-characterized and potent inducer of endothelial barrier disruption, after preincubation with WS® 1442. The macromolecular permeability-increase was analyzed *via* detection of the amount of FITC-labeled dextran diffusion through a HMEC monolayer. Figure 16A shows a clear concentration dependent decrease of macromolecular endothelial permeability. 1-100 µg/ml of WS® 1442 (30 min) significantly reduces macromolecular permeability. The time course (Figure 16B) points out that WS® 1442 (100 µg/ml) protects the endothelium during the whole 30 min of stimulation with thrombin. These findings demonstrate for the first time that WS® 1442 is a highly potent protective compound that affects the inflammation induced macromolecular permeability increase. For further experiments a concentration of 100 µg/ml was used.

A
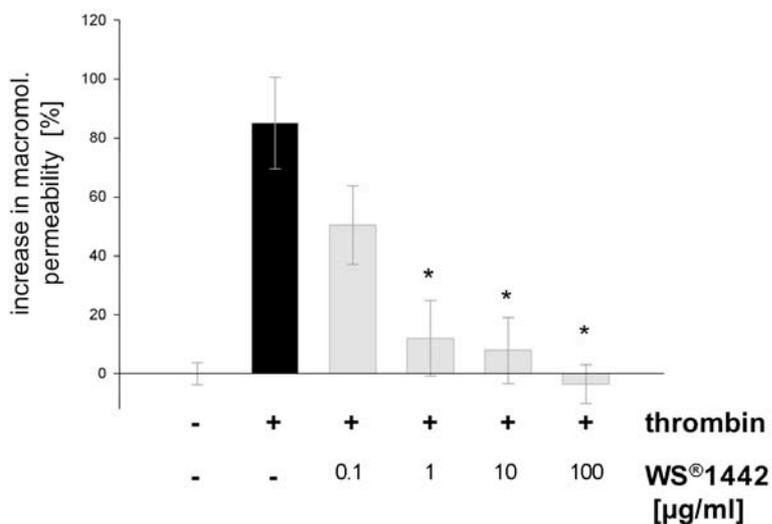
B
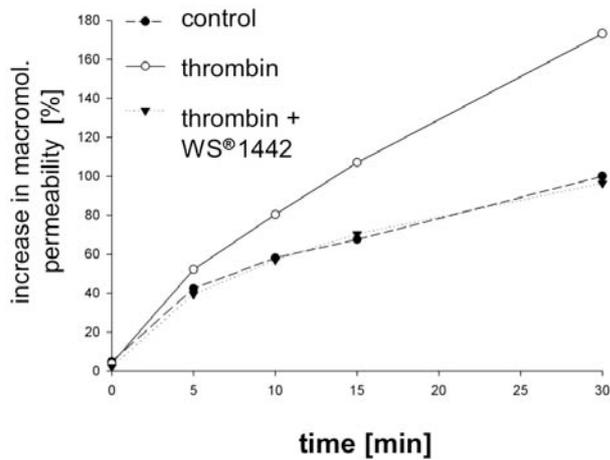
Figure 16: WS® 1442 blocks the increase in thrombin-induced hyperpermeability in a time and concentration dependent manner. **A** Concentration dependency: HMECs were left untreated, treated with thrombin (1 U/ml; 30 min), or with thrombin after preincubation with WS® 1442 (30 min) at indicated concentrations. **B** Time dependency: HMECs were left untreated, treated with thrombin (1 U/ml), or with thrombin after preincubation with WS® 1442 (100 µg/ml). Macromolecular permeability was measured as described in section II 9.

2.2 Inhibition of endothelial permeability *in vivo*

As an ultimate *in vivo* proof of the barrier protective properties of WS®1442, the measurement of macromolecular permeability at the mouse cremaster muscle model was used. Because of the prothrobotic activity of thrombin we used histamine for endothelium activation. Histamine was superfused on the cremaster muscle for 10 min, after pretreatment with WS® 1442 (30 min). The extravasation into the surrounding tissue after histamine treatment could be detected as a strong increase in fluorescence (Figure 17B). In comparison to treatment with histamine alone, WS®1442 significantly minimized macromolecule extravasation (Figure 17A). These *in vivo* data pointed out that WS®1442 clearly protects the endothelial barrier function against an inflammation-induced activation.

A

B
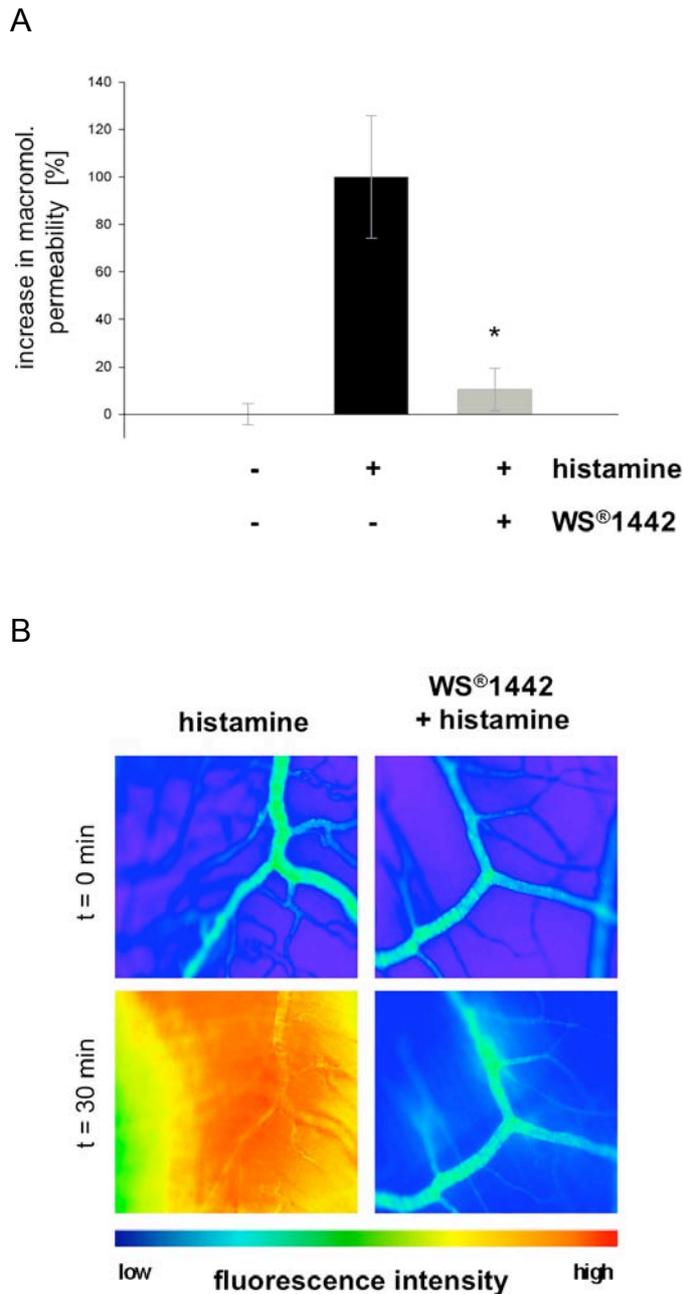
Figure 17: Effect of WS® 1442 on the inflammation-induced endothelial permeability *in vivo* measurement. **A**: 30 min after bolus treatment with WS® 1442 to reach 100 µg/ml plasma-concentration, histamine (50 µM) was superfused on the cremaster muscle for 10 min. We compared animals treated with histamine, with animals treated with histamine after pretreatment with WS® 1442. Fluorescence signal was measured right before histamine treatment (t=0) and 30 min later. **B**: Representative fluorescence images of the post-capillary venues. *In vivo* macromolecular permeability assay was performed as described in section II 15.

2.3 WS®1442 modulates key parameters of endothelial permeability

In order to figure out the underlying signaling mechanism of WS®1442 to protect endothelial barrier function, we focused on the key parameters of endothelial permeability. We had a look on the disruption of adhesion junctions, on cell-contraction and on the rearrangement of the actin cytoskeleton, which represent the three core events governing endothelial hyperpermeability, caused by inflammatory mediators like thrombin.

2.3.1 WS®1442 prevents the disruption of adhesion junctions

The inflammatory activation of the endothelium by thrombin (30 min) led to a disassembly of the adhesion junctions, with strong changes in morphology from a regular to a fringy and porous VEC seam, resulting in inter-endothelial gaps. This change is visualized in a histogram showing the fluorescence increase of VEC, giving the VEC protein levels along the white bar, which crosses two sites of cell-cell contacts (Figure 18). In this histogram, a properly formed cell-cell adhesion zone (untreated cells) is indicated as a single high and sharp peak. In contrast, a series of undefined 3 to 5 small peaks indicate the thrombin-activated unshaped and stretched VEC border. WS® 1442 itself does not affect the VEC border. Pretreatment with WS® 1442 completely abolished deleterious effects of thrombin, characterized by the sharp and high peak (Figure 18). Adhesion junctions show smooth and uninterrupted VEC borders, indicating that there are no tending forces between single cells. These images visualized that WS® 1442 pretreatment protect cells from thrombin induced morphological changes.
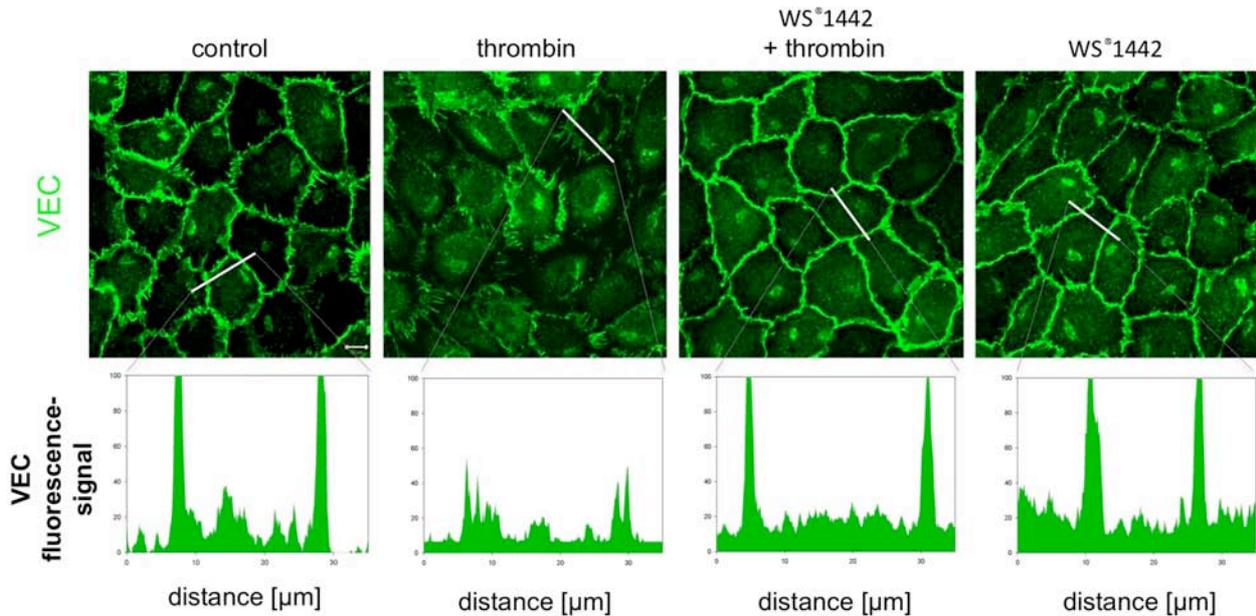
Figure 18: VEC seem protection by WS®1442 preincubation on thrombin activated endothelial cells. HUVECs were left untreated, treated with thrombin (1 U/ml; 30 min), or with thrombin after preincubation with WS®1442 (100 µg/ml; 30 min). Immunocytochemistry of VEC and confocal microscopy were performed as described in section II 12.1 Small white bar = 10 µm. One representative image out of 6 independently performed experiments is shown, each.

2.3.2 WS® 1442 prevents the translocation of adhesion junction proteins to the cytosol

According to the microscopic approach, the thrombin-induced endothelial barrier disruption was detected by a translocation of VEC from the cell membrane into the cytosol. WS® 1442 treatment totally blocked this translocation and therefore VEC internalization. Although the protein content of β-catenin and p120ctn in the cytosol did not increase after thrombin treatment, they were reduced after WS® 1442 treatment (Figure 19). These results show that the adhesion molecule VEC itself, and additionally its two major regulatory proteins as well, are protected by WS® 1442, underlining the above described morphological barrier protective effect of WS®1442.
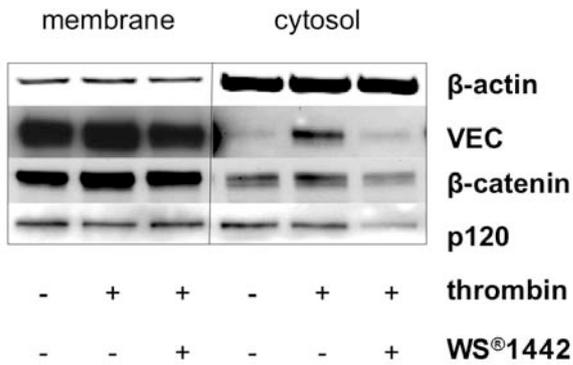
Figure 19: WS® 1442 affects thrombin-induces translocation of AJ complex proteins to the cytosol. HUVECs were left untreated, treated with thrombin (1 U/ml; 30 min), or with thrombin after preincubation with WS® 1442 (100 µg/ml; 30 min). Membrane fractionation and Western blot analysis was performed as described in section II 3.2 and II 5.

2.3.3 WS® 1442 prevents VEC tyrosine-phosphorylation

In the next step we intended to figure out if WS® 1442 affects the tyrosine-phosphorylation of VEC induced by thrombin leading to AJ complex dissociation. Especially the phosphorylation site Y 731 correlates with endothelial hyper-permeability.[18] Figure 20 displays a strong induction of tyrosine 731 phosphorylation by thrombin, which was abolished by the treatment with WS® 1442. Our data show that WS® 1442 inhibits VEC activation.
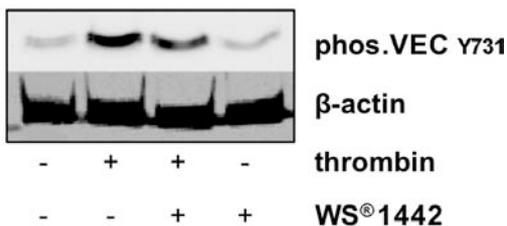
Figure 20: WS® 1442 inhibits the thrombin-induced VEC[Y731] phosphorylation. HUVECs were grown to confluence, were left untreated, treated with thrombin (1 U/ml; 30 min), or with thrombin after preincubation with WS® 1442 (100 µg/ml; 30 min). Protein sample preparation and Western blot analysis were performed as described in section II 3.1 and II 5.

2.3.4 WS® 1442 modulates the actin cytoskeleton

The second key parameter of inflammation-induced endothelial activation, leading to hyperpermability is the rearrangement of the actin cytoskeleton into stress fibers. Treating HUVEC with thrombin induced the formation of stress fibers. Pretreatment with WS® 1442 showed a complete inhibition of the cell spanning stress fiber formation. Interestingly WS® 1442 induced the formation of cortical actin, which is known to correlate with reduced endothelial permeability (Figure 21A). In order to measure the actin polymerization necessary for stress fiber formation, we biochemically quantified the formation of F-actin (Figure 21B). The induction of F-actin polymerization was significantly reduced by WS® 1442. As Figure 21 shows, WS® 1442 not only inhibits the formation of permeability-inducing stress fibers, but also evokes barrier-stabilizing cortical actin in the endothelium. Both effects are mediated by different signaling pathways, we therefore hypothesized that WS® 1442 has not just an anti-inflammatory action, but also activates barrier protective signaling pathways *per se*.

A
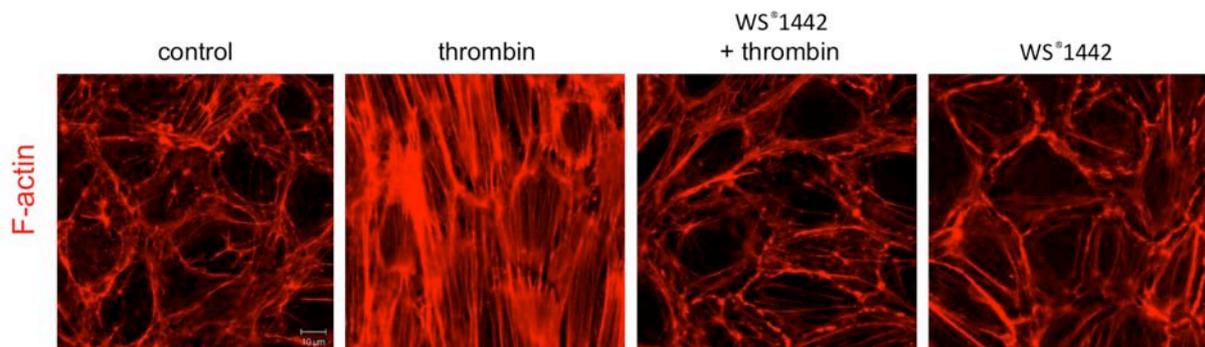
B
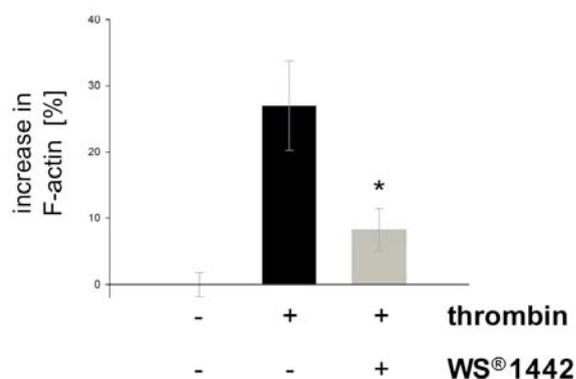
Figure 21: Modulation of the actin cytoskeleton by WS® 1442. **A** HUVECs were grown to confluence, were left untreated, treated with thrombin (1 U/ml; 30 min), or with thrombin after preincubation with WS® 1442 (100 µg/ml; 30 min). F-actin staining and confocal microscopy were performed as described in section II 12.1 White bar = 10 µm (control). One representative image out of 6 independently performed experiments is shown, each. **B** F-actin quantification. HUVECs were grown to confluence, were left untreated, treated with thrombin (1 U/ml; 30 min), or with thrombin after preincubation with WS® 1442 (100 µg/ml; 30 min). F-actin staining and quantification were performed as described in section II 14.

2.3.5 Live cell imaging of actin showed the formation of cortical actin by WS® 1442

To observe the cortical actin formation by WS® 1442 and to get an idea of the time flow of this process we performed actin live cell imaging microscopy (Figure 22). After 2 min of treatment with WS® 1442 the increase of actin at the cell membrane gets obvious. Actin polymerizes directly at the cell membrane, there is no transport of polymerized actin to the cell membrane. Finally, after 10 min the maximum in cortical actin formation has been reached.

GFP-actin
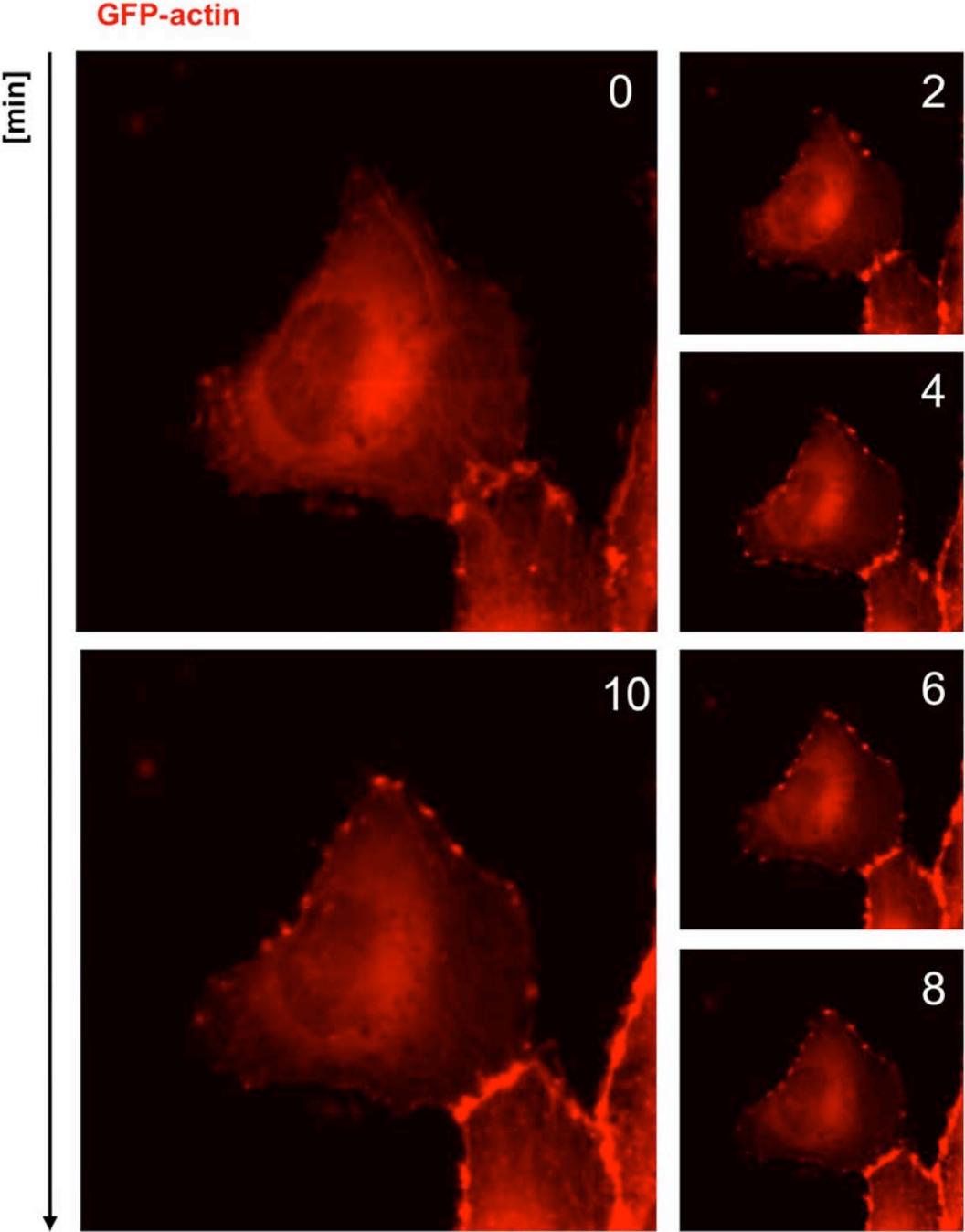
Figure 22: Live cell imaging of cortical actin induction by WS$^®$ 1442. WS$^®$ 1442 (100 µg/ml) was applied for 10 min. Cell transfection and life cell imaging was done according to section II 7 and II 12.2

2.3.6 WS® 1442 prevents the activation of cell contraction

Furthermore, we examined the influence of WS® 1442 on inflammation-induced endothelial cell contraction, the third key parameter of endothelial permeability. In the interplay between AJ disruption and actin rearrangement, cell contraction leads to inter-endothelial gap formation. Figure 23A shows the strong thrombin effect on the phosphorylation of myosin light chain 2 (MLC2), colocalized at the stress fibers, indicating the activation of cell contraction. In the microscopic approach as well as in the biochemical Western blot analysis, the extract clearly minimized the phosphorylation of MLC2 (Figure 23A/B). In consequence, these data suggest that WS® 1442 inhibits inflammation-induced cell contraction.

A
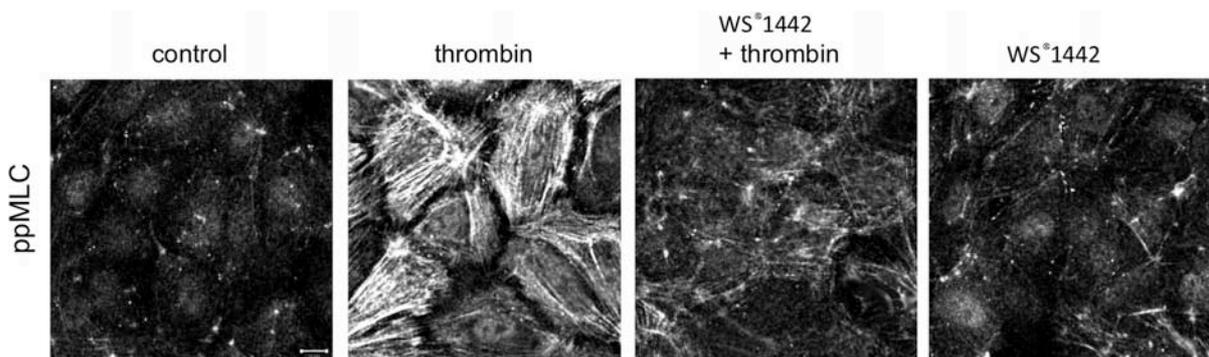
B
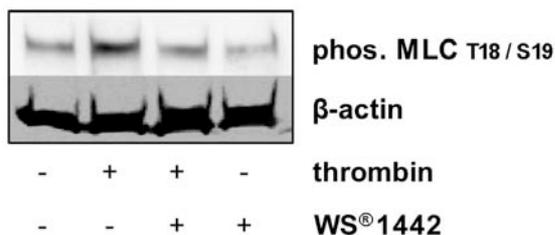
Figure 23: WS® 1442 inhibits thrombin induced MLC2 phosphorylation. HUVECs were grown to confluence, were left untreated, treated with thrombin (1 U/ml; 30 min), or with thrombin after preincubation with WS® 1442 (100 µg/ml; 30 min). **A** Immunocytochemistry of ppMLC and confocal microscopy were performed as described in section II 12.1 . White bar = 10 µm. One representative image out of 3 independently performed experiments is shown, each. **B** Protein sample preparation and Western blot analysis was performed as described in section II 3.1 and II 5. One representative image out of 3 independently performed experiments is shown, each.

2.4 NO does not affect the protective effect of WS® 1442 on the endothelial barrier function

2.4.1 The inhibition on the EHP by WS® 1442 is independent from NO

To analyze whether WS® 1442 affects endothelial barrier function by regulating NO-signaling we tested the effect of WS® 1442 and L-NAME (a NO synthase inhibitor) on the macromolecular permeability *in vitro*. L-NAME did not influence the barrier-protective effect of WS® 1442 (Figure 24), indicating that WS® 1442 works NO independently. This experiment was kindly performed by Elisabeth Willer.
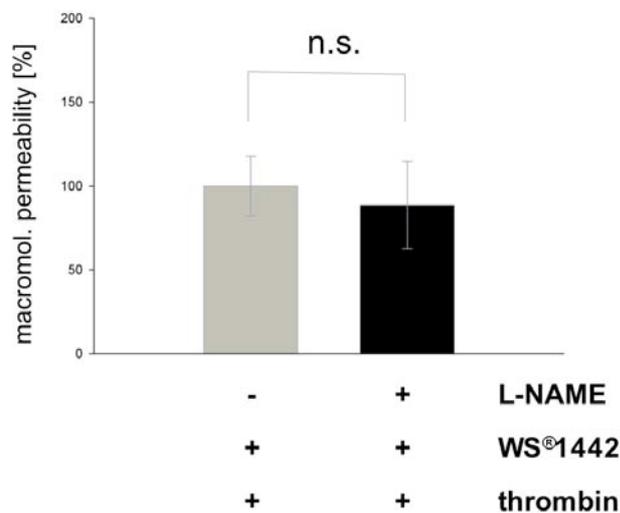

Figure 24: WS® 1442-induced macromolecular permeability decrease is NO independent. HMECs were treated with thrombin after preincubation with WS®1442 (100 µg/ml; 30 min) and additionally combined with or without 60 min preincubation of the NO synthase inhibitor L-NAME (100 µM). The *in vitro* macromolecular permeability assay was performed as described in section II 9.

2.4.2 WS® 1442 affects the key parameters of endothelial permeability NO independent.

After we could show that eNOS-inhibition did not alter the effects of WS®1442 on macromolecular permeability, we wanted to clarify if the key parameters of endothelial permeability also unaltered in the presence of L-NAME. Inhibition of the NO-synthase did not alter the influence of WS® 1442 on stress-fiber formation as well

as the stabilization of AJ. Hence, WS®1442 affects AJ and the actin cytoskeleton NO-independently.
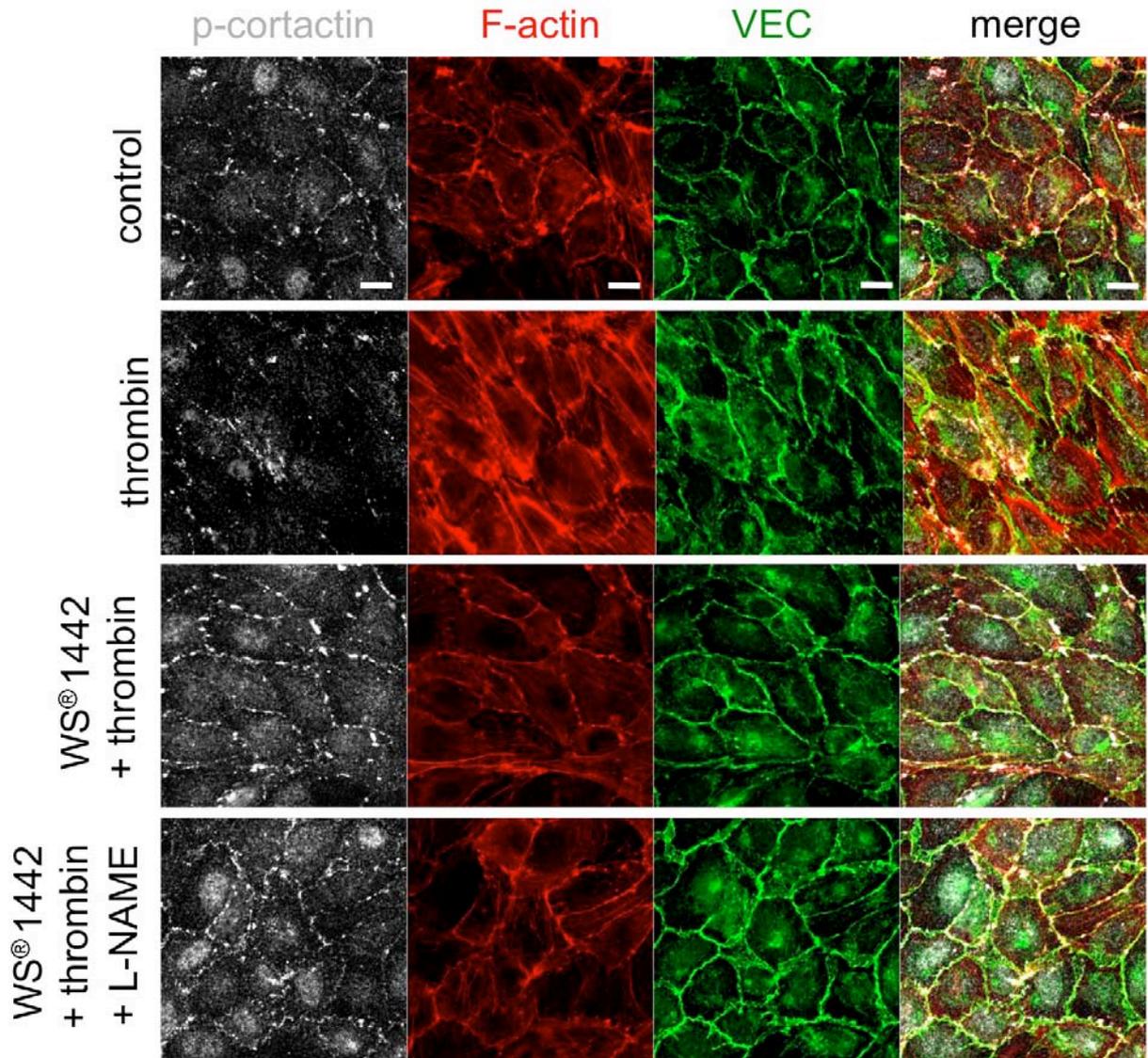
Figure 25: AJ and f-actin modulation by WS® 1442 is NO independent. HUVECs were grown to confluence, were left untreated, treated with thrombin (1 U/ml; 30 min), or with thrombin after preincubation with WS® 1442 (100 µg/ml; 30 min), combined with or without 60 min preincubation of the NO synthase inhibitor L-NAME (100 µM). F-actin staining and confocal microscopy were performed as described in section II 12.1 White bar = 10 µm (control). One representative image out of 3 independently performed experiments is shown, each.

Figure 25 continued
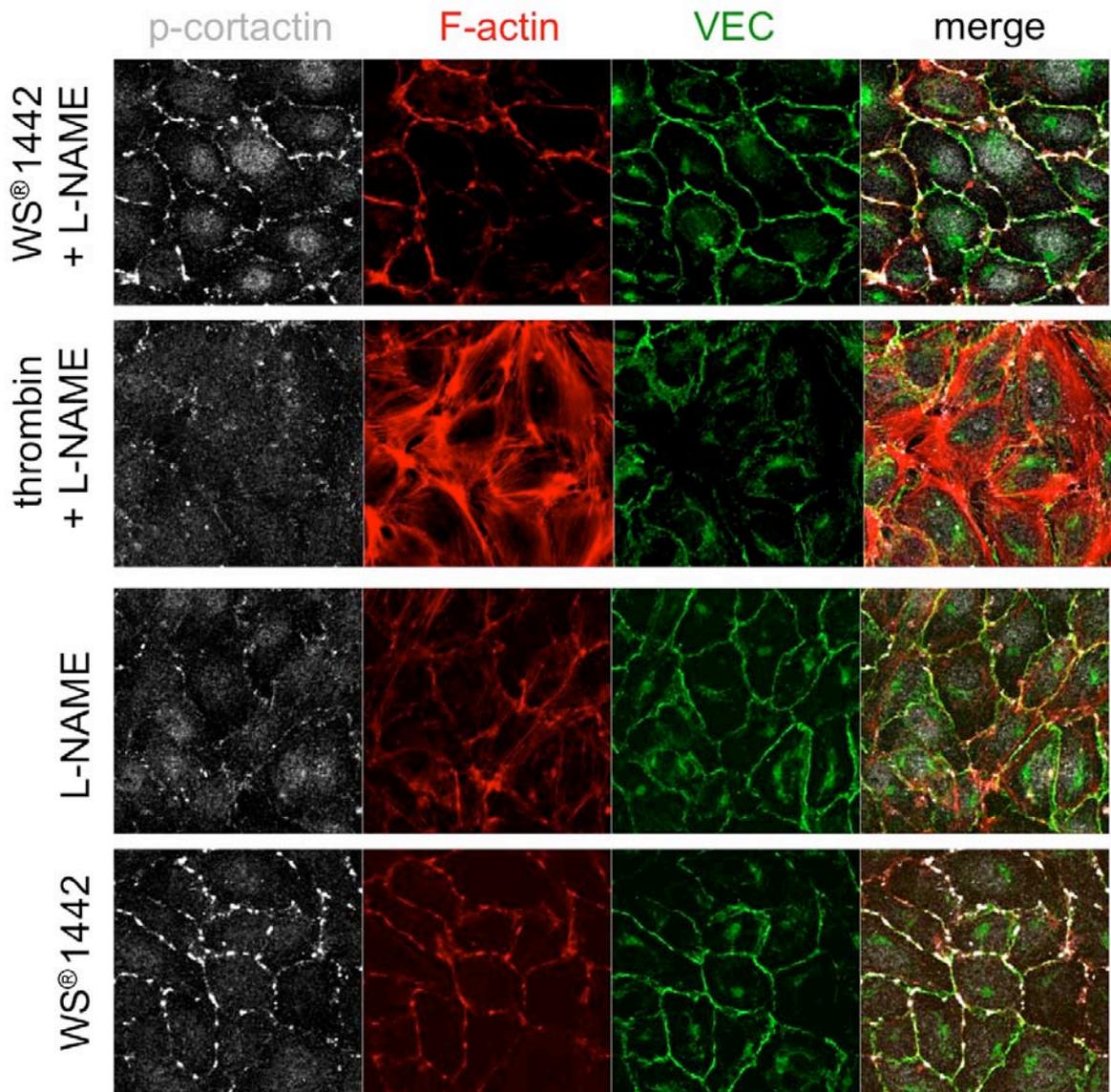
2.5 WS® 1442 inhibits the inflammatory Ca²⁺-signaling

Since we found that WS® 1442 blocks EHP in functional permeability assays and affects key parameters of endothelial permeability, we wanted to investigate which part of the upstream thrombin signaling is affected. Ca^{2+} is important for relaying signals of different EHP-inducing agents in the endothelium, leading to EC rounding and therefore to inter-endothelial gap formation, which is inevitably correlated to changes in endothelial permeability. We aimed to figure out if WS® 1442 affects the inflammatory Ca^{2+}-signaling at the endothelium.

2.5.1 WS®1442 inhibits the long lasting Ca^{2+}-signal of thrombin

The $[Ca^{2+}]_i$-increase was induced by thrombin treatment. The thrombin-dependent raise of $[Ca^{2+}]_i$ is very fast and strong at the beginning, but declines after 2 to 3 min to reach a plateau phase of low magnitude, that lasts for a minimum of 15 min. Preincubation with WS® 1442 blocked this long-lasting Ca^{2+} signal, which is crucial for the activation of many Ca^{2+} downstream targets (Figure 26A).[16] The fast $[Ca^{2+}]_i$ response directly following thrombin administration is not affected. Comparing the areas under the curve (AUCs) of these $[Ca^{2+}]_i$ measurements, WS® 1442 significantly lowers the total $[Ca2+]_i$-increase down to the basal level (Figure 26B).

A
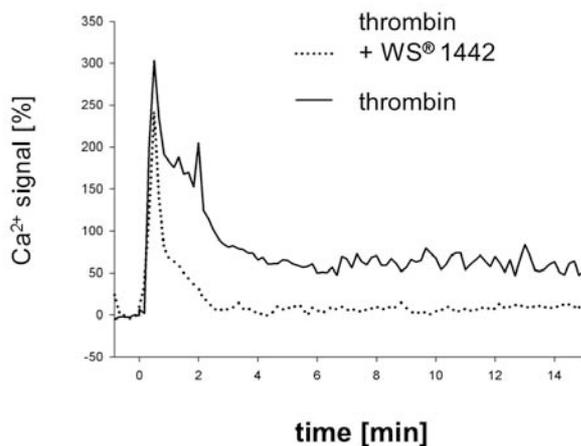
B
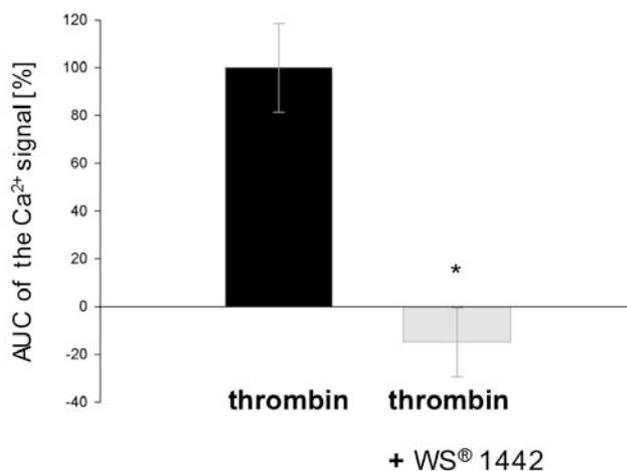
Figure 26: WS® 1442 inhibits the sustained Ca^{2+} signaling of thrombin-induced endothelial cells. HUVECs were grown to confluence, were left untreated, treated with thrombin (1 U/ml; 30 min) after preincubation with WS® 1442 (100 µg/ml; 30 min). $[Ca^{2+}]_i$ was detected by

fluorescence microscopy using Fura-2, as described in section II 10. **A** Time course of the Ca^{2+} measurement (15 min), thrombin *vs.* WS®1442 + thrombin. **B** AUC diagram of the Ca^{2+} measurement (15 min), thrombin *vs.* WS®1442 + thrombin.

2.5.2 WS® 1442 inhibits thrombin-induced extracellular Ca^{2+} influx

The $[Ca^{2+}]_i$ increase induced by thrombin is composed of two different phases: The first increase by the release of intracellularly stored Ca^{2+} and the second phase, the long lasting $[Ca^{2+}]_i$-increase, by extracellular influx of Ca^{2+}. To clarify if WS® 1442 inhibits the extracellular Ca^{2+}-influx, as discriebed by the previous findings, we repeated the experiment (2.5.1), but treated the cells with WS® 1442 not until the long lasting Ca^{2+}-plateau has been reached (after 4 min of thrombin treatment). WS® 1442 suddenly blocks the extracellular Ca^{2+}-influx down on control level (Figure 27A).

To clarify if WS®1442 selectively inhibits the extracellular Ca^{2+} influx, we performed the assay in a Ca^{2+}-free HEPES-buffer, treated the cells with thrombin (see section 2.5.1), and added (t = 4 min) 2 mM Ca^{2+} to the cells. Until Ca^{2+} treatment, the cells showed no Ca^{2+} plateau, and behave like WS®1442 pretreated cells, similar to 2.5.1 (Figure 27). This fact indicates that WS® 1442 modulates the Ca^{2+} signal of thrombin by inhibition of the extracellular Ca^{2+} influx. After Ca^{2+} treatment, the cells without WS®1442 form a normal Ca^{2+} plateau, in contrast to WS®1442 treated cells, which Ca^{2+} signal again decreases after 4 min. These data further support the hypotheses, that WS®1442 selectively inhibits the extracellular Ca^{2+} influx.

A
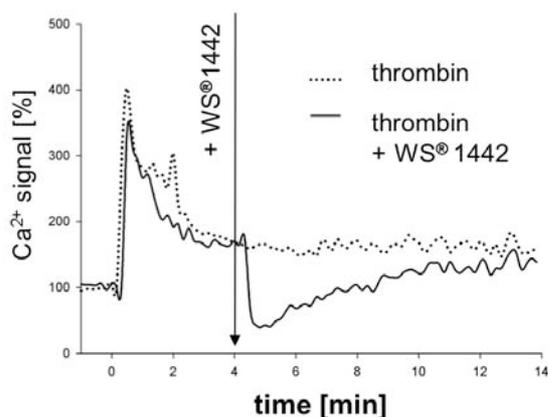
B
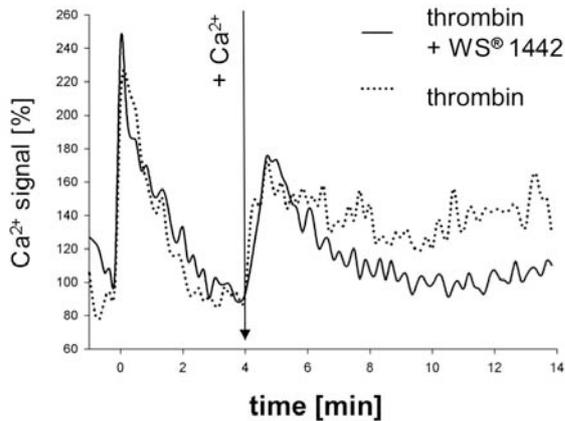
Figure 27: Measurement of the thrombin-induced inhibition of Ca^{2+}- nflux by WS[®] 1442. **A** Time course of HUVECs grown to long confluence treated with thrombin (t= 0 min; 1 U/ml; 14 min) after treatment with WS[®] 1442 (t=4min; 100 µg/ml). **B** Time course of HUVECs grown to long confluence treated with thrombin (t=0min; 1 U/ml; 14 min) after preincubation with WS[®] 1442 (30 min; 100 µg/ml) in Ca^{2+} free HEPES-buffer. At t = 4 min 2 mM Ca^{2+} was added to the cells. In both experiments, $[Ca^{2+}]_i$ was detected by fluorescence microscopy using Fura-2 as described in section II 10 (n=2).

2.5.3 WS[®]1442 does not lead to Ca^{2+} store depletion

To exclude that preincubation with WS[®]1442 does lead to Ca^{2+} store depletion, we compared the effect of WS[®]1442 treatment with that of thapsigargin, an inhibitor of the sarco/endoplasmatic reticulum Ca^{2+} ATPase, which is and known to induce Ca^{2+} store depletion and in consequence a reduction of EHP.[16] Thapsigargin raised intracellular Ca^{2+} first in an initial peak, but later on continuously, which indicates a Ca^{2+} store depletion. In contrast, WS[®] 1442 treatment reduced $[Ca^{2+}]_i$ at the beginning, but after 4 min the cells showed no difference in $[Ca^{2+}]_i$ increase to untreated cells (Figure 28). These findings pointed out that, WS[®]1442 does not lead to Ca^{2+} store depletion in endothelial cells.
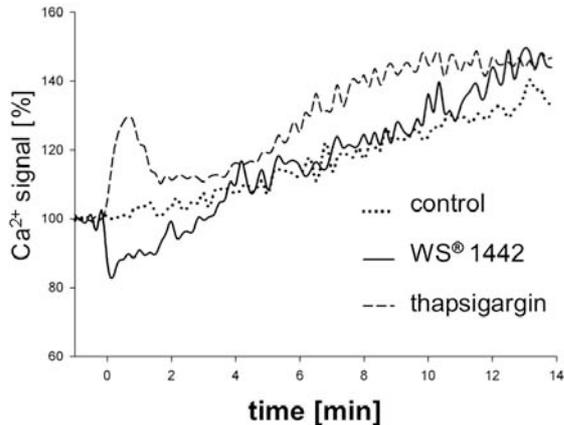
Figure 28: Time course of the measurement of $[Ca^{2+}]_i$ after treatment with WS[®] 1442 compared to thapsigargin. HUVECs were grown to long confluence, left untreated, treated with WS[®] 1442 (t = 0min; 100 µg/ml) or with thrombin after preincubation with WS[®] 1442 (100 µg/ml; 30 min). $[Ca^{2+}]_i$ was detected by fluorescence microscopy using Fura-2 as described in section II 10 (n=2).

2.5.4 WS[®]1442 inhibits the activation of PKC

We next investigated whether the inhibition of the sustained Ca^{2+} signal by WS[®] 1442 modifies the downstream effectors of Ca^{2+} signaling. Protein kinase C (PKC) has been shown to mediate the induction of stress fiber formation and cell contraction.[19] For analyzing the activity of PKC we looked at the phosphorylation site at PKC (T514) itself and at the phosphorylation of the PKC ((R/K)X(S*)(R/K)) substrate motive, both correlating with conventional PKC activity. As expected, thrombin activated PKC itself and induced the phosphorylation of its downstream targets. WS[®]1442 pretreated cells showed no raise in phosphorylation of PKC or PKC substrates (Figure 29). According to these findings, we assume that WS[®] 1442 affection of the sustained Ca^{2+} signal, inhibits the Ca^{2+} downstream target PKC.[19] But a direct inhibition of PKC could not be excluded.
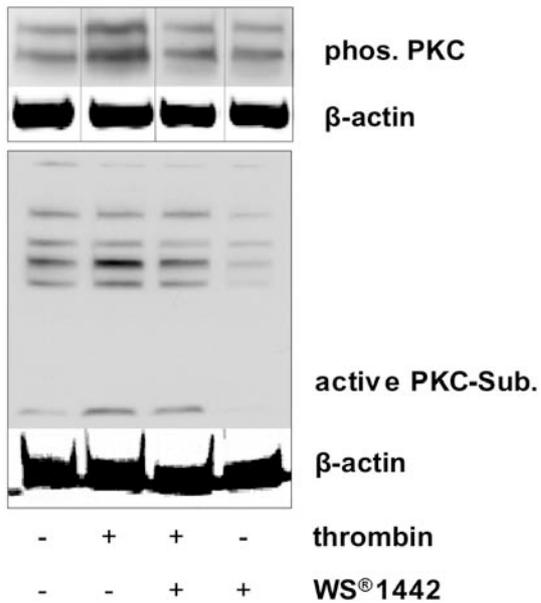
Figure 29: WB analysis of the inhibition of conventional PKC by WS® 1442 in inflammatory conditions.
HUVECs were grown to confluence, were left untreated, treated with thrombin (1 U/ml; 30
min), or with thrombin after preincubation with WS® 1442 (100 µg/ml; 30 min). Protein
sample preparation and Western blot analysis was performed as described in section II 3.1
and II 5.

2.5.5 WS® 1442 inhibits thrombin-induced RhoA activation

In analogy to the experiments regarding the inhibition of PKC activity, we checked
whether WS® 1442 treatment also effects a major regulator of stress fiber formation,
the small GTPase RhoA. Thrombin is known to activate RhoA in the endothelium,
which induces the formation of stress fiber.[4] WS® 1442 totally blocks thrombin-
induced Rho activation (Figure 30).
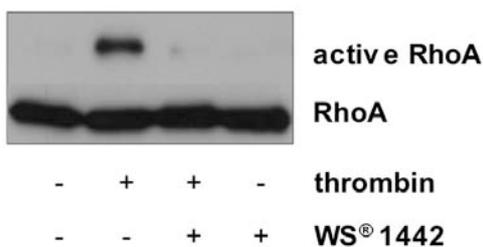
Figure 30: The inhibition of inflammation-induced RhoA activity. HUVECs were grown to confluence,
were left untreated, treated with thrombin (1 U/ml; 30 min), or with thrombin after

preincubation with WS® 1442 (100 µg/ml; 30 min). RhoA GTPase activation assay and Western blot analysis was performed as described in sections II 8, and II 5.

2.6 Activation of the barrier protective cAMP signaling by WS® 1442

Restoring the endothelial barrier function by controlling the inflammatory Ca^{2+}-signaling is an obvious and promising approach. In addition to the inhibition of the inflammatory barrier disruption, the activation of a *per se* barrier-stabilizing pathway also represents a promising approach. cAMP signaling is known as a strong stabilizer of the endothelial barrier (see section I 3). The first evidence that cAMP signaling might participate in the endothelial barrier stabilization by WS® 1442, could be noticed by the cortical actin formation (seen in IV 2.3.4), which is known to be cAMP-dependent. Therefore we hypothesized that WS® 1442 activates the barrier stabilizing cAMP signaling pathways.

2.6.1 WS® 1442 increases endothelial cAMP

We aimed to clarify if WS® 1442 increases cellular cAMP levels in cultured endothelial cells. The cAMP levels were measured by an enzyme-linked immunosorbant assay. Figure 31 shows that WS® 1442 concentration dependently increases the leves of cellular cAMP. WS® 1442 significantly raises cAMP in endothelial cells at 10 and 100 µg/ml. For further analysis of Crataegus influenced cAMP-dependent signaling-pathways we used 100 µg/ml extract.
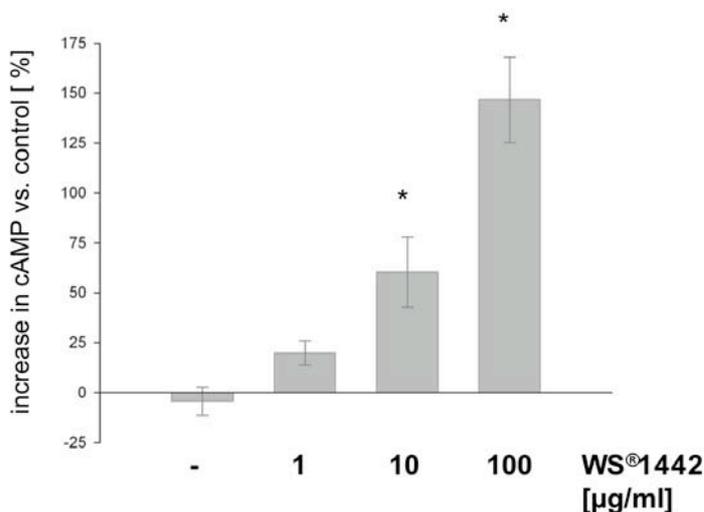
Figure 31: WS[®] 1442 increases cAMP levels concentration dependently in endothelial cells. HUVEC were grown to long confluence, either left untreated or treated for 15 min with the indicated WS[®] 1442 concentrations. cAMP levels were measured by ELISA according to section II 11. *, p ≤ 0.001 versus control (= 100%) (n=4).

2.6.2 Cause of WS[®] 1442-induced [cAMP]$_i$ increase

To clarify whether the cAMP increase is due to an activation of the adenylate cyclase (AC), or due to an inhibition of cAMP degradation *via* phosphodiesterases (PDE), we treated HUVECs with WS[®]1442 together with forskolin (AC activator) or IBMX (PDE inhibitor) (Figure 32). Additional cAMP increase could only be reached by a combination of forskolin together with WS[®]1442. Because forskolin induces maximal AC activity, Crataegus could only led to a further raise of forskolin-induced cAMP levels by inhibition of cAMP degradation. According to that finding, IBMX does not alter the WS[®]1442-induced cAMP increase at all, suggesting that WS[®]1442 leads to an inhibition of PDE.
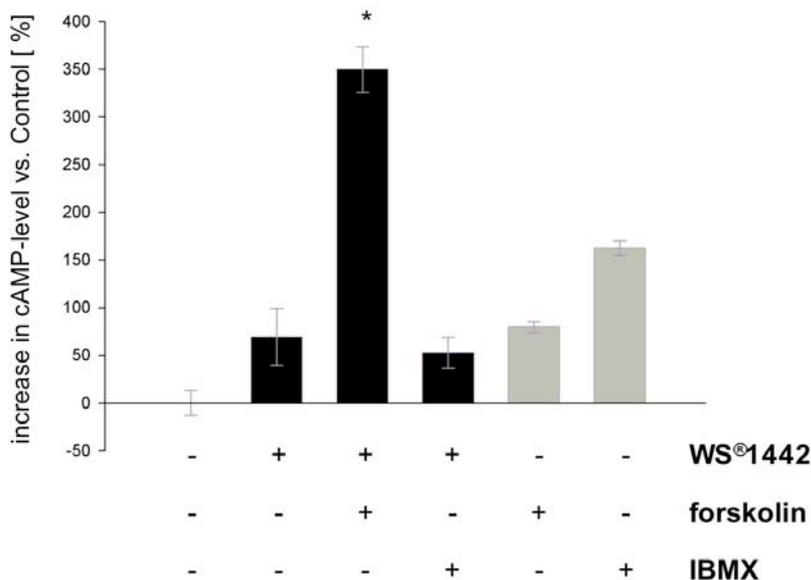

Figure 32: Crataegus inhibits cAMP degradation. HUVECs were grown to long confluence, either left untreated or treated with WS[®]1442 (100 µg/ml; 15min) or cotreated with forskolin (10 µM) or IBMX (500 µM) as indicated. cAMP levels were measured by ELISA according to section II 11. cAMP levels of control cells were set as 100% (n=2).

2.6.3 Induction of PKA activity by WS® 1442

We investigated whether the cAMP-dependent protein kinase A (PKA) pathway, of which the activity correlates with an inhibition of EP, is involved in mediating the WS® 1442 evoked barrier protection. We monitored PKA activation *via* determination of the phosphorylation of PKA substrates. Forskolin was used as a positive control. WS® 1442 raises PKA-substrate phosphorylation, but to a lower content than forskolin (Figure 33A). However, the WS® 1442-induced increase in phosphorylation is localized at the cell membrane and is comparable to that of the cAMP analogue 8-Br-cAMP (Figure 33B). These data suggest that WS® 1442 increases PKA activity at the cell membrane.

A
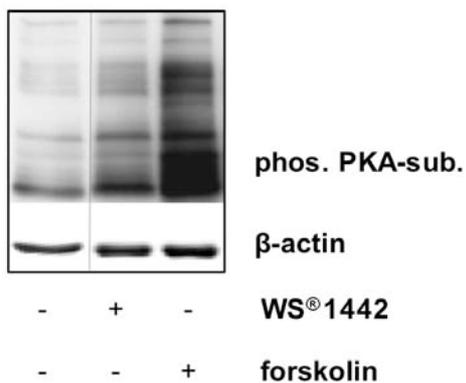
B
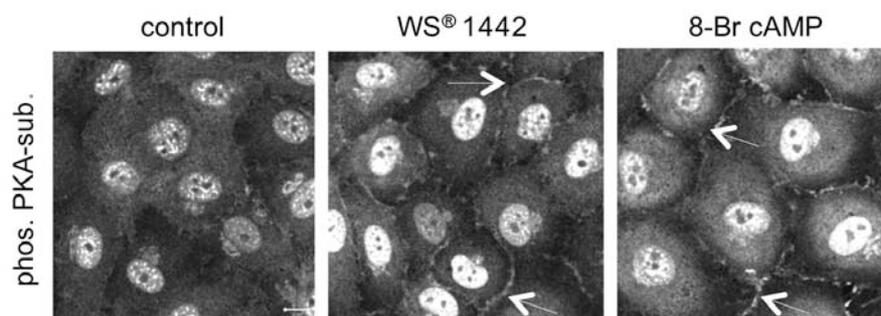
Figure 33: WS® 1442 induces PKA activity at the cell membrane. HUVECs were grown to long confluence, either left untreated or were treated with WS®1442 (30 min, 100 µg/ml) or forskolin (30 min, 1 µm), or 8-Br-cAMP (30 min, 100 µM). **A** Protein sample preparation and Western blot analysis was performed as described in section II 3.1 and II 5. **B** Immunocytochemistry of phos. PKA-substrates and confocal microscopy were performed as described in section II 12.1 . White bar = 10 µm (control). One representative image out of 3 independently performed experiments is shown, each.

2.6.4 VASP activity-induction by WS®1442

Since we found that PKA is activated by WS® 1442, we investigated downstream of PKA, if the cytoskeletal adaptor protein VASP is activated as well. Active VASP is phosphorylated at Ser[157]. WS® 1442 induced VASP phosphorylation and therefore led to activation of VASP (Figure 34A). In addition, the increase of phosphorylated VASP could be detected exclusively at the cell membrane (Figure 34B). In contrast to that, the positive control forskolin strongly induces VASP phosphorylation mainly in the cytosol. These data suggest that WS® 1442 activates VASP at the cell membrane.

A

phos. VASP^{S157}

β-actin

| - | - | + | WS®1442 |
| - | + | - | forskolin |

B

control   WS®1442   forskolin

phos. VASP^{S157}
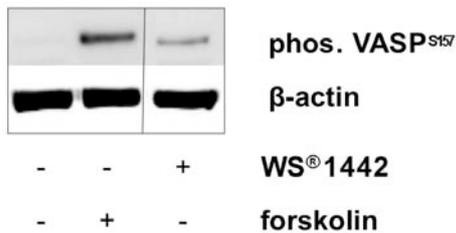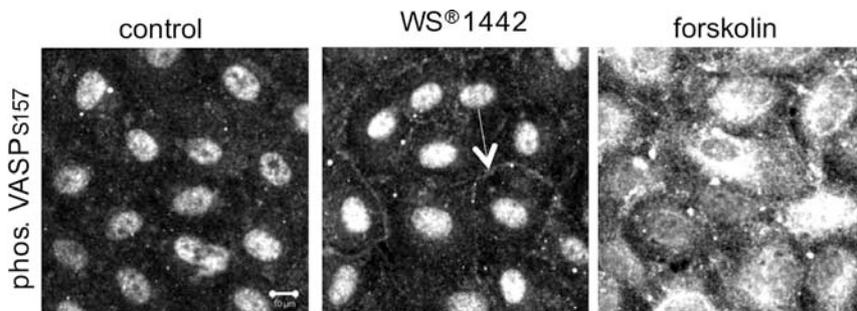
Figure 34: The induction of VASP activation by WS® 1442 at the cell membrane. HUVEC were grown to long confluence, either left untreated or were treated with WS® 1442 (30 min, 100 µg/ml) or forskolin (30 min, 1 µm). **A** Protein sample preparation and Western blot analysis was performed as described in section II 3.1 and II 5. **B** Immunocytochemistry of pVASP and confocal microscopy were performed as described in section II 12.1 . White bar = 10 µm (control). One representative image out of 3 independently performed experiments is shown, each.

2.6.5 The induction of barrier protection by WS®1442 is PKA independent.

Next, we wanted to clarify if PKA is involved in the WS® 1442-evoked barrier protection. Therefore, we modified the macromolecular permeability assay and preincubated the cells with the PKA inhibitor cAMPS-Rp. In this new setting WS® 1442 still clearly reduced the permeability increase (Figure 35A). Cells treated with WS® 1442 showed no significant difference to PKA-inhibited cells. In Figure 35B demonstrates that PKA activity was completely inhibited by cAMPS-Rp. This results point out that WS® 1442-induced barrier protection is PKA independent.

A
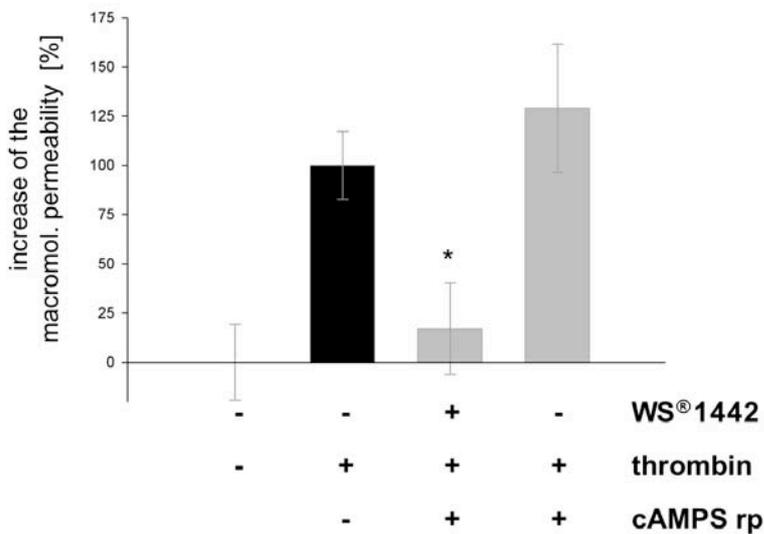
B
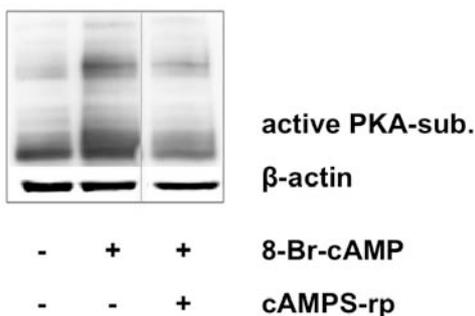
Figure 35: The inhibition of the endothelial hyperpermeability by WS® 1442 is PKA independent. **A** HMECs were left untreated, treated with thrombin (1 U/ml) or with thrombin after preincubation with WS®1442 (100 µg/ml; 30 min). Cells were additionally pretrated with the PKA inhibitor cAMPS-Rp (100 µM; 60 min). The permeability increase of WS® 1442 *vs*. thrombin was set as 100%. Macromolecular permeability assay was performed as described in section II 9. **B** HUVEC were grown to long confluence, left untreated, treated with 8-Br-

cAMP (30 min, 100 µM) or in combination with 30 min preincubation with cAMPS-Rp (100 µM). Protein sample preparation and Western blot analysis was performed as described in section II 3.1 II 5.

2.6.6 The induction of Rap1 by WS® 1442

Since we found that WS®1442 does not mediate its effect *via* activation of PKA, we wanted to figure out if the barrier-protective and cAMP-induceable Rap1pathway is activated by WS® 1442. In a Rap1 activation pull-down assay, WS®1442 was able to strongly activate Rap1 (Figure 36), which is known to be a central regulator of AJ formation and maintenance.
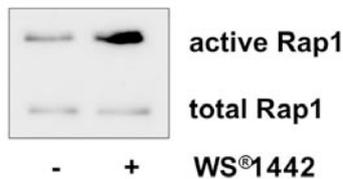
Figure 36: The induction of Rap1 by WS®1442 activates Rap1. HUVECs were grown to long confluence, either left untreated or were treated with WS®1442 (30 min, 100 µg/ml). Rap1 pull-down assay was performed according to section II 8.

2.6.7 The induction of Rac1 by WS®1442

The GTPase Rac1 is one of the downstream targets of Rap1 signaling and a main regulator of the cytoskeleton, but is also involved in AJ stabilization. Figure 37 shows the strong activation of Rac1 by WS®1442 treatment.
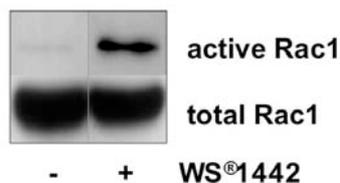

Figure 37: WS®1442 activates Rac1. HUVEC were grown to long confluence, either left untreated or were treated with WS®1442 (30 min, 100 µg/ml). Rac1 pull-down assay was performed according to section II 8.

2.6.8 The induction of cortactin activation by WS®1442

In a third step we observed the activation of cortactin, a downstream target of Rac1. As an actin binding protein, activated cortactin is known to mediate the cortical actin rearrangement. Its activity can be displayed by Tyr[421]-phosphorylation.[68] WS® 1442 induces cortactin phosphorylation after 5 min, and sustained it during the period of preincubation with WS® 1442 (Figure 38A). By CLSM we found that phosphorylated cortactin is colocalized with cortical actin at the cell borders (Figure 38B). These experiments show that treatment with WS® 1442 activates cortactin at the cell border.

A

phos. cortactin

β-actin

0   5   10   20   30   WS® 1442 [min]

B

control   WS®1442

F-actin
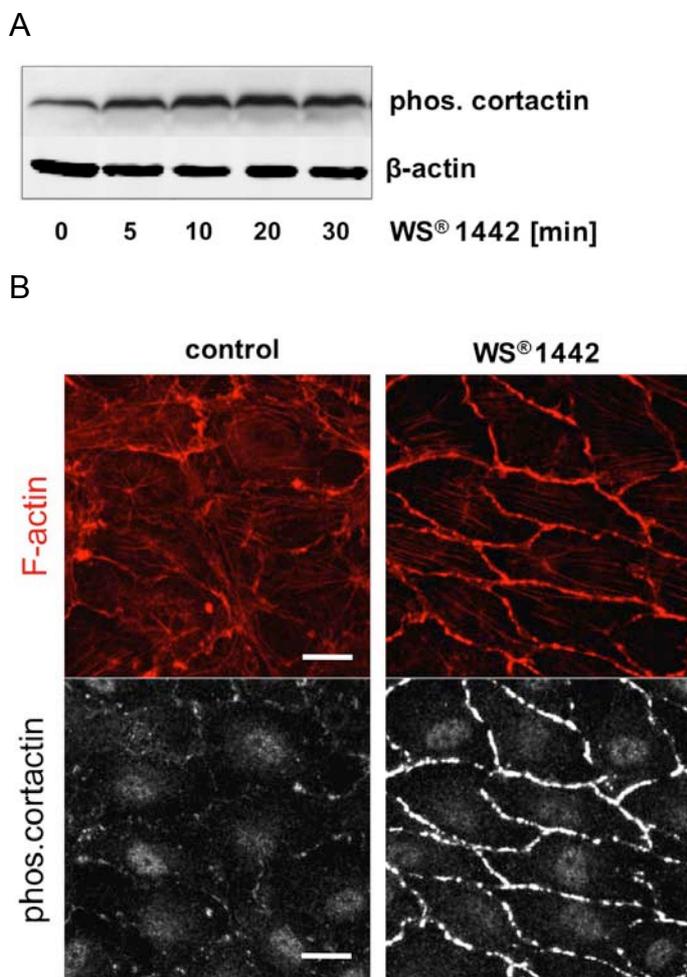
phos. cortactin

Figure 38: Cortactin activation at the cell border by WS® 1442. **A** HUVECs were grown to long confluence, left untreated or treated with WS® 1442 (100 µg/ml) for the indicated time points. Protein sample preparation and Western blot analysis was performed as described in section II 3.1 II 5. **B** HUVECs were grown to long confluence, left untreated or treated with WS® 1442 (100 µg/ml; 30 min). Immunocytochemistry and confocal microscopy were

performed as described in section II 12.1 . White bar = 10 µm (control). One representative image out of 5 independently performed experiments is shown, each.

2.7 Protection of the endothelial barrier function by WS[®] 1442 fractions

Since we found several actions of WS[®] 1442 on the inflammatory EP signaling, we wanted to figure out whether specific actions could be associated to single WS[®] 1442 fractions. Therefore, we repeated several key experiments with four different WS[®] 1442 fractions (described in section II 1.1).

2.7.1 WS[®] 1442 fractions 32-36 inhibit endothelial hyperpermeability.

First of all, we wanted to clarify which fraction shows EHP-inhibiting properties. Therefore we performed the macromolecular permeability *in vitro* assay. Fractions 32-36 reduced significantly the thrombin-induced hyperpermeability increase (Figure 39). Fraction 30 does not have a barrier protective potential. These data clearly demonstrate that there must be more then one active component in the total WS[®] 1442 extract.
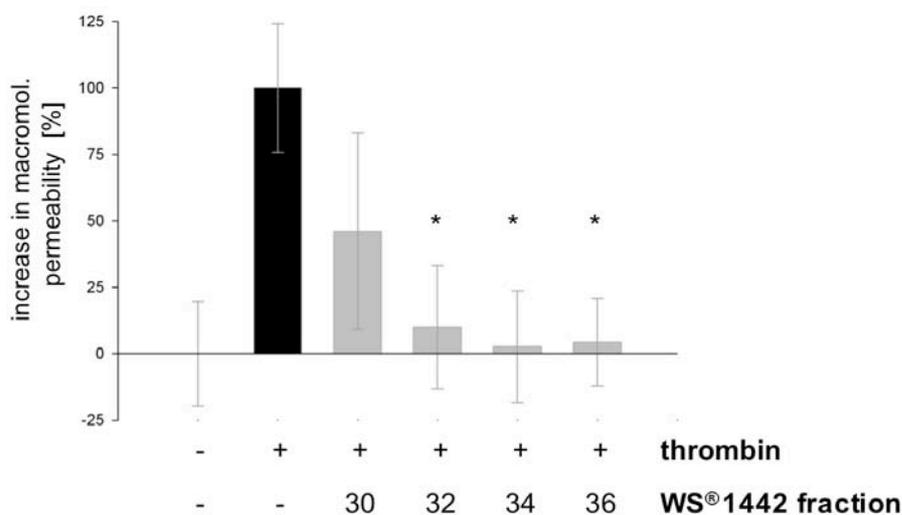

Figure 39: Inhibition of EHP by the WS[®] 1442 fractions 32-36 *in vitro*. HMECs were left untreated, treated with thrombin (1 U/ml) or treated with thrombin after preincubation with WS[®] 1442 fractions 32-36 (single concentrations are calculated on 100 µg/ml of the total extract; 30 min). Macromolecular permeability assay was performed as described in section II 9.

2.7.2 WS® 1442 fractions 32-36 affect the key parameters of endothelial permeability

In analogy to the experiments with the total WS® 1442 extract, we now wanted to figure out if and how these active fractions target the key parameters of EHP. The Western blot analysis of phosphorylated VEC showed a protective effect of WS® 1442 fractions 34 and 36. The phosphorylation of MLC2 was reduced to control level only by fraction 32 (Figure 40A).

Congruent to these findings, fraction 30 did not inhibit the activation of the monolayer by thrombin as we could see by CLSM (Figure 40B). However, fraction 32 showed an obvious reduction of stress fibers and a less fringy VEC seam indicating a reduced cell contraction. Fraction 34 exhibited the strongest morphological protection of the monolayer. There are no intercellular gaps, no fringy seams, and no stress fibers. Additionally, fraction 34 induced cortical actin and cortactin translocation to the cell membrane as well. Fraction 36 did not protect the VEC seam, from stress-fiber formation. Importantly, we found that each of the WS® 1442 fractions targets a different spectrum of key parameters.

A
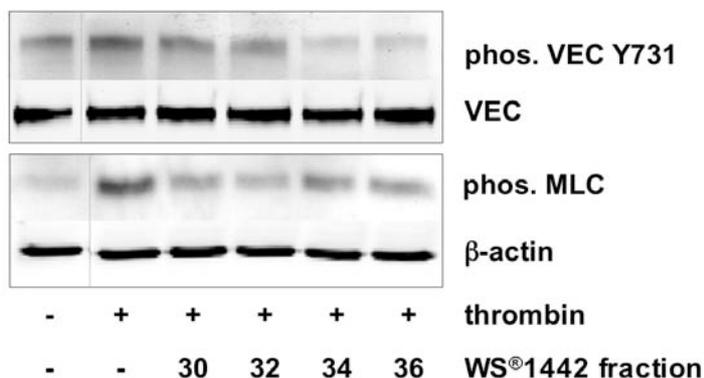
Figure 40 A/B: Different WS® 1442 fractions target different key parameters of EHP. HUVECs were grown to confluence, left untreated, treated with thrombin (1 U/ml; 30 min) or treated with thrombin after preincubation with WS® 1442 fractions (single concentrations are calculated on 100 µg/ml of the total extract; 30 min) **A** Protein sample preparation and Western blot analysis was performed as described in section II 3.1 II 5. **B** Immunocytochemistry and confocal microscopy were performed as described in section II 12.1 . White bar = 10 µm (control). One representative image out of 3 independently performed experiments is shown, each.

Figure 40B
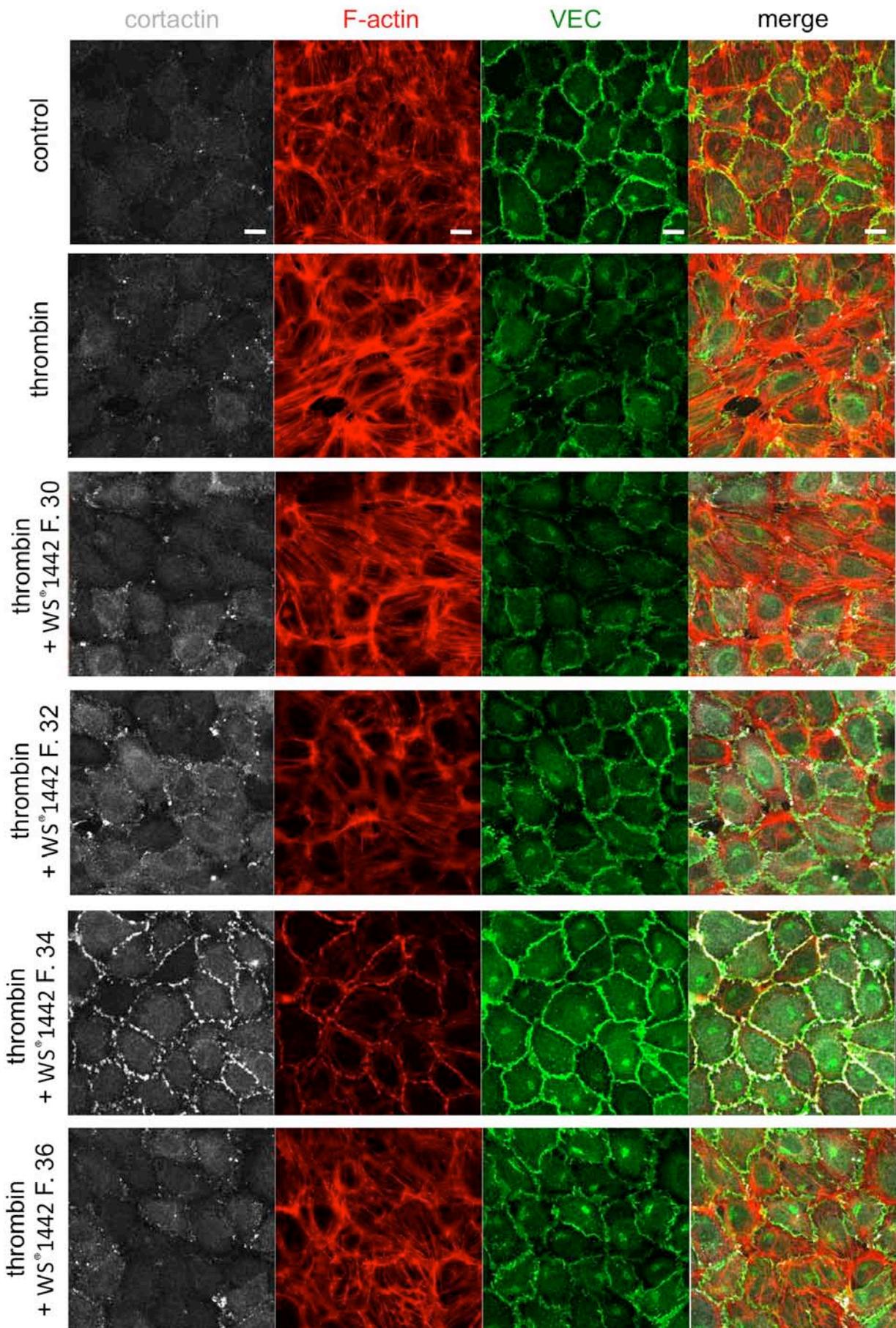
2.7.3 WS® 1442 fraction 32 modified the thrombin-induced $[Ca^{2+}]_i$ increase

Next we intended to figure out which fractions influence the $[Ca^{2+}]_i$ signal . Interestingly, only fraction 32 changed the initial thrombin-induced $[Ca^{2+}]_i$ signal , but did not inhibit the long lasting $[Ca^{2+}]_i$ signal for the whole measurement, compared to the total WS® 1442 extract (Figure 41).
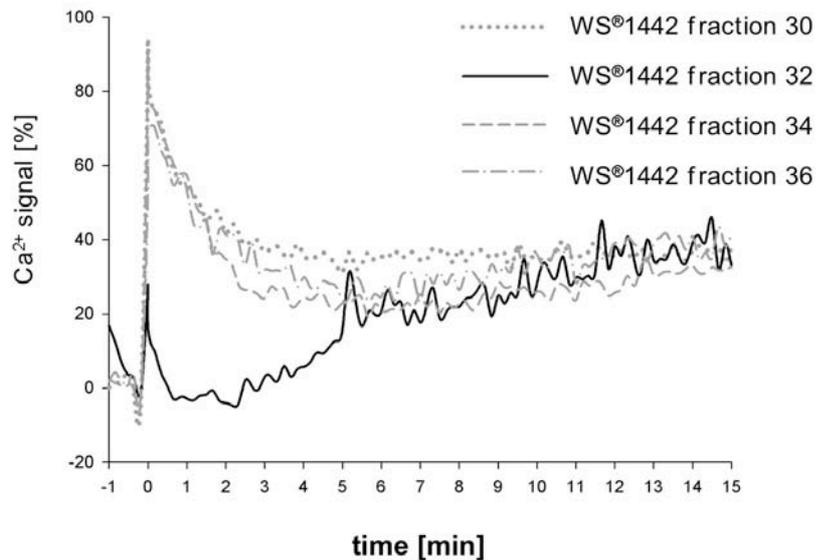
Figure 41: WS® 1442 fraction 32 modifies the thrombin-activated $[Ca^{2+}]_i$ signal. HUVECs were grown to long confluence, were treated with thrombin (1 U/ml; t = 0) after preincubation of WS® 1442 fractions (single concentrations are calculated on 100 µg/ml of the total extract; 30 min). $[Ca^{2+}]_i$ was detected by fluorescence microscopy using Fura-2 as described in section II 10. Basal $[Ca^{2+}]_i$ was set as 100%, the $[Ca^{2+}]_i$-increase is shown [%]; (n = 3).

2.7.4 Inhibition of RhoA activation by WS® 1442 fraction 30 and 32

To study if the affection of the $[Ca^{2+}]_i$ signal by WS® 1442 fraction 32, or a $[Ca^{2+}]_i$ signal independent affection by WS® 1442 fraction 30, 34, and 36 inhibits central downstream targets of the $[Ca^{2+}]_i$ signaling pathway, we analyzed their effects on RhoA in an RhoA activation pull down assay. Congruent to Ca^{2+} measurements (see 2.7.3), WS® 1442 fraction 32, inhibited the thrombin-induced activation of RhoA (Figure 42), which could be explained by the modulation of the $[Ca^{2+}]_i$ signal. The WS® 1442 fraction 34 and 36 exhibited no effect on RhoA-activation. WS® 1442 fraction 30, which showed no effect

on the macromolecular permeability increase, completely blocked the activation of RhoA. These are preliminary data and have to be corroborated by further experiments.
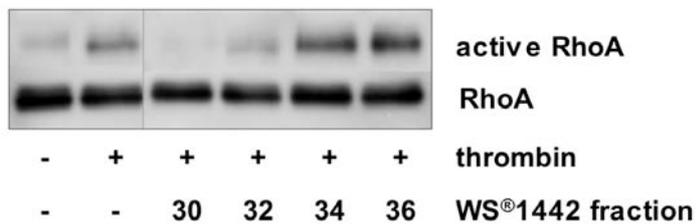
Figure 42: Inhibition of RhoA activation by WS[®] 1442 fraction 30 and 32. HUVECs were grown to long confluence, were treated with thrombin (t = 0min; 1 U/ml; 14 min) or with thrombin after preincubation of the WS[®] 1442 fractions (single concentrations are calculated on 100 µg/ml of the total extract) preincubation. RhoA activation assay and Western blot analysis was performed as described in sections II 8/II 5 (n = 1).

2.7.5 The increase of cAMP level by WS[®] 1442 fraction 34 and 36

Besides targeting the Ca^{2+} signaling, WS[®]1442 increases cellular cAMP-levels. The preliminary cAMP-measurements of the WS[®] 1442 fractions showed that fraction 34/36 significantly increased cAMP levels (Figure 43).
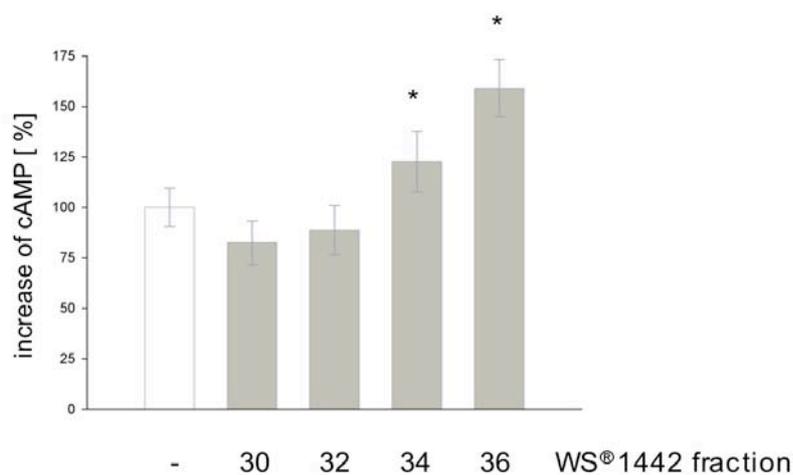
Figure 43: The increase of cAMP by WS[®] 1442 fraction 34 and 36. HUVECs were grown to long confluence, either left untreated or treated for 15 min with WS[®] 1442 fraction (single concentrations are calculated on 100 µg/ml of the total extract). cAMP levels were measured by ELISA according to section II 11 (n = 2).

2.7.6 WS® 1442 fraction 34 and 36 influence the PKA dependent activation of VASP

Since we found a cAMP increase evoked by fraction 34/36 we wanted to clarify if the downstream targets of the cAMP signaling are affected, too. According to the previous findings, PKA dependent VASP was activated after treatment with WS® 1442 fraction 34 and 36 (Figure 44). WS® 1442 fraction 30 and 32 showed a slight increase.
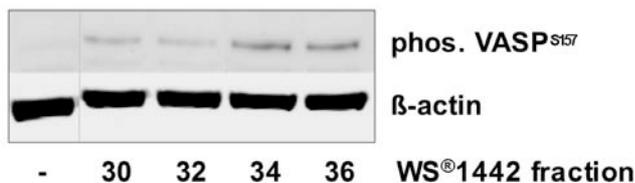
Figure 44: VASP is activated by the WS® 1442 fraction 34 and 36. HUVECs were grown to long confluence, either left untreated or were treated with WS® 1442 fraction (30 min; single concentrations are calculated on 100 µg/ml of the total extract). Protein sample preparation and Western blot analysis was performed as described in section II 3.1 II 5 (n = 2).

2.7.7 The activation of Rac1 by WS® 1442 fraction 30 and 34

The downstream effector of the Epac1/Rap1-signaling, Rac1, regulates cortical actin formation and AJ complex stabilization. A clear activity induction is caued by fraction 34 as expected by the cAMP-increasing action of this fraction. Surprisingly WS®1442 fraction 36 showed no activation, although we found a cAMP increase. WS®1442 fraction 30 on the contrary, does not induce cAMP, but activates Rac1 (Figure 45).
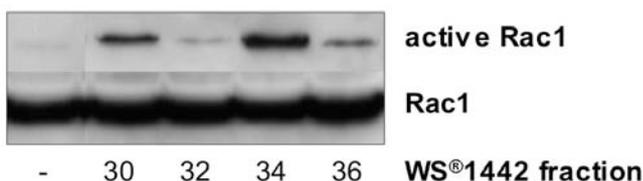
Figure 45: Rac1 is activated by fraction 30 and 34. HUVECs were grown to long confluence, either left untreated or were treated with WS® 1442 fraction (30 min; single concentrations are calculated on 100 µg/ml of the total extract). Rac1 pull-down assay was performed according to section II 8 (n = 1).

2.7.8 The increase in cortactin activation by WS®1442 fraction 34

Cortactin as an effector of the Rac1 signaling is crucial for cortical actin formation. WS®1442 fraction 34 shows a strong activation of cortical actin by increasing phosphorylation localized at the cell membrane. WS® 1442 fraction 36 shows similar effects, but to a lesser degree. Fraction 30 and 32 showed no difference to the control cells. These data suggest that cAMP-inducing fractions, especially the fraction 34, mediate the cytoskeleton rearrangement to cortical actin in the preincubation period, which stabilizes the endothelial barrier function.

Figure 46: Fraction 34 and 36 induce phosphorylation of cortactin and induce cortical actin formation. HUVECs were grown to confluence, left untreated or with 30 min WS® 1442 fractions (single concentrations are calculated on 100 µg/ml of the total extract) preincubation. Immunocytochemistry and confocal microscopy were performed as described in section II 12.1 . Small white bar = 10 µm (control). One representative image out of 3 independently performed experiments is shown, each.

Figure 46
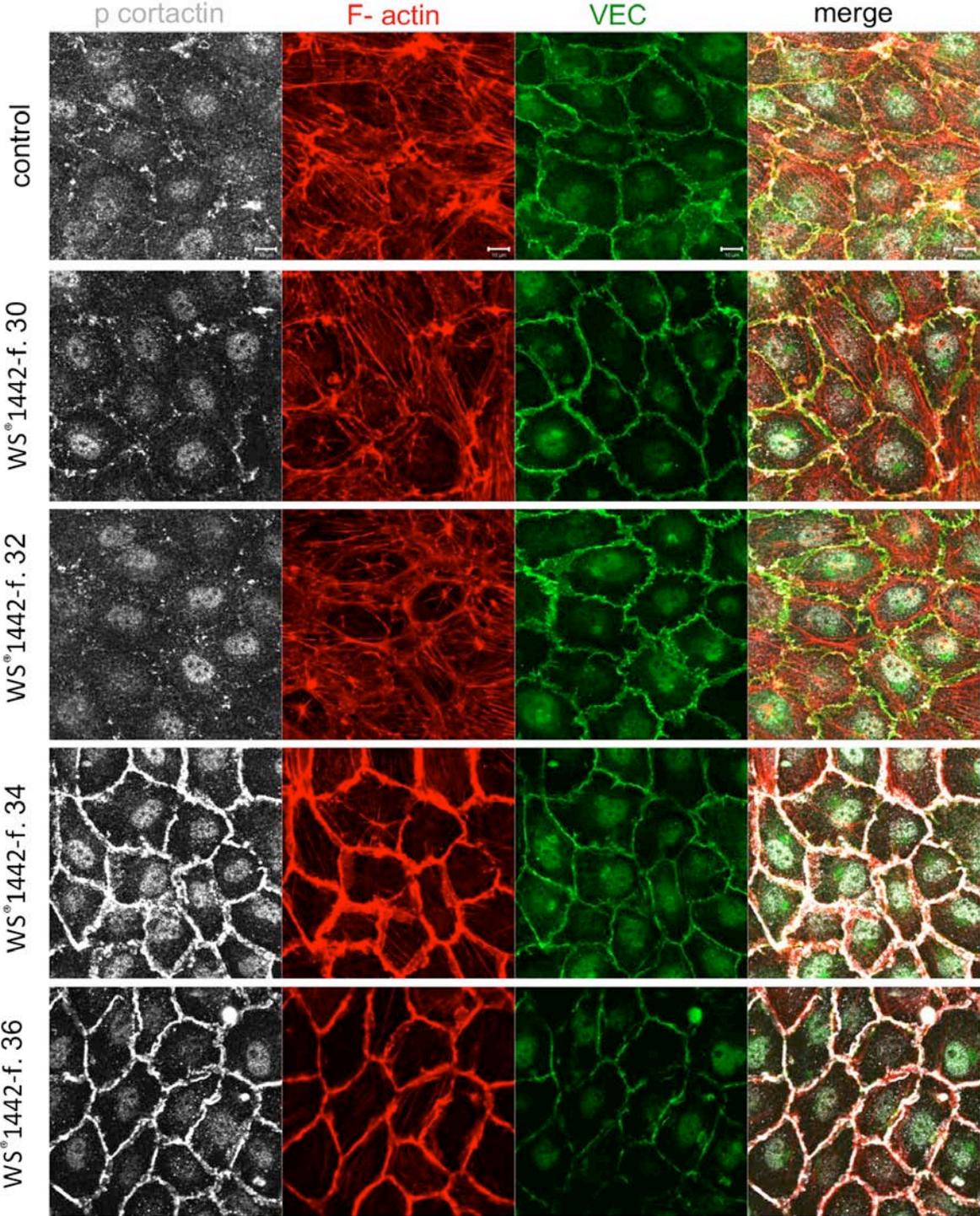
IV **DISCUSSION**

This work presents a novel mode of action for the well-established Crataegus extract WS®1442: Crataegus inhibits inflammation-induced endothelial hyperpermeability and therefore beneficially affects the endothelial barrier function. To understand the relevance of this action it is important to know that endothelial hyperpermeability is a hallmark of endothelial inflammation leading to endothelial dysfunction. This mechanism takes part in the pathophysiology of a multitude of diseases (Figure 47). In most of the common human vascular diseases there is an inflammatory response of the endothelium to stress, prolonging the activation of the endothelium.[69] The inductors of endothelial stress are identical to the known risk factors for CVD: arterial hypertension, smoking, high blood cholesterol levels, or diabetes mellitus, which are all associated with the release of proinflammatory cytokines (e.g., IL-6, TNFα) and a consecutive induction of a systemic inflammatory state.[70-73] Bonetti et al. and de Jager et al. linked the exposure of CVD risk factors to the impairment of endothelial function,[74, 75] which again leads to the progression to CVD.[5, 76-80] Hence anti-inflammatory therapies became more and more important for patients suffering from CVD, especially atherosclerosis, and started with the use of statins.[81, 82] In recent years, agents interfering with TNFα, interleukin-1, and leukotriene pathways are evaluated in clinical trials for patients suffering from coronary artery disease.[83] Even the immunosuppressive drug methotrexate will be tested for the secondary prevention in patients suffering from CHF.[84] But beside this central role of endothelial dysfunction in CVD and many other diseases, this cell layer is not amenable to traditional physical diagnostic maneuvers of inspection. Therefore, other organs or clinical parameters are in the focus in patient monitoring or in evaluating the pathophysiology of diseases. The endothelium has been out of the focus as a potential drug target for a long time period. But now great efforts are done to find successful novel therapy options. These efforts point out that there is an enormous need for new tools to target inflammation-induced endothelial activation. Thus, the endothelium still has an immense untapped potential as a therapeutic target.

This work is divided into two parts, both of them focusing on one distinct mechanism of inflammatory endothelial activation:

(I)   the endothelial ICAM expression

(II)   the endothelial permeability increase
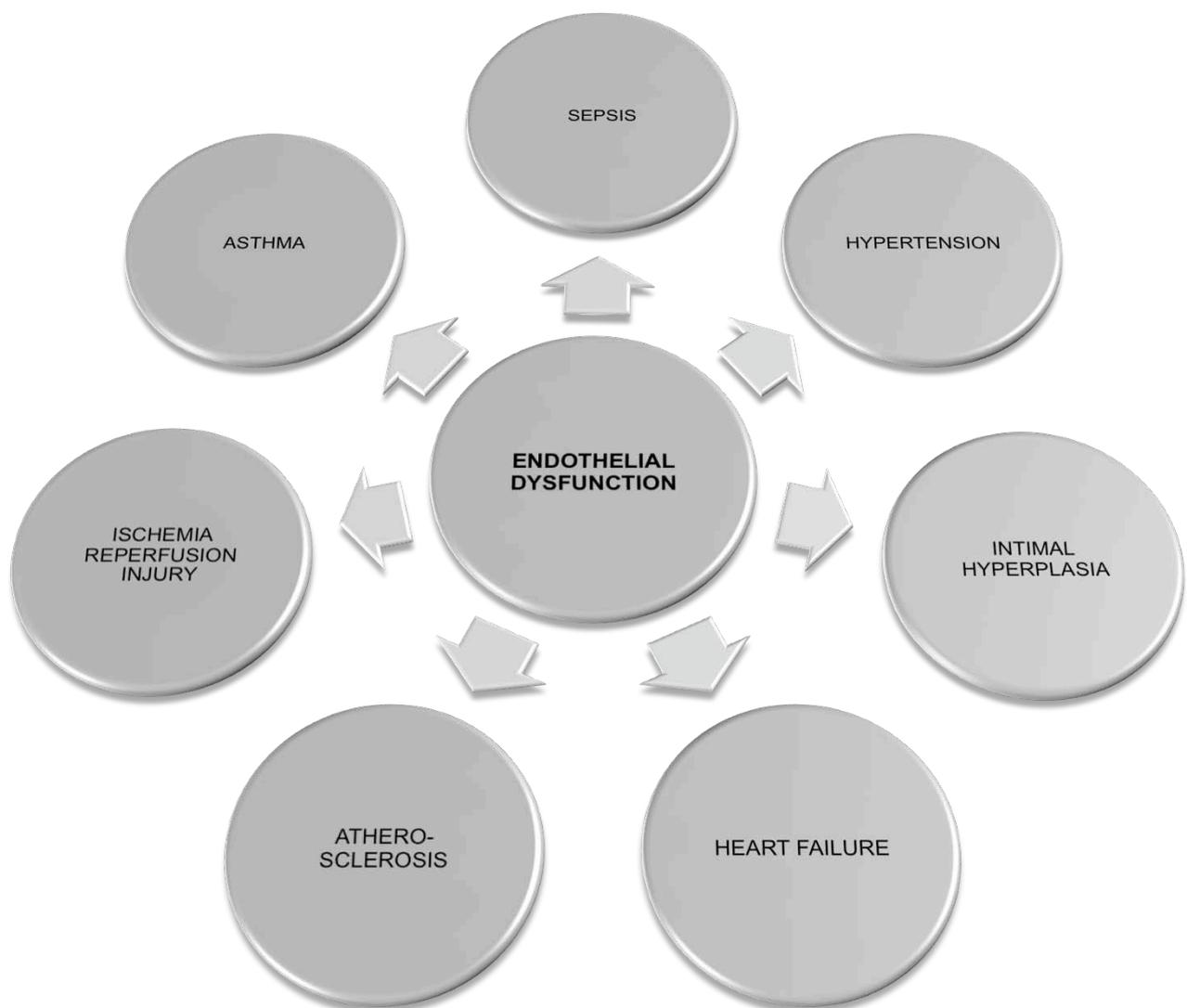
Figure 47: Overview of the participation of endothelial dysfunction in the pathophysiology of a multitude of disease.

1 Effect of WS® 1442 on ICAM-1 expression

The inflammatory response is the stereotyped reaction of the body to tissue damage. Beside rapid and transient delivery of soluble elements from the blood to the site of injury, there is a more prolonged transmigration of leukocytes to the tissue.[85] Leukocytes have to be recruited to the site of inflammation, a process guided by cytokines. Subsequently, they attach to the vessel wall, where they are locomoted to the endothelial cell borders to migrate through the endothelium into the inflammatory interstitial tissue.[86] This transendothelial migration or diapedesis represents the "point of no return" in the context of inflammatory response. The inflammatory endothelial activation is a pivotal step to prepare the endothelium for leukocyte adhesion by the expression of CAM on the surface of EC. But this mechanism is not only initiated by tissue damage, it also occurs as a response of the endothelium to stress, e.g. shear stress in hypertension, leading in consequence to local inflammatory reactions and has been implicated in the pathophysiology of many CVD.[87]

To reveal a potential of WS® 1442 to inhibit distinct steps of endothelial activation, we analyzed the impact of the Crataegus extract WS® 1442 on inhibiting ICAM-1 cell surface expression. This is a common and very specific marker for inflammatory endothelial activation.[88,89] Corresponding to Leeuwenberg et al. we used TNFα to induce ICAM-1 expression in HUVECs.[89] The TNFα-induced expression of ICAM1 was reduced about 25% by WS® 1442.

To elucidate the mechanism of WS®1442 to reduce TNFα induced ICAM-1 expression, we focused on the three central pathways responsive to an induction of stress stimuli and cytokines: the c-Jun N-terminal kinases (JNKs) pathway, the p38 mitogen-activated protein kinase (p38 MAPK) pathway, and the NFκB pathway.[14] The DNA-binding activity of AP-1 or NFκB to the ICAM-1 promotor sequence induced by TNFα was not affected by preincubation with WS®1442. Additionally translocation of the p65 subunit of NFκB to the nucleus was not influenced by WS® 1442. Also the activation of the p38 MAPK-signaling seems not to be a target of WS® 1442 action. These findings point out that the reduction of ICAM-1 cell surface expression is not due to the inhibition of these distinct targets. WS®1442 seems to interfere other downstream targets of TNFα leading to an inhibition of ICAM-1 expression. To determine whether the effects of WS® 1442 were specific to adhesion molecule expression or rather to cytokine-induced gene expression in general further experiments have to be done. But before the exact signaling

mechanism of this effect will be analyzed the relevance of this effect hast to be characterize (diapedesis of leukocytes). Gerritsen et al. showed a similar effect of the flavonoid apigenin on TNFα induced ICAM-1 expression.[90] Apigenin showed no effect on the activation of the transcription factor NF-KB (nuclear translocation or binding to the consensus oligonucleotide), but they found a inhibitory effect on the transcriptional activation of NF-KB (reporter gene assay).

1.1 Conclusion

WS[®] 1442 showed a weak effect on a central marker of inflammatory endothelial activation, the expression of ICAM-1 on the cell surface. However, WS[®] 1442 had no influence on some of the major pathways leading to ICAM-1 expression. This suggests that WS[®] 1442 might influence ICAM-1 cell surface expression distal of the analyzed targets, or WS[®] 1442 targets a further TNFα-induced signal pathway. Thus, there are still interesting aspects, which might open a new field of research connected to the diapedesis of leukocytes and WS[®]1442:

(I)   Is a reduction of 25% of TNFα-induced ICAM-1 expression on cell surface by WS[®]1442 sufficient to decrease the diapedesis of leukocytes from the blood vessels to the tissue *in vivo*? Taking into account that most of the leukocytes that once initiated contact with the endothelium at sites of inflammation lose the adhesion contact and reenter the circulation,[85] 25% less ICAM-1 would possibly be enough for a significant reduction in diapedesis. For this purpose it would be interesting to analyze leukocyte diapedesis *in vivo* (e.g. intravital microscopy).[91]

(II)   To what extend is the vascular cell adhesion molecule (VCAM) affected by WS[®]1442? VCAM governs transendothelial migration, and is vital in the mechanism of diapedesis of leukocytes through the endothelium.[92]

2 Effects of WS® 1442 on inflammation-activated endothelial hyper-permeability

Endothelial barrier dysfunction is responsible for protein-rich tissue edema, which is a significant pathogenic component in multiple diseases, such as atherosclerosis[93], cardiovascular disease,[12] acute lung injury,[94] or sepsis.[54] Treatment with diuretics represents the standard therapy of edema.[95] Inflammation plays a crucial role in edema formation and inflammation-induced hyperpermeability showed up to be the capable target to affect edema.[5, 6, 83] The screening for novel permeability-inhibiting compounds has recently been intensified focusing on the discovery of lead structures that affect aberrant inflammation-induced endothelial hyperpermeability. We investigated the effect of WS® 1442 on inflammation-induced endothelial hyperpermeability, by two different settings:

(I)   As prove of principle the macromolecular vascular permeability in the mouse cremaster muscle *in vivo*.

(II)   The measurement of endothelial macromolecular permeability *in vitro* was used as a basal functional assay for analyzing the underlying signaling mechanisms.

WS® 1442 clearly inhibited the barrier disruption *in vivo* induced by histamine (90% reduction) - a strong mediator of endothelial permeability increase. The histamine-induced permeability increase in mice pretreated with WS® 1442 was not significantly different from the control animals. If we compare these findings with those of the atrial natriuretic peptide (ANP) done in the same setting (60% reduction), WS® 1442 showed a much stronger effect on endothelial hyperpermeability.[96] This difference in effect intensity might be due to the affection of different targets. Also *in vitro* WS® 1442 was able to completely block the endothelial permeability induced by thrombin, the best characterized mediator of endothelial hyperpermeability, down to control levels.

In conclusion of these findings, we could exhibit for the first time that WS® 1442 is a strong protector of endothelial barrier function *in vivo* and *in vitro*. Thus, we found not only a new extracardial function of WS® 1442 involved in the control of CHF symptoms, but also elucidated an action, which is discussed to affect the underlying mechanisms of CHF pathophysiology. Therefore, WS® 1442 might be beneficial for CHF prevention.

2.1 Influence of WS® 1442 on endothelial hyperpermeability signaling

To understand how WS® 1442 interferes with the mechanisms of endothelial hyperpermeability we observed the underlying signaling cascades. A short pretreatment with WS® 1442 (30 min) lead to a barrier protection, suggesting that WS® 1442 might directly affect the underlying signaling mechanism. Promising targets for beneficially influencing endothelial hyperpermeability (EHP) are the central signaling molecules of the pathways leading to the activation of the three key parameters of endothelial permeability:[23] Cytoskeletal protein reorganization, activation of the contractile machinery and disassembly of VEC complex (AJ),[23] all depending on the change of intracellular Ca^{2+} concentrations.[21, 97]

2.1.1 WS® 1442 and the key parameters of the endothelial permeability

We examined potential effects of WS® 1442 on these three key parameters of EHP. Interestingly, WS® 1442 affected all these three key systems: adherent junctions disassembly, cell contraction, and the cytoskeleton rearrangement. WS® 1442 inhibited the thrombin-induced inflammatory endothelial activation.[17, 18, 98-101] Live cell imaging of the cytoskeleton showed increased cortical actin formation after treatment with WS® 1442, known to be barrier protective and AJ stabilizing.[17, 101]

It is obvious that WS® 1442 affects EHP-signaling upstream of the key parameters. This regulation of endothelial permeability indicates that there might be a central step affected by WS® 1442 in EHP signaling, such as the Ca^{2+}-signaling, which plays a central role in the acute inflammation-induced endothelial activation.

2.1.2 WS® 1442 and Ca^{2+} signaling in endothelial hyperpermeability

Almost every permeability-increasing mediator raises intracellular Ca^{2+} levels.[16, 19] Therefore, it seems of special interest to clarify if WS® 1442 targets the thrombin induced $[Ca^{2+}]_i$ increase. Thrombin increases $[Ca^{2+}]_i$ within two distinct phases.[102,26] WS® 1442 completely inhibited the increase in $[Ca^{2+}]_i$ in the second sustained phase, the first phase stayed unaffected. In cardiac myocytes, Crataegus raises $[Ca^{2+}]_i$ cAMP-independently by inhibition of the Na^+/K^+-ATPase, which leads to the positive inotropic

effect.[44] However, there exists no data describing the regulation of Ca^{2+} signaling in the endothelium. Interestingly, the sustained second phase of thrombin-induced $[Ca^{2+}]_i$ increase is known to be mediated by store-operated cation channels (SOCs: TRP1 and TRP2). Moreover, thrombin induced endothelial hyperpermeability, MLC2 phosporylation, and stress-fiber formation are based on the opening of TRP1 and TRP2. [19, 25, 26, 103, 104] We could exclude that WS® 1442 mediates the inhibition of the second phase of $[Ca^{2+}]_i$ increase *via* Ca^{2+} store depletion, and seems to be causing a direct inhibition of the Ca^{2+} influx into the cytosol of the second phase. Therefore, we hypothesize that WS® 1442 mediates its Ca^{2+} effect *via* SOC inhibition.

In the next step we wanted to figure out if this inhibition of the second phase of $[Ca^{2+}]_i$ increase affects the key parameters of EHP. The activation of the Ca^{2+} dependent protein kinase C (PKC) isoform PKCα leads to the disassembly of the VEC junctional complex and to the activation of the small Rho GTPase RhoA.[104, 105] RhoA is the central regulator of stress fiber formation, it inactivates MLCP resulting in contraction of endothelial cells.[106] PKCα as well as RhoA are activated by thrombin. In WS®1442 pretreated cells the thrombin-induced PKC and RhoA activation is completely blocked. These findings indicate, that the action of WS®1442 affects both of these central signaling parameters.

The impact of WS® 1442 on the key parameters of EP and therefore on the endothelial permeability itself seems to be due to the modulation of the Ca^{2+}-signaling (PKC and RhoA inhibition). Interestingly, until now, permeability-inhibiting compounds, which affect these targets, are very rare. Moreover, they are, with only few exceptions, not effective, unselective, or too toxic for therapeutical use. For instance, inhibitors of MLCK that prevent MLC phosphorylation, failed to completely abolish the hyperpermeability response[107]. Fusadil, a ROCK inhibitor,[108] showed permeability inhibiting characteristics *in vitro*[109]. However, *in vivo* data or clinical studies are missing up to now. In initial studies, Ruboxistaurin, an inhibitor selective for the PKCβ isoform, decreased the development of sight-threatening macula edema[110]. Nevertheless, most inflammatory edema correlate with an activation of PKCα and not PKCβ and a total block of PKCα can activity increases basal endothelial permeability as well[32]. The approach to affect single targets in Ca^{2+} signaling seems not to be effective enough to completely prevent inflammation induced vascular leakage. Barrier protective signaling cascades have to be activated as well. In this regard, WS® 1442 showed beside its inhibitory potential on

Ca^{2+} signaling an effect, connected to endothelial barrier protection, the cortical actin arrangement.

2.1.3 WS® 1442 and the barrier protective cAMP-signaling

A further promising strategy for an anti-hyperpermeability therapy is to target barrier stabilization signaling pathways, which antagonize vascular leakage and protect endothelial barrier function. It is assured that cAMP elevating drugs like Beraprost[108] and the atrial natiuretic peptide[96, 111]reduce inflammation-induced permeability and edema-formation.[28-31] In contrary, EHP-increasing mediators, such as thrombin reduce basal cAMP levels in the cell.[112]

cAMP exerts its effect primarily *via* direct activation of protein kinase A (PKA) and of the guanine nucleotide exchange factor Epac1, an activator of Rap1. Both pathways are parallel and independent of each other.[113] Additionally, it is known that the formation of cortical actin is a cAMP-dependent process.[19] Even though there are citations claiming Crataegus extracts as a cAMP-raising herbal remedy, until now, there exists no publication showing that WS® 1442 increases cAMP levels. Only an inhibition of isolated PDE was shown once. [114]

In order to clarify the involvement of WS® 1442 in cAMP signaling, endothelial cAMP levels were measured. We showed for the first time that WS® 1442 raises the cAMP content in endothelial cells. Therefore, a participation of the cAMP-dependent barrier protective signaling seems to be obvious. How does WS® 1442 increase cAMP levels, by activation of AC or by inhibition of PDE? Based on our findings, we hypothesized that Crataegus raises cAMP by an inhibition of PDE. There are several strong hints emphasizing this hypothesis: (I) WS® 1442 shows slower kinetics for maximum increase of cAMP than it is known for AC agonists. (II) The WS® 1442–induced increase of cAMP could not be forced up by additional PDE inhibition via IBMX. However, the forskolin-induced cAMP increase *via* AC activation was elevated by WS® 1442 pretreatment. (III) WS® 1442 selectively increases the activation of the Rap1-pathway *via* cAMP. This specificity of the second messenger cAMP to activate a distinct signaling pathway is regulated by individual PDE isoforms, modulating distinct signaling pathways in the cell, provided by their remarkably selective cellular and sub-cellular localization,[115] and only

subsidiary by ACs. (IV) Inhibitors of the PDE2 isoform decrease endothelial permeability in inflammatory conditions.[116] Accordingly, TNFα induces vascular leakage *via* increasing PDE2A expression [117]. PDE are known targets for the treatment of EHP. Although selective PDE2 inhibitors are available, clinical studies, which evaluate the therapeutic efficiency of these compounds, are still missing.[116]

In the present work we could show that WS[®] 1442 activates PKA and its downstream target VASP. However, the inhibition of PKA showed no significant influence on the WS[®]1442 mediated barrier protection *in vitro*. Therefore, we excluded the PKA signaling pathway to be the main target of WS[®] 1442 in the regulation of EHP inhibition. We next focused on the Epac1 downstream effector Rap1, the most important regulator of AJ stability and cortical actin formation.[27, 34, 41, 118, 119] WS[®] 1442 showed up to be a strong activator Rap1/Rac1/cortatcin signaling cascade.[68, 120] Beside the effect on Ca^{2+} signaling, WS[®] 1442 posseses a second strong effect on the activation of the Rap1-signaling pathway, which is in the focus of today's EHP research.

2.1.4 NO and the WS[®] 1442 barrier protective signaling

As WS[®] 1442 is known to increase endothelial NO formation, which can regulate endothelial permeablity.[19] We could exclude that NO formation,[121,58] is responsible for the barrier protective effects of WS[®] 1442.[122] Upon cotreatment with NO-synthase inhibitor, WS[®] 1442 still exhibited its barrier protective properties. Moreover morphological changes like cortactin activation and cortical actin formation induced by WS[®] 1442 were not affected by NO synthase inhibition.

2.1.5 Effects of WS[®] 1442 fractions on the barrier protective signaling

To clarify if the effect of WS[®] 1442 on the Ca^{2+} and the cAMP signaling is due two separate actions, based on different components of the total extract, and to get further hints which chemical class of biological compounds mediate this effects, we used four fractions of WS[®] 1442. We repeated the *in vitro* key experiments, which were used to analyze the signaling-pathways regarding endothelial hyperpermeability. The following Figure 48 shows a summary of these experiments and displays the effects of each fraction.

	WS® 1442 fractions			
Effects on thrombin induced endothelial cell activation	**30**	**32**	**34**	**36**
inhibition of macromolecular permeability		✓	✓	✓
inhibition of intracellular Ca^{2+}-increase		✓		
inhibition of MLC phosphorylation		✓		
inhibition of VEC phosphorylation	✓	✓	✓	✓
inhibition of AJ-disruption		✓	✓	
inhibition of stress-fiber formation		✓	✓	
inhibition of RhoA activity	✓	✓		

Effects on cAMP signaling	**30**	**32**	**34**	**36**
increase of cellular cAMP-concentration			✓	✓
phosphorylation of PKA-substrat			✓	✓
induction of VASP phosphorylation			✓	✓
activation of Rac1	✓		✓	
formation of cortical actin			✓	✓
induction of cortactin phosphorylation			✓	✓

Figure 48: Summary of all experiments done with WS® 1442 fractions. Active WS® 1442 fractions in each experiment setting were marked in green. Some of the experiments have to be regarded as preliminary data (s. Results).

After analyzing the activity pattern of the single WS® 1442 fractions they can be divided into groups by there potential to target distinct pathways. The first group consists of, WS®1442-fraction 32, containing mainly flavones and flavonols, and mediates the inhibition of the thrombin-induced $[Ca^{2+}]_i$ increase and of its downstream targets (cell contraction, AJ and actin-cytoskeleton). The second group fraction, 34 and 36, contains mainly oligomeric procyanidines of different polymerization degree and mediates the effects on the cAMP signaling. WS® 1442 fraction 34 showed generally stronger effects than 36. These data clearly proved that WS® 1442 mediates two independent effects. Both of them lead to the same result, the inhibition of the thrombin-induced endothelial permeability. These completely different signaling cascades, which of course can influence each other, complement one another, leading to that strong impact of WS® 1442 on endothelial hyperpermeability. These two effects might explains the difference

between ANP and WS[®] 1442 in the effect intensity on EHP *in vivo*. Althought both affect all of the key parameters of endothelial permeability, WS[®] 1442 in contrast to ANP does additionally affect the Ca^{2+} signaling cascade.[96, 111]

These findings also consort with the data from experimental literature. Oligomeric procyanidines of different origin showed permeability- and edema-inhibiting effects *in vivo*. Fitting to our data, a correlation between the polymerization degree and the effect intensity was found. A reduced polymerization degree (n) increases the effect, as seen with WS[®] 1442 fractions 34 (n= 1-4) and WS[®] 1442 fractions 36 (n>4).[123, 124] Also flavanoids showed anti-edema effects in venous disease, which are strongly related to a inflammatory pathogenesis.[125]

2.2 Conclusion

Our work showed that Crataegus extract WS[®] 1442 is highly barrier protective. It inhibits the inflammation-induced endothelial permeability increase *in vivo* and *in vitro*. Thus, we present a completely new extracardiac effect of this well studied drug, in addition to the previous known WS[®] 1442 functions related to the treatment of CHF. Inflammation-induced endothelial activation is discussed to take part in CVD-pathophysiology. Because of its direct intervention with inflammatory endothelial activation, WS[®]1442 might be a new therapeutic option for the prevention of CVD, and would perfectly complement existing drugs, with an impact on basal anti-inflammatory mechanisms in CVD.

Moreover, we elucidated the underlying mechanisms. If we compare the mechanisms of WS[®] 1442 to other substances affecting the endothelial hyperpermeability signaling pathway, the particular benefit of WS[®] 1442 is to target all of the key parameters leading to EHP in two different modalities: The inflammatory activation of the endothelium by Ca^{2+}/PKC/RhoA signaling, and the activation of the highly barrier protective cAMP/Rap1/Rac1 signaling pathway. These pathways were affected at a very early and essential signaling step, complementing one another in handling vascular permeability.[94, 126] This character is unique compared to other hyperpermeability-inhibiting compounds, and it is likewise conceivable that it enables WS[®] 1442 to flexibly inhibit the induction of vascular leakage by a wide range of different permeability-inducing mediators, which is of importance to handle such a complex mechanism like EHP. Each of these two effects can be related to distinct WS[®] 1442 fractions, and is

therefore related to different chemical classes of bioactive compounds including flavonoids or oligomeric procyanidins. Certainly, this multi-component character of WS®1442 is comparable to the principle of modern combinatory drug therapies: causing synergistic effects by multi-targeting, which is doubtless an advantage for the prevention of such complex dysfunctions, such as inflammatory vascular leakage, and is not at all a handicap of a herbal remedy extract. In addition, the safety of WS®1442 is proved in several studies and centuries of therapeutical use.

3 Possible aspects of future research

Certainly it will be a long way to close the gap between these findings and drug targeting, between bench and bedside. Although these data show a great potential in controlling endothelial permeability also *in vivo*, the question if these effects are appropriate in CVD prevention or in the control of inflammation-induced edema, will be one possible aspect of future research.

The main questions are:
(I)   What are the active compounds in these WS® 1442 fractions? To answer this question, further sub fractionations are needed to reduce the number of compounds, to isolate and test some of the candidates separately of each other. These single compounds could be the source to characterize new leading structures for EHP targeting.

(II)   Are there further cell targets involved, which could lead to further effects? For example effects on tight junctions, integrins or microtubuli.

(III)   Does WS® 1442 influence processes, that are based on related signaling mechanisms, such as leukocyte transmigration through the endothelium[85] or vascular endothelial growth factor-induced brain edema formation after ischemic stroke.[127]

(IV)   What is the exact mechanism of WS® 1442 to inhibit the Ca^{2+} increase and to increase cAMP levels?

(V)   Does WS® 1442 possess potential to prevent CVD, e.g. in an atherosclerotic model?

V SUMMARY

WS$^®$ 1442 and endothelial ICAM expression

This study shows for the first time that WS$^®$ 1442 exerts anti-inflammatory effects. **WS$^®$ 1442 reduced the expression of ICAM-1** on the surface of endothelial cell. Based on these findings, further investigations into the anti-inflammatory profile of WS$^®$ 1442 would be highly interesting.

WS$^®$ 1442 and inflammation-induced endothelial hyperpermeability

WS$^®$ 1442 is successfully used in the treatment of CHF. We found a **completely new extracardial effect** of the Crataegus extract WS$^®$ 1442 on the endothelial permeability induction, which is a hallmark of inflammation activated endothelial cells and a crucial mechanism in the pathophysiology of cardiovascular diseases. This study we for the first time elucidates that WS$^®$ 1442 blocks inflammation-induced endothelial dysfunction *in vivo* and *in vitro*. WS$^®$ 1442 affects all three key parameters of endothelial permeability: cell contraction, rearrangement of the actin cytoskeleton, and disruption of adhesion junctions (
Figure 49). WS$^®$ 1442 strongly protects endothelial barrier function by two distinct mechanism:

(I)   WS$^®$ 1442 inhibits the **thrombin-induced sustained Ca^{2+} increase**. It blocks the activation of MLC2, which leads to an inhibition of cell contraction. It abolishes activation of PKC and thus the disruption of adhesion junctions. WS$^®$ 1442 also affects the activation of RhoA resulting in reduced stress fiber formation and sustained MLC2 phosphorylation.

(II)   WS$^®$ 1442 activates the **barrier protective cAMP signaling**. WS$^®$ 1442 activates two barrier stabilizing pathways. It activates PKA and its downstream effector VASP. The more pronounced effect, however, is the activation of the Ras like GTPase Rap1 by WS$^®$ 1442. This results in a stabilization of the VEC-complex and therefore of the adhesion junctions.

Additionally, *via* Rap1, WS® 1442 mediates the activation of Rac1 leading to the formation of cortical actin, resulting in a stabilization of AJ as well.

(III)   WS® 1442 mediates these **two independent effects** *via* different chemical classes of biological compounds, which are contained in two different fractions.

The unique feature of WS®1442 is that it is on the one hand an inhibitor of inflammation-induced hyperpermeability and on the other hand a stabilizer of endothelial barrier function.
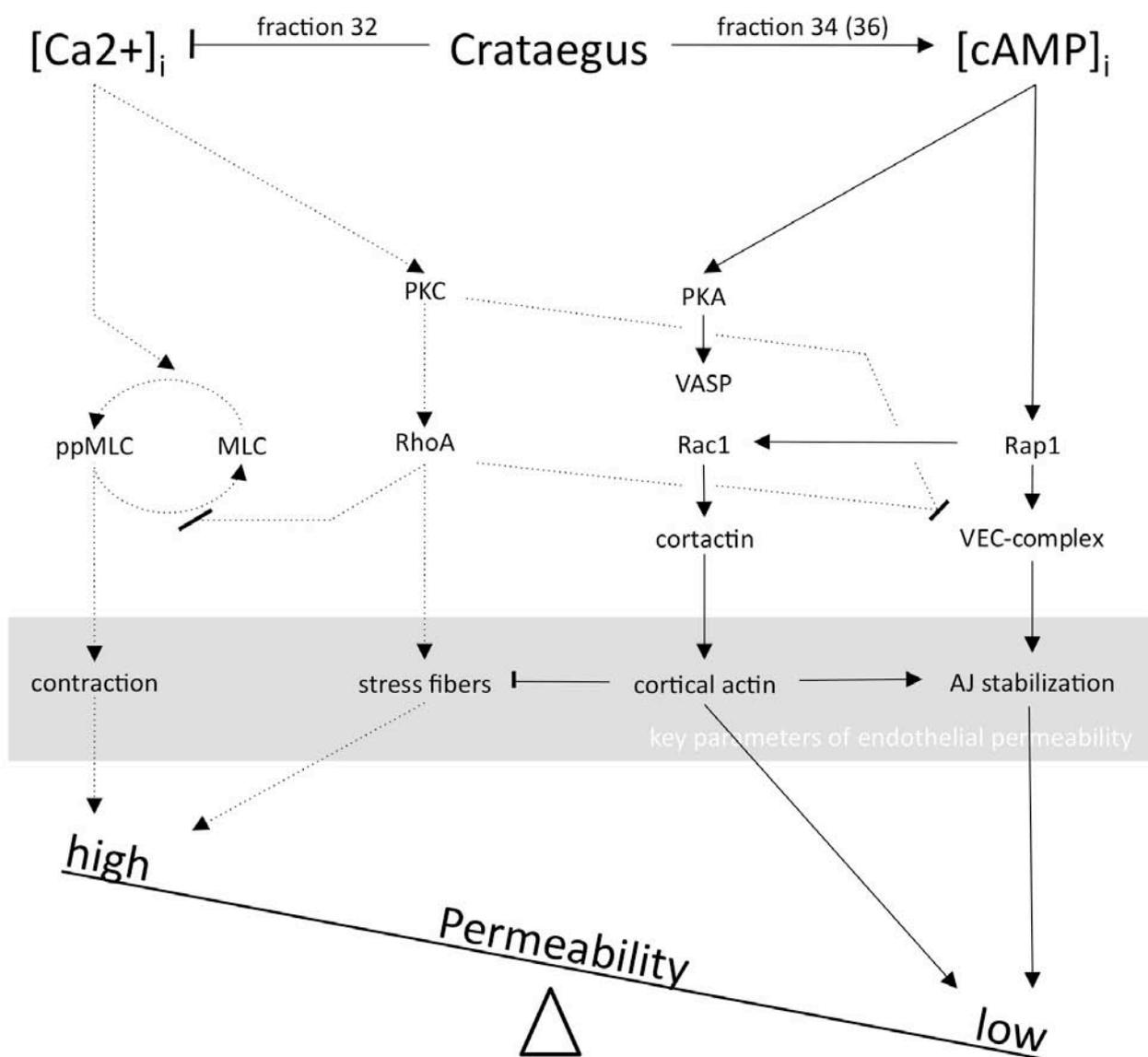

Figure 49: Summary of barrier stabilizing signaling cascades of the Crataegus extract WS® 1442.

VI **ANP**

The cardiovascular hormone atrial natriuretic peptid (ANP) has been recognized to possess important additional functions beyond blood pressure regulation: ANP is expressed by macrophages and is able to influence these immune cells by attenuating their inflammatory response (Kiemer et al., 2005) Thus, we proposed the working hypothesis that ANP could open new therapeutical options for protecting against endothelial barrier dysfunction. In fact, some evidence is given from in vitro and ex vivo experiments that ANP influences an inflammation-increased permeability (Inomata et a., 1987; Lofton et al., Kiemer et al., 2002a). However, data precisely demonstrating a beneficial effect of administrated ANP on inflammatory-induced endothelial barrier dysfunction in vivo were lacking. Moreover, data concerning the effect of ANP on subcellular systems that control permeability were missing.

Therefore, we analyzed the in vivo barrier protective potential, and figured out the sub cellular targets of ANP: adherens junctions and the contractile apparatus. We could show that ANP is an interesting pharmacological compound opening a new therapeutic option for the prevention of vascular leakage.

This study was completed in 2007 and published as an accelerated communication in Mol. Pharmacol. in 2008:

Fürst R, Bubik MF, Bihari P, Mayer BA, Khandoga AG, Hoffmann F, Rehberg M, Krombach F, Zahler S, Vollmar AM. Atrial natriuretic peptide protects against histamine-induced endothelial barrier dysfunction in vivo. ***Mol Pharmacol***. 2008;74(1):1-8.

The manuscript of this publication is subsequently added.

Atrial natriuretic peptide protects against histamine-induced endothelial barrier dysfunction *in vivo*

Robert Fürst, Martin F. Bubik, Peter Bihari, Bettina A. Mayer, Alexander G. Khandoga,

Florian Hoffmann, Markus Rehberg, Fritz Krombach, Stefan Zahler, and Angelika M. Vollmar

Department of Pharmacy, Pharmaceutical Biology, University of Munich, Germany (R.F., M.F.B., B.A.M., F.H., S.Z., A.M.V.); Institute for Surgical Research, University of Munich, Germany (P.B., A.G.K., M.R., F.K.)

Abstract

Endothelial barrier dysfunction is a hallmark of many severe pathologies including sepsis or atherosclerosis. The cardiovascular hormone atrial natriuretic peptide (ANP) has increasingly been suggested to counteract endothelial leakage. Surprisingly, the precise *in vivo* relevance of these observations has never been evaluated. Thus, we aimed to clarify this issue and, moreover, to identify the permeability-controlling subcellular systems that are targeted by ANP. Histamine was used as important pro-inflammatory, permeability-increasing stimulus. Measurements of FITC-dextran extravasation from venules of the mouse cremaster muscle and rat hematocrit values were performed to judge changes of endothelial permeability *in vivo*. Importantly, ANP strongly reduced the histamine-evoked endothelial barrier dysfunction *in vivo*. *In vitro*, ANP blocked the breakdown of transendothelial electrical resistance (TEER) induced by histamine. Moreover, as judged by immunocytochemistry and Western blot analysis, ANP inhibited changes of vascular endothelial (VE)-cadherin, β-catenin, and p120^{ctn} morphology, VE-cadherin and myosin light chain 2 (MLC2) phosphorylation, and F-actin stress fiber formation. These changes seem to be predominantly mediated by the natriuretic peptide receptor (NPR)-A, but not by NPR-C. In summary, we revealed ANP as a potent endothelial barrier protecting agent *in vivo* and identified adherens junctions and the contractile apparatus as subcellular systems targeted by ANP. Thus, our study highlights ANP as an interesting pharmacological compound opening new therapeutic options for preventing endothelial leakage.

The endothelium crucially participates in the regulation of important physiological functions, such as blood pressure, coagulation, or host defense, and it represents a barrier that controls the passage of cells, macromolecules, and fluid between the blood and the adjacent tissue interstitium. Beyond its physiological role, the endothelium is also involved in pathological conditions: Endothelial barrier dysfunction is a hallmark of inflammatory processes and still poses an important therapeutical challenge, since a causal pharmacological treatment is as yet widely lacking.

Endothelial barrier function is mainly governed by the balance between interendothelial cell adhesion. Adherens junctions (AJs) are important subcellular structures responsible for endothelial cell-cell attachment and they represent multiprotein complexes that consist of vascular endothelial (VE)-cadherin, β-catenin, and p120^{ctn}. Under inflammatory conditions VE-cadherin junctions disassemble, thus facilitating paracellular passage, and show an increased tyrosine phosphorylation. Endothelial cell retraction is caused by the activation of the contractile machinery, i.e. the interaction between actin and myosin, which is controlled by phosphorylation of the myosin light chain (MLC). These two regulatory systems could be targets of a successful therapeutic principle.

The cardiovascular hormone atrial natriuretic peptide (ANP) is secreted by the cardiac atria as response to an increased plasma volume. In general, ANP binds to the guanylate cyclase-coupled natriuretic peptide receptor (NPR)-A and NPR-C, which lacks guanylate cyclase function. ANP exerts a hypotensive effect by its natriuretic, diuretic, and vasodilating action. The role of ANP as an important regulator of the cardiovascular system is highlighted by the fact that ANP (carperitide, HANP$^®$) has been approved as drug for the treatment of acute heart failure in Japan. Recently, however, ANP has been recognized to possess important additional functions beyond blood pressure regulation: ANP is expressed by macrophages and is able to influence these immune cells by attenuating their inflammatory response (Kiemer and Vollmar, 2001). Most importantly, ANP exerts anti-inflammatory properties in the endothelium (Kiemer et al.,

2005). Thus, we posed the working hypothesis that ANP could open new therapeutical options for protecting against endothelial barrier dysfunction. In fact, some evidence is given from *in vitro* and *ex vivo* experiments that ANP influences an inflammation-increased permeability (Kiemer et al., 2002a; Lofton et al., 1991; Inomata et al., 1987). However, data precisely demonstrating a beneficial effect of administered ANP on inflammation-induced endothelial barrier dysfunction *in vivo* are lacking. Moreover, data concerning the effect of ANP on subcellular systems that control permeability are missing.

Therefore, aim of the study was (i) to examine the *in vivo* potential of ANP as pharmacological agent counteracting endothelial leakage and (ii) to investigate the influence of ANP on key regulators of endothelial permeability, i.e. the endothelial cell adhesion (VE-cadherin) and contraction system (MLC).

Materials and Methods

Measurement of vascular permeability in the mouse cremaster muscle *in vivo*. Male C57BL/6NCrl mice (Charles River, Sulzfeld, Germany) with 23-25 g bodyweight were used. All experiments were performed according to the German legislation for the protection of animals. Surgery was performed as described by Baez (Baez, 1973). Vascular permeability was analyzed according to Hatekeyama *et al.* (Hatakeyama et al., 2006). Briefly, mice were anesthetized *i.p.* using a ketamine (Pfizer, Karlsruhe, Germany)/xylazine (Bayer, Leverkusen, Germany) mixture. Fluorescein isothiocyanate-dextran (150 kDa, Sigma-Aldrich, Taufkirchen, Germany), Ringer solution (control) and ANP (bolus sufficient to reach 200 nM plasma concentration, AnaSpec/MoBiTec, Göttingen, Germany) were applied into the left femoral artery. 20 min after ANP application, the cremaster was superfused with histamine (30 µM, Sigma-Aldrich) for 10 min. Dexamethasone 21-phosphate (disodium salt, Sigma-Aldrich) was administered *i.p.* (10 mg/kg bodyweight) 2 h before histamine. Postcapillary venules with diameters of 18-30 µm were analyzed. Ten regions of interests (50x50 µm²) in the interstitial tissue (approx. 50 µm distant from the venule) were randomly selected. Intravital microscopic images were recorded with an IMAGO S/N 382KLO345 CCD-camera (TILL Photonics, Gräfelfing, Germany) and subjected to digital image analysis (TILLvisION 4.0, TILL Photonics).

Measurement of rat hematocrit. Male Sprague-Dawley rats (Charles River) with 190-240 g bodyweight were used. All experiments were performed according to the German legislation for the protection of animals. Rats were anesthetized *i.p.* using a fentanyl (Jansen-Cilag, Neuss, Germany)/midazolam (Ratiopharm, Ulm, Germany) mixture and anesthesia was maintained by 1.5% isoflurane (Abbott, Wiesbaden, Germany). Rats were pre-treated for 15 min with ANP (bolus sufficient to reach 200 nM plasma concentration) or PBS, followed by histamine (bolus sufficient to reach 1 µM plasma concentration). Reagents were applied into the jugular vein. 30

min after administration of histamine, blood samples were collected *via* a jugular artery catheter and hematocrit was determined by centrifugation in hematocrit capillaries.

Cell culture. Human umbilical vein endothelial cells (HUVECs) were prepared as previously described (Kiemer et al., 2002a) and cultured in Endothelial Cell Growth Medium (Provitro, Berlin, Germany) containing 10% FBS (Biochrom, Berlin, Germany). Cells were used for experiments at passages 1-3.

Measurement of transendothelial electric resistance (TEER). HUVECs were cultured on collagen A (Biochrom)-coated Millicell 12 mm PCF inserts (Millipore, Schwalbach, Germany). TEER measurements were performed with an Ussing-type chamber. The incubation fluid (HEPES-buffer containing 10% FBS) was circulated by means of humidified air streams at 37°C. A custom-built voltage/current clamp unit in connection with a computer-aided evaluation program was used. Bidirectional square current pulses of 50 µA and 200 ms duration were applied across the monolayer every 2 second. The resistance of the monolayer was calculated by Ohm's law from the induced deflection of the transendothelial voltage.

Immunocyto/histochemistry and confocal laser scanning fluorescence microscopy. HUVECs were cultured on collagen-treated µ-Slides (ibidi, Martinsried, Germany). The NPR-A/B antagonist HS-142-1 (Morishita et al., 1991) was kindly provided by Dr. Y. Matsuda, Kyowa Hakko Kogyo Co., Ltd. (Shizuoka, Japan). cANP was from Bachem (Weil am Rhein, Germany). HUVECs and samples of the mouse cremaster muscle (immediately dissected after histamine treatment) were analyzed immunocyto/ histochemically and by confocal fluorescence microscopy as previously described (Fürst et al., 2005). The following antibodies and reagents were used: mouse monoclonal anti-VE-cadherin (Santa Cruz, Heidelberg, Germany), rabbit polyclonal anti-phospho-Tyr[731]-VE-cadherin (Biosource/Invitrogen, Karlsruhe, Germany), rabbit

polyclonal anti-phospho-MLC2 (Thr[18]/Ser[19]) (Cell Signaling/New England Biolabs, Frankfurt a. M., Germany), rhodamine phalloidin (Invitrogen, Karlsruhe, Germany), Alexa Fluor 633-linked goat anti-mouse (Invitrogen), and Alexa Fluor 488-linked goat anti-rabbit (Invitrogen).

Western blot analysis. HUVEC were cultured in collagen-treated 6-well plates or 60 mm-dishes. Western blot analysis was performed as previously described (Kiemer et al., 2002a). The following antibodies were used: rabbit polyclonal anti-phospho-Tyr[731]-VE-cadherin (Biosource), mouse monoclonal anti-VE-cadherin (Santa Cruz), rabbit polyclonal anit-phospho-MLC2 (Thr[18]/Ser[19]) (Cell Signaling), and MLC2 (Santa Cruz).

Statistical analysis. Statistical analysis was performed with the GraphPad Prism software version 3.03 (GraphPad Software, San Diego, CA). Unpaired *t* test was used to compare two groups. To compare three or more groups, one-way ANOVA followed by Newman-Keuls post hoc test was used.

Results

ANP protects against an inflammation-impaired endothelial barrier function *in vivo*. To judge endothelial permeability *in vivo*, we measured the extravasation of FITC-dextran (150 kDa) *via* intravital fluorescence microscopy in postcapillary venules of the mouse cremaster muscle. 20 min after *i.a.*-application of ANP (bolus sufficient to reach 200 nM plasma concentration), histamine (30 µM) was superfused for 10 min. Histamine evoked a strong leak of FITC-dextran from the blood into the adjacent tissue. ANP clearly abrogated the histamine-induced extravasation (Figure 1A, upper panel). Movies of this extravasation are presented as supplemental data (movie1: control; movie2: histamine; movie3: ANP+histamine). ANP alone (at least in the observed 20 min pre-treatment) seems to slightly increase basal permeability (please note the different ordinate scales in Figure 1A), but this effect is statistically not significant (Figure 1A, lower left panel). Moreover, we aimed to appraise the therapeutical impact of ANP by comparing its beneficial effect to that of a strong anti-inflammatory drug. Thus, we treated mice with a high dose of dexamethasone (*i.p.*, 10 mg/kg, 2 h) before applying histamine (30 µM). The glucocorticoid completely prevented the histamine-induced extravasation of FITC-dextran.

As a second approach for detecting changes of endothelial permeability *in vivo*, we measured hematocrit levels. Rats were treated with histamine (*i.v.* bolus sufficient to reach 1 µM plasma concentration) and hematocrit was determined after 30 min. Due to a reduction of plasma volume, i.e. augmented fluid extravasation, histamine evoked a strong hematocrit increase. ANP (bolus injection sufficient to reach 200 nM plasma concentration, 15 min pre-treatment) significantly reduced the permeability-increasing effect of histamine (Figure 1B).

Characterization of the barrier protecting effect of ANP *in vitro*. Data about an influence of ANP on histamine-induced endothelial leakage *in vitro* are completely lacking. Thus, we first

aimed to verify the effect of ANP in human umbilical vein endothelial cells (HUVECs). To judge permeability changes, transendothelial electrical resistance (TEER) was measured. Upon applying histamine, the electrical resistance of a HUVEC monolayer rapidly drops within seconds and recovers after approx. 10 min. The extent of this effect depends on the histamine concentration used: the resistance is lowered to 55% by 10 µM and to 85% by 1 µM histamine (Figure 1C, left). ANP (1 µM, 30 min pre-treatment) attenuates the drop-down of electrical resistance evoked by histamine (Figure 1C, middle). The statistic analysis of all experiments (n = 4) performed is depicted in the right panel of Figure 1C. The large variability of the ANP+histamine group expresses the fact that in 2 of the 4 experiments ANP did not only attenuate the effect of histamine, but even increased the endothelial resistance, i.e. led to a less permeable endothelium, even if compared to the basal resistance under control conditions. In summary, ANP strongly alleviates endothelial barrier dysfunction induced by histamine *in vitro*. This warrants the usage of this system for the following investigations into the action of ANP on adherens junctions and the contractile machinery.

ANP abolishes the histamine-evoked changes of adherens junction morphology and inhibits the histamine-induced VE-cadherin tyrosine phosphorylation. Histamine (1 µM) leads to strong changes of AJ morphology: the VE-cadherin, β-catenin, and p120^{ctn} seam, properly build in untreated endothelial cells (control), becomes fringy, indicating an AJ disassembly, i.e. the retraction of the inter-endothelial VE-cadherin homodimers and/or an intra-membranous lateral shift (Figure 2 A-C). Endothelial cells treated with ANP alone did not show any effect on AJs. Most importantly, ANP (1 µM, 30 min pretreatment) clearly abolishes the detrimental effects induced by histamine (Figure 2, A-C).

To clarify which natriuretic peptide receptor is involved in mediating the beneficial actions of ANP, we treated cells with the NPR-A/B antagonist HS-142-1 (10 µg/ml, 10 min before ANP) and found that the effects on VE-cadherin disassembly were prevented by this inhibitor. The

NPR-C receptor agonist cANF (1 µM, 30 min before histamine) was not able to mimic the effects of ANP (Figure 2A). Compared to NPR-B, NPR-A binds ANP with a much higher affinity. Thus, our results suggest that the action of ANP is mainly transduced by NPR-A. The C-receptor seems not to be involved.

Phosphorylation of the VE-cadherin Tyr^{731} residue is associated with AJ disassembly and strong endothelial leakage *in vitro* (Potter et al., 2005). First, we verified that Tyr^{731} is also phosphorylated by histamine *in vivo*: Vessels of the mouse cremaster muscle show a strong increase of Tyr^{731} phosphorylation induced by histamine (30 µM, 10 min, Figure 3A) and the same pronounced localization at cell fringes (Figure 3A, longitudinal vessel section) as in the *in vitro* situation (Figure 3B). Most importantly, as shown both by microscopic (Figure 3B) and by Western blot analysis (Figure 3C), ANP completely blocked the histamine-induced VE-cadherin Tyr^{731} phosphorylation. ANP alone did not evoke any alterations of the phosphorylation (Figure 2B). Our data clearly point towards a protecting effect of ANP on the integrity of endothelial adherens junctions.

ANP reduces the histamine-evoked activation of myosin light chain (MLC) and the formation of F-actin stress fibers. The generation of contractile forces (interaction of actin and myosin) is governed by MLC Thr^{18}/Ser^{19}-phosphorylation. Histamine treatment time-dependently leads to a strong phosphorylation of MLC, which was analyzed microscopically (Figure 4A) and by Western blotting (Figure 4B). Moreover, histamine evokes a strong change in F-actin organization. While quiescent endothelial cells show a cortical F-actin localization, histamine induces the formation of long, cell-spanning stress fibers (Figure 4C). ANP clearly reduces both MLC phosphorylation (Figure 4, A and B) and F-actin stress fiber formation (Figure 4C). ANP alone had no effect on these parameters (Figure 4, A-C). These results indicate that ANP prevents histamine-evoked activation of the endothelial cell contraction system.

Furthermore, we investigated which NP receptor subtype was involved in mediating these effects. The NPR-A/B inhibitor HS-142-1 (10 µg/ml, 10 min before ANP) blocked the effects of ANP on MLC phosphorylation (Figure 4A) and stress fiber formation (Figure 4C). The NPR-C agonist cANF (1 µM, 30 min) was not able to show beneficial effects (Figure 4, A and C). Thus, NPR-A/B could be regarded as the major receptors for transducing the actions of ANP in our setting.

Discussion

Many severe pathologies like sepsis or atherosclerosis are associated with an inflammation-impaired endothelial barrier function leading to an increased plasma extravasation, and thus edema formation (Volk and Kox, 2000; Poredos, 2001). Proinflammatory mediators, such as TNF-α or histamine, are involved in the pathogenesis of these disorders and are strong inducers of vascular leakage. Current therapies against an inflammation-evoked barrier dysfunction (e.g. the administration of glucocorticoids or antihistamines) are often insufficient or even fail (van Nieuw Amerongen and van Hinsbergh, 2002). Therefore, new therapeutical options are needed. Strong progress has been made in the recent years concerning the mechanisms involved in the regulation of endothelial permeability (Mehta and Malik, 2006). However, substances that counteract an inflammation-induced vascular leakage by specifically influencing these mechanisms are still largely lacking (van Nieuw Amerongen and van Hinsbergh, 2002).

Initially, the physiological action of the cardiovascular hormone ANP, i.e. the reduction of blood pressure, was mainly ascribed to its natriuretic, diuretic, and vasodilating action. However, ANP was also found to increase endothelial permeability (Huxley et al., 1987). Recently, this effect was proven to be crucial for the chronic control of plasma volume by ANP (Sabrane et al., 2005). Beyond these permeability increasing effects on *quiescent* endothelial cells, ANP has increasingly been recognized to possess barrier protecting actions on an inflammation-*activated* endothelium: We could demonstrate that ANP attenuates the TNF-α-induced expression of adhesion molecules and monocyte chemoattractant protein-1 (MCP-1) by inhibiting NF-κB activation and p38 mitogen-activated protein kinase (MAPK) signaling (Weber et al., 2003; Kiemer et al., 2002b). In this context, we showed that ANP protects against TNF-α-evoked endothelial barrier dysfunction in HUVECs (Kiemer et al., 2002a). ANP was also shown to lower

endothelial leakage *in vitro* induced by the pro-inflammatory stimuli thrombin (Baron et al., 1989) and VEGF (Pedram et al., 2002).

Thus, ANP has commonly been suggested to work as a barrier protecting agent. Surprisingly, an obvious question has as yet not been answered precisely: Can ANP be used as pharmacological agent to prevent endothelial barrier dysfunction *in vivo*? This issue is of special interest, since the drug ANP (carperitide, HANP®) could open new therapeutical options for protecting endothelial barrier function. In the present study, we for the first time show that ANP administered at a pharmacological concentration is able to prevent endothelial leakage in a (histamine-induced) inflammatory setting *in vivo*. Different aspects of endothelial permeability were used as read-out parameters and were all beneficially influenced by ANP: macromolecular permeability (FITC-dextran extravasation), plasma volume/fluid changes (hematocrit), and electrical resistance (TEER measurement). Compared to the maximal increase of FITC-dextran extravasation induced by histamine (time point 45 min in Figure 1A), ANP led to approx. 65% reduction. Due to this pronounced effect, a therapeutical impact of ANP is not unlikely. A complete blockage of the deleterious effect of histamine was observed in the presence of a extraordinary high dosage of the glucocorticoid dexamethasone, a highly potent anti-inflammatory drug.

Former studies dealing with ANP and vascular permeability served as valuable hints toward an *in vivo* relevance of ANP as barrier protecting agent. However, these reports did not concisely test the hypothesis that administered ANP exerts beneficial effects on endothelial barrier dysfunction *in vivo*, because they (i) either used *ex vivo* models or (ii) focused on the *endogenous* ANP system: (i) Three older reports demonstrate that pharmacological concentrations of ANP attenuate changes of pulmonary wet weight induced by toxic agents like reactive oxygen metabolites, paraquat, or arachidonic acid in *ex vivo* models of isolated-perfused lungs from rabbits or guinea pigs (Lofton et al., 1991; Inomata et al., 1987; Imamura et al., 1988). (ii) Blockade of *endogenous* ANP was shown to deteriorate pulmonary edema

formation in rats suffering from high altitude-induced (Irwin et al., 2001) or HCl-evoked (Wakabayashi et al., 1990) pulmonary vascular leakage, whereas mice lacking the major ANP-degrading enzyme neutral endopeptidase were found to be less susceptible for pulmonary leakage (Irwin et al., 2005a). Interestingly, Pedram *et al.* showed that VEGF-induced vascular leakage is attenuated in ANP-overexpressing mice, whereas these mice are not protected against histamine-evoked leakage (Pedram et al., 2002). This might be due to the much lower ANP levels in these animals (plasma level: ~40 pM) compared to our setting, in which ANP is exogenously supplied to reach a pharmacological plasma concentration of 200 nM. Recently, our group could demonstrate that ANP-treated mice (plasma level: ~35 nM) are protected against LPS-induced septic shock (Ladetzki-Baehs et al., 2007). Since endothelial hyperpermeability is an important pathological feature of sepsis, it can be speculated that the barrier protecting effect of ANP contributes to the beneficial action in the mouse septic shock model. Our results suggest that pharmacological concentrations of ANP show additional, highly valuable effects beyond its action as an endogenous regulator of permeability.

Adherens junctions and the contractile apparatus are key players in the regulation of endothelial permeability. Both the loss of VE-cadherin function and the activation of MLC result in decreased transendothelial electrical resistance (Garcia et al., 1997; van Buul et al., 2005) and increased macromolecular permeability (Nwariaku et al., 2002; Garcia et al., 1995). Studies investigating the action of ANP on these key systems are as yet completely lacking. We provide for the first time evidence that ANP interacts with these systems, since we showed that ANP attenuates both adherens junction disassembly (morphological changes and Tyr[731] phosphorylation of VE-cadherin) and activation of the contractile apparatus (phosphorylation of MLC and rearrangement of F-actin) induced by histamine. Furthermore, we could demonstrate that ANP exerts these effects predominantly via the natriuretic peptide receptor (NPR)-A. Since this receptors represent particulate guanylate cyclases, it can be speculated that the actions of ANP might be mediated via the second messenger cyclic guanosine monophosphate (cGMP).

Our results add further support to the hypothesis that ANP is an endothelium protecting agent, since it directly counteracts the detrimental effects of proinflammatory mediators on endothelial barrier function.

Only few data exist about the action of ANP on subcellular systems contributing to permeability regulation. We and others could demonstrate that ANP inhibits F-actin stress fiber formation induced by TNF-α (Kiemer et al., 2002a; Irwin et al., 2005b) or VEGF (Pedram et al., 2002). Interestingly, one study reports that ANP influences tight junctions in bovine aortic endothelial cells (Pedram et al., 2002). In contrast to the dense aortic endothelium, the occurrence of tight junctions is limited in the venous endothelium (Ogunrinade et al., 2002), which represents the predominant site of endothelial hyperpermeability and was investigated in the present study.

In summary, we have revealed ANP as a potent endothelial barrier protecting agent *in vivo*. Moreover, we have identified adherens junctions and the contractile apparatus as important subcellular systems targeted by ANP. Most importantly, our study highlights ANP as an interesting pharmacological compound opening a new therapeutic option for the prevention of vascular leakage. This warrants further efforts aiming for an expansion of the therapeutic indications of natriuretic peptides.

References

Baez S (1973) An Open Cremaster Muscle Preparation for the Study of Blood Vessels by in Vivo Microscopy. *Microvasc Res* **5**:384-394.

Baron DA, Lofton CE, Newman WH and Currie MG (1989) Atriopeptin Inhibition of Thrombin-Mediated Changes in the Morphology and Permeability of Endothelial Monolayers. *Proc Natl Acad Sci U S A* **86**:3394-3398.

Fürst R, Brueckl C, Kuebler WM, Zahler S, Krötz F, Görlach A, Vollmar AM and Kiemer AK (2005) Atrial Natriuretic Peptide Induces Mitogen-Activated Protein Kinase Phosphatase-1 in Human Endothelial Cells Via Rac1 and NAD(P)H Oxidase/Nox2-Activation. *Circ Res* **96**:43-53.

Garcia JG, Davis HW and Patterson CE (1995) Regulation of Endothelial Cell Gap Formation and Barrier Dysfunction: Role of Myosin Light Chain Phosphorylation. *J Cell Physiol* **163**:510-522.

Garcia JG, Schaphorst KL, Shi S, Verin AD, Hart CM, Callahan KS and Patterson CE (1997) Mechanisms of Ionomycin-Induced Endothelial Cell Barrier Dysfunction. *Am J Physiol* **273**:L172-L184.

Hatakeyama T, Pappas PJ, Hobson RW, Boric MP, Sessa WC and Duran WN (2006) Endothelial Nitric Oxide Synthase Regulates Microvascular Hyperpermeability in Vivo. *J Physiol* **574**:275-281.

Huxley VH, Tucker VL, Verburg KM and Freeman RH (1987) Increased Capillary Hydraulic Conductivity Induced by Atrial Natriuretic Peptide. *Circ Res* **60**:304-307.

Imamura T, Ohnuma N, Iwasa F, Furuya M, Hayashi Y, Inomata N, Ishihara T and Noguchi T (1988) Protective Effect of Alpha-Human Atrial Natriuretic Polypeptide (Alpha-HANP) on Chemical-Induced Pulmonary Edema. *Life Sci* **42**:403-414.

Inomata N, Ohnuma N, Furuya M, Hayashi Y, Kanai Y, Ishihara T, Noguchi T and Matsuo H (1987) Alpha-Human Atrial Natriuretic Peptide (Alpha-HANP) Prevents Pulmonary Edema Induced by Arachidonic Acid Treatment in Isolated Perfused Lung From Guinea Pig. *Jpn J Pharmacol* **44**:211-214.

Irwin DC, Patot MT, Tucker A and Bowen R (2005a) Neutral Endopeptidase Null Mice Are Less Susceptible to High Altitude-Induced Pulmonary Vascular Leak. *High Alt Med Biol* **6**:311-319.

Irwin DC, Rhodes J, Baker DC, Nelson SE and Tucker A (2001) Atrial Natriuretic Peptide Blockade Exacerbates High Altitude Pulmonary Edema in Endotoxin-Primed Rats. *High Alt Med Biol* **2**:349-360.

Irwin DC, Tissot van Patot MC, Tucker A and Bowen R (2005b) Direct ANP Inhibition of Hypoxia-Induced Inflammatory Pathways in Pulmonary Microvascular and Macrovascular Endothelial Monolayers. *Am J Physiol Lung Cell Mol Physiol* **288**:L849-L859.

Kiemer AK, Fürst R and Vollmar AM (2005) Vasoprotective Actions of the Atrial Natriuretic Peptide. *Curr Med Chem Cardiovasc Hematol Agents* **3**:11-21.

Kiemer AK and Vollmar AM (2001) The Atrial Natriuretic Peptide Regulates the Production of Inflammatory Mediators in Macrophages. *Ann Rheum Dis* **60 Suppl 3**:iii68-iii70.

Kiemer AK, Weber NC, Fürst R, Bildner N, Kulhanek-Heinze S and Vollmar AM (2002a) Inhibition of P38 MAPK Activation Via Induction of MKP-1: Atrial Natriuretic Peptide

Reduces TNF-a-Induced Actin Polymerization and Endothelial Permeability. *Circ Res* **90**:874-881.

Kiemer AK, Weber NC and Vollmar AM (2002b) Induction of IkB: Atrial Natriuretic Peptide As a Regulator of the NF-KB Pathway. *Biochem Biophys Res Commun* **295**:1068-1076.

Ladetzki-Baehs K, Keller M, Kiemer AK, Koch E, Zahler S, Wendel A and Vollmar AM (2007) Atrial Natriuretic Peptide, a Regulator of Nuclear Factor-KappaB Activation in Vivo. *Endocrinology* **148**:332-336.

Lofton CE, Baron DA, Heffner JE, Currie MG and Newman WH (1991) Atrial Natriuretic Peptide Inhibits Oxidant-Induced Increases in Endothelial Permeability. *J Mol Cell Cardiol* **23**:919-927.

Mehta D and Malik AB (2006) Signaling Mechanisms Regulating Endothelial Permeability. *Physiol Rev* **86**:279-367.

Morishita Y, Sano T, Ando K, Saitoh Y, Kase H, Yamada K and Matsuda Y (1991) Microbial Polysaccharide, HS-142-1, Competitively and Selectively Inhibits ANP Binding to Its Guanylyl Cyclase-Containing Receptor. *Biochem Biophys Res Commun* **176**:949-957.

Nwariaku FE, Liu Z, Zhu X, Turnage RH, Sarosi GA and Terada LS (2002) Tyrosine Phosphorylation of Vascular Endothelial Cadherin and the Regulation of Microvascular Permeability. *Surgery* **132**:180-185.

Ogunrinade O, Kameya GT and Truskey GA (2002) Effect of Fluid Shear Stress on the Permeability of the Arterial Endothelium. *Ann Biomed Eng* **30**:430-446.

Pedram A, Razandi M and Levin ER (2002) Deciphering Vascular Endothelial Cell Growth Factor/Vascular Permeability Factor Signaling to Vascular Permeability. Inhibition by Atrial Natriuretic Peptide. *J Biol Chem* **277**:44385-44398.

Poredos P (2001) Endothelial Dysfunction in the Pathogenesis of Atherosclerosis. *Clin Appl Thromb Hemost* **7**:276-280.

Potter MD, Barbero S and Cheresh DA (2005) Tyrosine Phosphorylation of VE-Cadherin Prevents Binding of P120- and Beta-Catenin and Maintains the Cellular Mesenchymal State. *J Biol Chem* **280**:31906-31912.

Sabrane K, Kruse MN, Fabritz L, Zetsche B, Mitko D, Skryabin BV, Zwiener M, Baba HA, Yanagisawa M and Kuhn M (2005) Vascular Endothelium Is Critically Involved in the Hypotensive and Hypovolemic Actions of Atrial Natriuretic Peptide. *J Clin Invest* **115**:1666-1674.

van Buul JD, Anthony EC, Fernandez-Borja M, Burridge K and Hordijk PL (2005) Proline-Rich Tyrosine Kinase 2 (Pyk2) Mediates Vascular Endothelial-Cadherin-Based Cell-Cell Adhesion by Regulating Beta-Catenin Tyrosine Phosphorylation. *J Biol Chem* **280**:21129-21136.

van Nieuw Amerongen GP and van Hinsbergh VW (2002) Targets for Pharmacological Intervention of Endothelial Hyperpermeability and Barrier Function. *Vascul Pharmacol* **39**:257-272.

Volk T and Kox WJ (2000) Endothelium Function in Sepsis. *Inflamm Res* **49**:185-198.

Wakabayashi G, Ueda M, Aikawa N, Naruse M and Abe O (1990) Release of ANP and Its Physiological Role in Pulmonary Injury Due to HCl. *Am J Physiol* **258**:R690-R696.

Weber NC, Blumenthal SB, Hartung T, Vollmar AM and Kiemer AK (2003) ANP Inhibits TNF-Alpha-Induced Endothelial MCP-1 Expression - Involvement of P38 MAPK and MKP-1. *J Leukoc Biol* **74**:932-941.

Figures

A
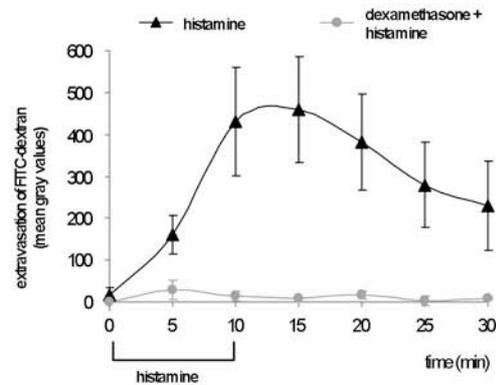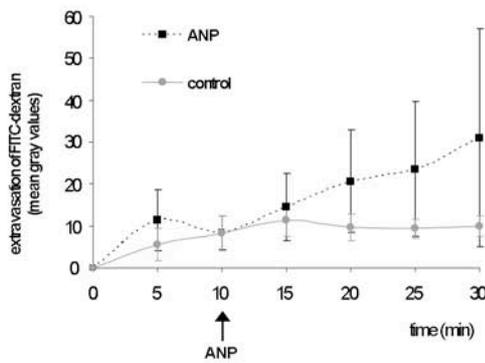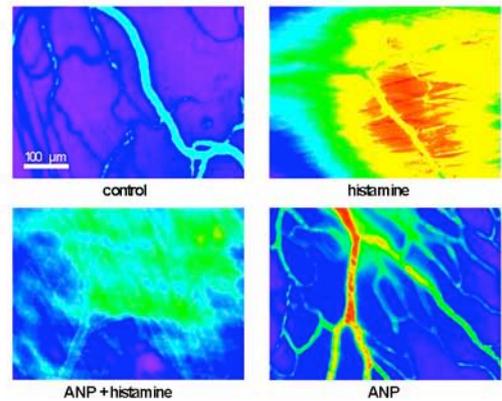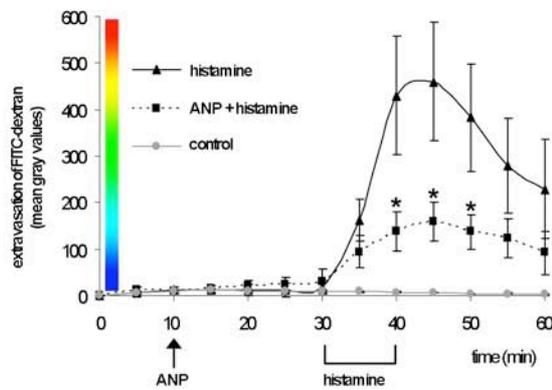
B
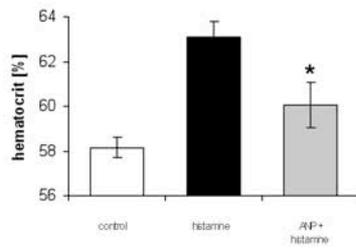
C
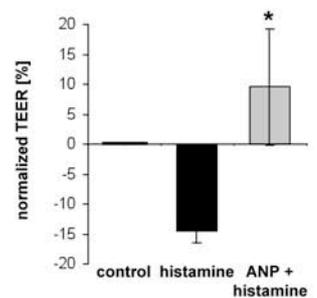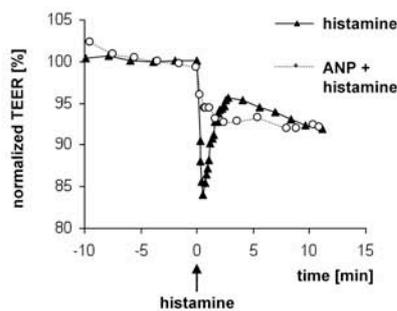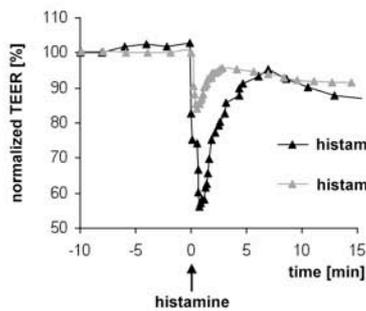
Figure 1. ANP attenuates histamine-induced increase of endothelial permeability *in vivo* and *in vitro*.

A, Extravasation of FITC-dextran (150 kDa) from venules of the mouse cremaster muscle was measured. Upper left panel: Mice were pre-treated with Ringer solution (control and histamine group), or with ANP (*i.a.* bolus injection sufficient to reach 200 nM plasma concentration). After 20 min, histamine (30 µM) was superfused for 10 min (histamine and ANP+histamine group). Data are expressed as mean ± SEM (*n* = 6). *$p \leq 0.05$ vs. histamine. Upper right panel: One representative image is shown for each group of treatment (at time point 45 min for control, histamine, and histamine+ANP; at time point 30 min for ANP alone). Videos showing this FITC-dextran extravasation (movie1: control; movie2: histamine; movie3: ANP+histamine) are available as supplemental data. Lower left panel: Mice were treated with Ringer solution (control group) or with ANP (*i.a.* bolus injection sufficient to reach 200 nM plasma concentration). Data are expressed as mean ± SEM (*n* = 6). Lower right panel: Mice were pre-treated with Ringer solution (histamine group) or with dexamethasone (*i.p.*, 10 mg/kg bodyweight) for 2 h. Histamine (30 µM) was superfused for 10 min. Data are expressed as mean ± SEM (*n* = 2).

B, Plasma volume changes were determined by measuring hematocrit values. Rats were pre-treated with PBS (control) or with ANP (*i.v.*, bolus injection sufficient to reach 200 nM plasma concentration). After 15 min, histamine was applied (*i.v.*, bolus injection sufficient to reach 1 µM plasma concentration). 30 min later, blood samples were taken and hematocrit was measured. Data are expressed as mean ± SEM (*n* = 3). *$p \leq 0.05$ vs. histamine.

C, Transendothelial electrical resistance (TEER) was used to judge changes in endothelial permeability of HUVECs. Left panel: Histamine concentration-dependently decreases TEER values. Middle panel: ANP (1 µM, 30 min pre-treatment) attenuates the histamine-induced decrease of electrical resistance. One representative graph out of 4 independent experiments is shown, each. Right panel: Statistical analysis of all experiments performed (*n* = 4). Data are expressed as mean ± SEM. *$p \leq 0.05$ vs. histamine.

A

B

C
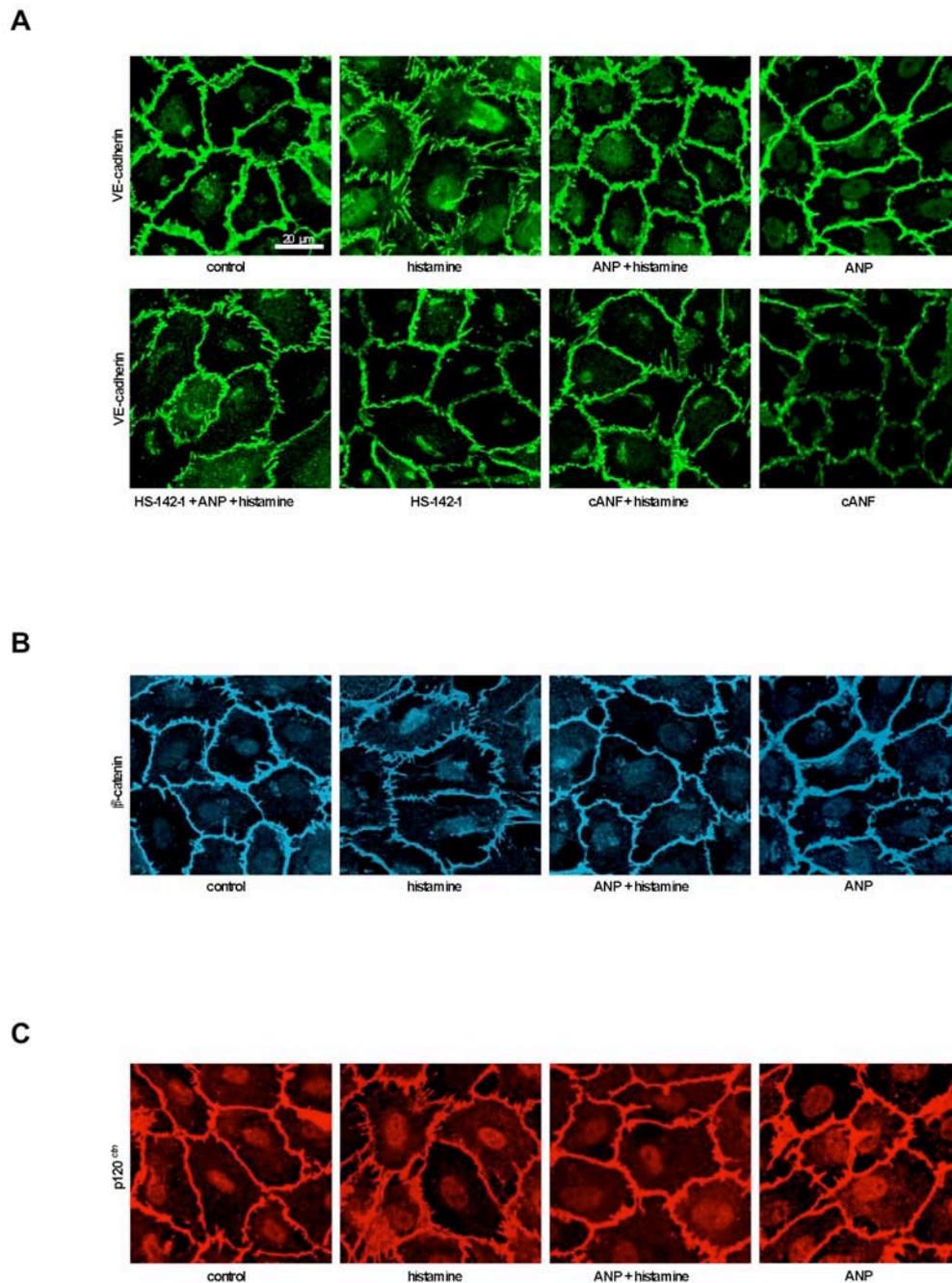
Figure 2. ANP inhibits the histamine-evoked morphological changes of adherens junctions. HUVECs were left untreated (control) or were treated with histamine (1 µM, 2 min) alone or in combination with ANP (1 µM, 30 min pre-treatment) or the NPR-C agonist cANF (1 µM, 30 min pre-treatment). The NPR-A/B receptor antagonist HS142-1 (10 µg/ml) was given 10 min before ANP. Immunocytochemistry and confocal fluorescence microscopy were performed to analyze

morphological changes of (A) VE-cadherin, (B) β-catenin, and (C) p120^{ctn}. One representative

image out of three independent experiments is shown, each.
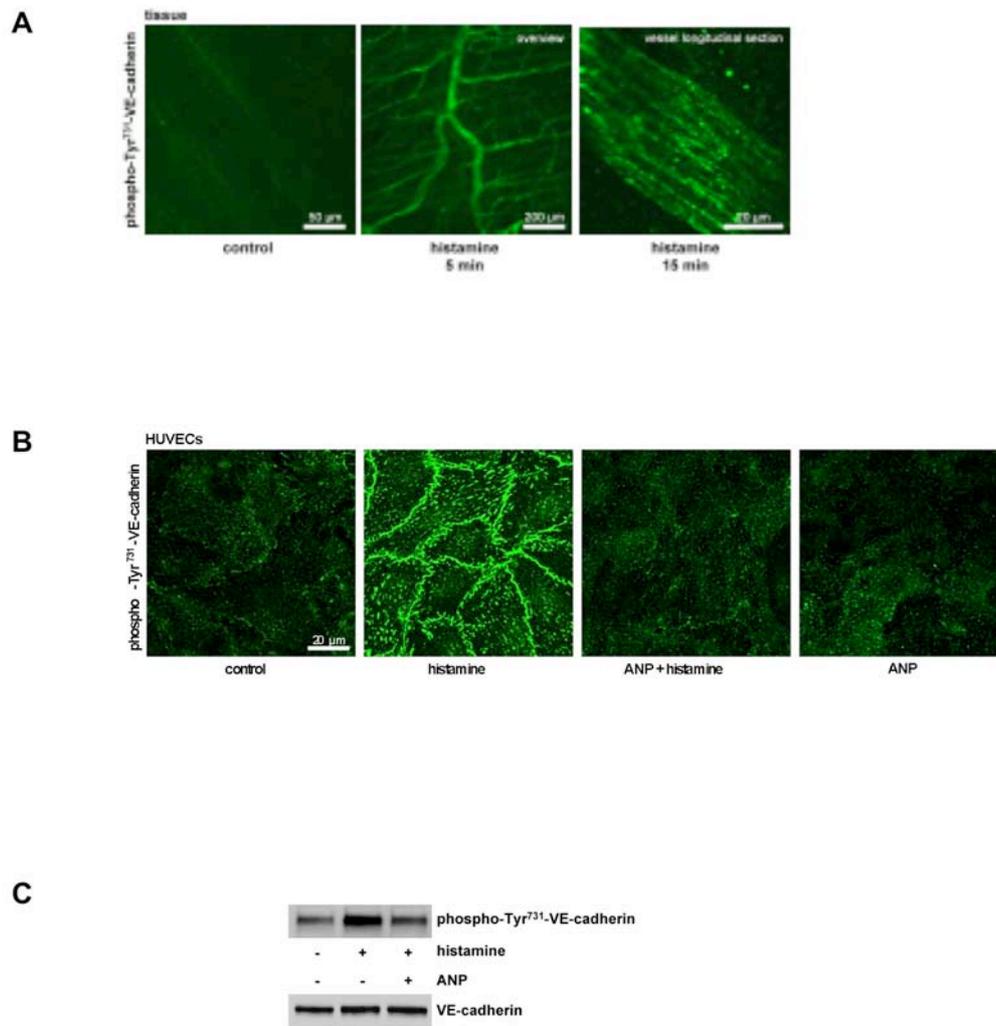
Figure 3. ANP blocks histamine-induced VE-cadherin Tyr^{731}-phosphorylation. A, Histamine

induces phosphorylation of VE-cadherin at Tyr^{731} *in vivo*. Mice were treated as described in

Figure 1A. Samples of the mouse cremaster muscle were analyzed via immunohistochemistry

and confocal fluorescence microscopy. Histamine (30 μM) was superfused for the indicated

times. One representative image out of 3 independent experiments is shown. B-C, ANP inhibits

histamine-induced VE-cadherin Tyr^{731}-phosphorylation *in vitro*. HUVECs were left untreated

(control),   were   treated   with   histamine

(1 μM, 5 min) or ANP (1 μM, 30 min) alone, or with ANP (1 μM) 30 min before histamine was

applied. The VE-cadherin Tyr[731]-phosphorylation was analyzed via immunocytochemistry and confocal fluorescence microscopy (B, *n* = 3) or biochemically via Western blot (C, *n* = 2).
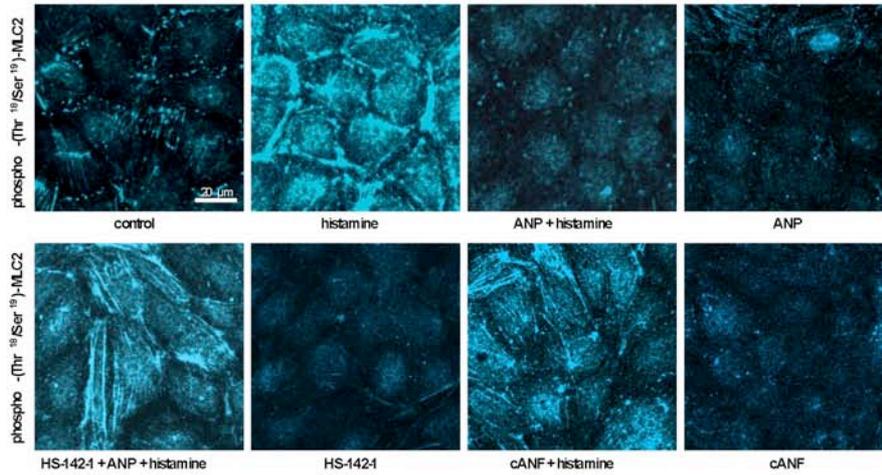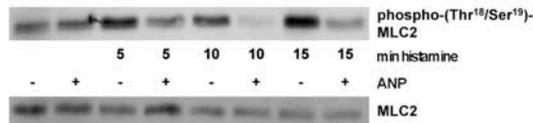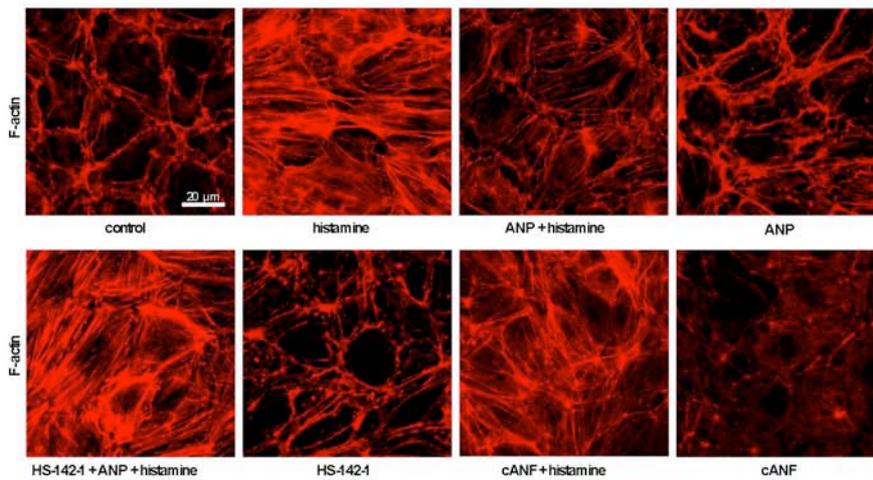

Figure 4. ANP inhibits histamine-induced MLC2 Thr[18]/Ser[19]-phosphorylation and stress fiber formation. A-C, HUVECs were left untreated (control) or were treated with histamine (1 µM, 5

min) alone or in combination with ANP (1 µM, 30 min pre-treatment) or the NPR-C agonist cANF (1 µM, 30 min pre-treatment). The NPR-A/B receptor antagonist HS142-1 (10 µg/ml) was given 10 min before ANP. MLC2 Thr[18]/Ser[19]-phosphorylation and F-actin were analyzed via immunocytochemistry and confocal fluorescence microscopy (A, C). MLC2 Thr[18]/Ser[19]-phosphorylation was additionally analyzed via Western blot (B). One representative image out of at least three independent experiments is shown, each.

VII REFERENCES

1.   Aird WC. Endothelium in health and disease. *Pharmacol Rep.* 2008;60(1):139-143.
2.   Pries AR, Secomb TW, Gaehtgens P. The endothelial surface layer. *Pflugers Arch.* 2000;440(5):653-666.
3.   Pasyk KA, Jakobczak BA. Vascular endothelium: recent advances. *Eur J Dermatol.* 2004;14(4):209-213.
4.   Vandenbroucke E, Mehta D, Minshall R, Malik AB. Regulation of endothelial junctional permeability. *Ann N Y Acad Sci.* 2008;1123:134-145.
5.   Blum A. Heart failure--new insights. *Isr Med Assoc J.* 2009;11(2):105-111.
6.   Mann DL. Inflammatory mediators and the failing heart: past, present, and the foreseeable future. *Circ Res.* 2002;91(11):988-998.
7.   Hansson GK. Inflammatory mechanisms in atherosclerosis. *J Thromb Haemost.* 2009;7 Suppl 1:328-331.
8.   Libby P. Inflammation in atherosclerosis. *Nature.* 2002;420(6917):868-874.
9.   von Haehling S, Schefold JC, Lainscak M, Doehner W, Anker SD. Inflammatory biomarkers in heart failure revisited: much more than innocent bystanders. *Heart Fail Clin.* 2009;5(4):549-560.
10.   Ryan S, Taylor CT, McNicholas WT. Systemic inflammation: a key factor in the pathogenesis of cardiovascular complications in obstructive sleep apnoea syndrome? *Thorax.* 2009;64(7):631-636.
11.   Sprague AH, Khalil RA. Inflammatory cytokines in vascular dysfunction and vascular disease. *Biochem Pharmacol.* 2009;78(6):539-552.
12.   Weis SM. Vascular permeability in cardiovascular disease and cancer. *Curr Opin Hematol.* 2008;15(3):243-249.
13.   Lopez AD, Mathers CD, Ezzati M, Jamison DT, Murray CJ. Global and regional burden of disease and risk factors, 2001: systematic analysis of population health data. *Lancet.* 2006;367(9524):1747-1757.
14.   Lawson C, Wolf S. ICAM-1 signaling in endothelial cells. *Pharmacol Rep.* 2009;61(1):22-32.
15.   Dejana E, Tournier-Lasserve E, Weinstein BM. The control of vascular integrity by endothelial cell junctions: molecular basis and pathological implications. *Dev Cell.* 2009;16(2):209-221.
16.   Sandoval R, Malik AB, Naqvi T, Mehta D, Tiruppathi C. Requirement for Ca2+ signaling in the mechanism of thrombin-induced increase in endothelial permeability. *Am J Physiol Lung Cell Mol Physiol.* 2001;280(2):L239-247.
17.   Prasain N, Stevens T. The actin cytoskeleton in endothelial cell phenotypes. *Microvasc Res.* 2009;77(1):53-63.
18.   Dejana E, Orsenigo F, Lampugnani MG. The role of adherens junctions and VE-cadherin in the control of vascular permeability. *J Cell Sci.* 2008;121(Pt 13):2115-2122.
19.   Mehta D, Malik AB. Signaling mechanisms regulating endothelial permeability. *Physiol Rev.* 2006;86(1):279-367.
20.   Malik AB, Lo SK, Bizios R. Thrombin-induced alterations in endothelial permeability. *Ann N Y Acad Sci.* 1986;485:293-309.
21.   Rabiet MJ, Plantier JL, Rival Y, Genoux Y, Lampugnani MG, Dejana E. Thrombin-induced increase in endothelial permeability is associated with

changes in cell-to-cell junction organization. *Arterioscler Thromb Vasc Biol.* 1996;16(3):488-496.

22. Konstantoulaki M, Kouklis P, Malik AB. Protein kinase C modifications of VE-cadherin, p120, and beta-catenin contribute to endothelial barrier dysregulation induced by thrombin. *Am J Physiol Lung Cell Mol Physiol.* 2003;285(2):L434-442.

23. Tiruppathi C, Minshall RD, Paria BC, Vogel SM, Malik AB. Role of Ca2+ signaling in the regulation of endothelial permeability. *Vascul Pharmacol.* 2002;39(4-5):173-185.

24. Nilius B, Droogmans G. Ion channels and their functional role in vascular endothelium. *Physiol Rev.* 2001;81(4):1415-1459.

25. Cioffi DL, Stevens T. Regulation of endothelial cell barrier function by store-operated calcium entry. *Microcirculation.* 2006;13(8):709-723.

26. Tiruppathi C, Ahmmed GU, Vogel SM, Malik AB. Ca2+ signaling, TRP channels, and endothelial permeability. *Microcirculation.* 2006;13(8):693-708.

27. Sehrawat S, Cullere X, Patel S, Italiano J, Jr., Mayadas TN. Role of Epac1, an exchange factor for Rap GTPases, in endothelial microtubule dynamics and barrier function. *Mol Biol Cell.* 2008;19(3):1261-1270.

28. Waschke J, Drenckhahn D, Adamson RH, Barth H, Curry FE. cAMP protects endothelial barrier functions by preventing Rac-1 inhibition. *Am J Physiol Heart Circ Physiol.* 2004;287(6):H2427-2433.

29. Farmer PJ, Bernier SG, Lepage A, Guillemette G, Regoli D, Sirois P. Permeability of endothelial monolayers to albumin is increased by bradykinin and inhibited by prostaglandins. *Am J Physiol Lung Cell Mol Physiol.* 2001;280(4):L732-738.

30. Langeler EG, van Hinsbergh VW. Norepinephrine and iloprost improve barrier function of human endothelial cell monolayers: role of cAMP. *Am J Physiol.* 1991;260(5 Pt 1):C1052-1059.

31. Hippenstiel S, Witzenrath M, Schmeck B, Hocke A, Krisp M, Krull M, Seybold J, Seeger W, Rascher W, Schutte H, Suttorp N. Adrenomedullin reduces endothelial hyperpermeability. *Circ Res.* 2002;91(7):618-625.

32. Yuan SY. Protein kinase signaling in the modulation of microvascular permeability. *Vascul Pharmacol.* 2002;39(4-5):213-223.

33. Kawasaki H, Springett GM, Mochizuki N, Toki S, Nakaya M, Matsuda M, Housman DE, Graybiel AM. A family of cAMP-binding proteins that directly activate Rap1. *Science.* 1998;282(5397):2275-2279.

34. Kooistra MR, Corada M, Dejana E, Bos JL. Epac1 regulates integrity of endothelial cell junctions through VE-cadherin. *FEBS Lett.* 2005;579(22):4966-4972.

35. de Rooij J, Zwartkruis FJ, Verheijen MH, Cool RH, Nijman SM, Wittinghofer A, Bos JL. Epac is a Rap1 guanine-nucleotide-exchange factor directly activated by cyclic AMP. *Nature.* 1998;396(6710):474-477.

36. Schlegel N, Waschke J. VASP is involved in cAMP-mediated Rac 1 activation in microvascular endothelial cells. *Am J Physiol Cell Physiol.* 2009;296(3):C453-462.

37. Roscioni SS, Elzinga CR, Schmidt M. Epac: effectors and biological functions. *Naunyn Schmiedebergs Arch Pharmacol.* 2008;377(4-6):345-357.

38. Bos JL. Epac proteins: multi-purpose cAMP targets. *Trends Biochem Sci.* 2006;31(12):680-686.

39. Baumer Y, Spindler V, Werthmann RC, Bunemann M, Waschke J. Role of Rac 1 and cAMP in endothelial barrier stabilization and thrombin-induced barrier breakdown. *J Cell Physiol.* 2009.

40. Baumer Y, Drenckhahn D, Waschke J. cAMP induced Rac 1-mediated cytoskeletal reorganization in microvascular endothelium. *Histochem Cell Biol.* 2008;129(6):765-778.

41. Pannekoek WJ, Kooistra MR, Zwartkruis FJ, Bos JL. Cell-cell junction formation: the role of Rap1 and Rap1 guanine nucleotide exchange factors. *Biochim Biophys Acta.* 2009;1788(4):790-796.

42. Joseph G, Zhao Y, Klaus W. [Pharmacologic action profile of crataegus extract in comparison to epinephrine, amirinone, milrinone and digoxin in the isolated perfused guinea pig heart]. *Arzneimittelforschung.* 1995;45(12):1261-1265.

43. Popping S, Rose H, Ionescu I, Fischer Y, Kammermeier H. Effect of a hawthorn extract on contraction and energy turnover of isolated rat cardiomyocytes. *Arzneimittelforschung.* 1995;45(11):1157-1161.

44. Schwinger RH, Pietsch M, Frank K, Brixius K. Crataegus special extract WS 1442 increases force of contraction in human myocardium cAMP-independently. *J Cardiovasc Pharmacol.* 2000;35(5):700-707.

45. Müller A, Linke W, Klaus W. Crataegus extract blocks potassium currents in guinea pig ventricular cardiac myocytes. *Planta Med.* 1999;65(4):335-339.

46. Brixius K, Willms S, Napp A, Tossios P, Ladage D, Bloch W, Mehlhorn U, Schwinger RH. Crataegus special extract WS 1442 induces an endothelium-dependent, NO-mediated vasorelaxation via eNOS-phosphorylation at serine 1177. *Cardiovasc Drugs Ther.* 2006;20(3):177-184.

47. Veveris M, Koch E, Chatterjee SS. Crataegus special extract WS 1442 improves cardiac function and reduces infarct size in a rat model of prolonged coronary ischemia and reperfusion. *Life Sci.* 2004;74(15):1945-1955.

48. Chatterjee SS, Koch E, Jaggy H, Krzeminski T. [In vitro and in vivo studies on the cardioprotective action of oligomeric procyanidins in a Crataegus extract of leaves and blooms]. *Arzneimittelforschung.* 1997;47(7):821-825.

49. Zapfe jun G. Clinical efficacy of crataegus extract WS 1442 in congestive heart failure NYHA class II. *Phytomedicine.* 2001;8(4):262-266.

50. Tauchert M. Efficacy and safety of crataegus extract WS 1442 in comparison with placebo in patients with chronic stable New York Heart Association class-III heart failure. *Am Heart J.* 2002;143(5):910-915.

51. Pittler MH, Schmidt K, Ernst E. Hawthorn extract for treating chronic heart failure: meta-analysis of randomized trials. *Am J Med.* 2003;114(8):665-674.

52. Holubarsch CJ, Colucci WS, Meinertz T, Gaus W, Tendera M. The efficacy and safety of Crataegus extract WS 1442 in patients with heart failure: the SPICE trial. *Eur J Heart Fail.* 2008;10(12):1255-1263.

53. Tamargo J, Caballero R, Gomez R, Barana A, Amoros I, Delpon E. Investigational positive inotropic agents for acute heart failure. *Cardiovasc Hematol Disord Drug Targets.* 2009;9(3):193-205.

54. Volk T, Kox WJ. Endothelium function in sepsis. *Inflamm Res.* 2000;49(5):185-198.

55. Cho S, Atwood JE. Peripheral edema. *Am J Med.* 2002;113(7):580-586.

56. Poredos P. Endothelial dysfunction in the pathogenesis of atherosclerosis. *Clin Appl Thromb Hemost.* 2001;7(4):276-280.

57. Wilson J. The bronchial microcirculation in asthma. *Clin Exp Allergy.* 2000;30 Suppl 1:51-53.

58. Anselm E, Socorro VF, Dal-Ros S, Schott C, Bronner C, Schini-Kerth VB. Crataegus special extract WS 1442 causes endothelium-dependent relaxation via a redox-sensitive Src- and Akt-dependent activation of endothelial NO synthase but not via activation of estrogen receptors. *J Cardiovasc Pharmacol.* 2009;53(3):253-260.

59. Sica DA. Edema mechanisms in the patient with heart failure and treatment options. *Heart Fail Clin.* 2008;4(4):511-518.

60. Ades EW, Candal FJ, Swerlick RA, George VG, Summers S, Bosse DC, Lawley TJ. HMEC-1: establishment of an immortalized human microvascular endothelial cell line. *J Invest Dermatol.* 1992;99(6):683-690.

61. Bouis D, Hospers GA, Meijer C, Molema G, Mulder NH. Endothelium in vitro: a review of human vascular endothelial cell lines for blood vessel-related research. *Angiogenesis.* 2001;4(2):91-102.

62. Li H, Oehrlein SA, Wallerath T, Ihrig-Biedert I, Wohlfart P, Ulshofer T, Jessen T, Herget T, Forstermann U, Kleinert H. Activation of protein kinase C alpha and/or epsilon enhances transcription of the human endothelial nitric oxide synthase gene. *Mol Pharmacol.* 1998;53(4):630-637.

63. Schreiber E, Matthias P, Muller MM, Schaffner W. Rapid detection of octamer binding proteins with 'mini-extracts', prepared from a small number of cells. *Nucleic Acids Res.* 1989;17(15):6419.

64. Bradford MM. A rapid and sensitive method for the quantitation of microgram quantities of protein utilizing the principle of protein-dye binding. *Anal Biochem.* 1976;72:248-254.

65. Smith PK, Krohn RI, Hermanson GT, Mallia AK, Gartner FH, Provenzano MD, Fujimoto EK, Goeke NM, Olson BJ, Klenk DC. Measurement of protein using bicinchoninic acid. *Anal Biochem.* 1985;150(1):76-85.

66. Laemmli UK. Cleavage of structural proteins during the assembly of the head of bacteriophage T4. *Nature.* 1970;227(5259):680-685.

67. Kurien BT, Scofield RH. Protein blotting: a review. *J Immunol Methods.* 2003;274(1-2):1-15.

68. Head JA, Jiang D, Li M, Zorn LJ, Schaefer EM, Parsons JT, Weed SA. Cortactin tyrosine phosphorylation requires Rac1 activity and association with the cortical actin cytoskeleton. *Mol Biol Cell.* 2003;14(8):3216-3229.

69. Cines DB, Pollak ES, Buck CA, Loscalzo J, Zimmerman GA, McEver RP, Pober JS, Wick TM, Konkle BA, Schwartz BS, Barnathan ES, McCrae KR, Hug BA, Schmidt AM, Stern DM. Endothelial cells in physiology and in the pathophysiology of vascular disorders. *Blood.* 1998;91(10):3527-3561.

70. Hankey GJ. Smoking and risk of stroke. *J Cardiovasc Risk.* 1999;6(4):207-211.

71. D'Agostino RB, Sr., Vasan RS, Pencina MJ, Wolf PA, Cobain M, Massaro JM, Kannel WB. General cardiovascular risk profile for use in primary care: the Framingham Heart Study. *Circulation.* 2008;117(6):743-753.

72. Ridker PM, Morrow DA. C-reactive protein, inflammation, and coronary risk. *Cardiol Clin.* 2003;21(3):315-325.

73. Willerson JT, Ridker PM. Inflammation as a cardiovascular risk factor. *Circulation.* 2004;109(21 Suppl 1):II2-10.

74. Bonetti PO, Lerman LO, Lerman A. Endothelial dysfunction: a marker of atherosclerotic risk. *Arterioscler Thromb Vasc Biol.* 2003;23(2):168-175.

75. de Jager J, Dekker JM, Kooy A, Kostense PJ, Nijpels G, Heine RJ, Bouter LM, Stehouwer CD. Endothelial dysfunction and low-grade inflammation explain much of the excess cardiovascular mortality in individuals with type 2 diabetes: the Hoorn Study. *Arterioscler Thromb Vasc Biol.* 2006;26(5):1086-1093.

76. Ku IA, Imboden JB, Hsue PY, Ganz P. Rheumatoid arthritis: model of systemic inflammation driving atherosclerosis. *Circ J.* 2009;73(6):977-985.

77. Feletou M, Vanhoutte PM. Endothelial dysfunction: a multifaceted disorder (The Wiggers Award Lecture). *Am J Physiol Heart Circ Physiol.* 2006;291(3):H985-1002.

78. Stoll G, Bendszus M. Inflammation and atherosclerosis: novel insights into plaque formation and destabilization. *Stroke.* 2006;37(7):1923-1932.

79. Bauersachs J, Widder JD. Endothelial dysfunction in heart failure. *Pharmacol Rep.* 2008;60(1):119-126.

80. Trepels T, Zeiher AM, Fichtlscherer S. The endothelium and inflammation. *Endothelium.* 2006;13(6):423-429.

81. Steffens S, Mach F. Drug insight: Immunomodulatory effects of statins--potential benefits for renal patients? *Nat Clin Pract Nephrol.* 2006;2(7):378-387.

82. Ridker PM, Cannon CP, Morrow D, Rifai N, Rose LM, McCabe CH, Pfeffer MA, Braunwald E. C-reactive protein levels and outcomes after statin therapy. *N Engl J Med.* 2005;352(1):20-28.

83. Klingenberg R, Hansson GK. Treating inflammation in atherosclerotic cardiovascular disease: emerging therapies. *Eur Heart J.* 2009.

84. Ridker PM. Testing the inflammatory hypothesis of atherothrombosis: scientific rationale for the cardiovascular inflammation reduction trial (CIRT). *J Thromb Haemost.* 2009;7 Suppl 1:332-339.

85. Muller WA. Mechanisms of transendothelial migration of leukocytes. *Circ Res.* 2009;105(3):223-230.

86. Ley K, Laudanna C, Cybulsky MI, Nourshargh S. Getting to the site of inflammation: the leukocyte adhesion cascade updated. *Nat Rev Immunol.* 2007;7(9):678-689.

87. Androulakis ES, Tousoulis D, Papageorgiou N, Tsioufis C, Kallikazaros I, Stefanadis C. Essential hypertension: is there a role for inflammatory mechanisms? *Cardiol Rev.* 2009;17(5):216-221.

88. Dustin ML, Rothlein R, Bhan AK, Dinarello CA, Springer TA. Induction by IL 1 and interferon-gamma: tissue distribution, biochemistry, and function of a natural adherence molecule (ICAM-1). *J Immunol.* 1986;137(1):245-254.

89. Leeuwenberg JF, Smeets EF, Neefjes JJ, Shaffer MA, Cinek T, Jeunhomme TM, Ahern TJ, Buurman WA. E-selectin and intercellular adhesion molecule-1 are released by activated human endothelial cells in vitro. *Immunology.* 1992;77(4):543-549.

90. Gerritsen ME, Carley WW, Ranges GE, Shen CP, Phan SA, Ligon GF, Perry CA. Flavonoids inhibit cytokine-induced endothelial cell adhesion protein gene expression. *Am J Pathol.* 1995;147(2):278-292.

91. Zarbock A, Ley K. New insights into leukocyte recruitment by intravital microscopy. *Curr Top Microbiol Immunol.* 2009;334:129-152.

92. Weber C, Fraemohs L, Dejana E. The role of junctional adhesion molecules in vascular inflammation. *Nat Rev Immunol.* 2007;7(6):467-477.

93. Libby P, Aikawa M, Jain MK. Vascular endothelium and atherosclerosis. *Handb Exp Pharmacol.* 2006(176 Pt 2):285-306.

94. Lucas R, Verin AD, Black SM, Catravas JD. Regulators of endothelial and epithelial barrier integrity and function in acute lung injury. *Biochem Pharmacol.* 2009;77(12):1763-1772.

95. O'Brien JG, Chennubhotla SA, Chennubhotla RV. Treatment of edema. *Am Fam Physician.* 2005;71(11):2111-2117.

96. Fürst R, Bubik MF, Bihari P, Mayer BA, Khandoga AG, Hoffmann F, Rehberg M, Krombach F, Zahler S, Vollmar AM. Atrial natriuretic peptide protects against histamine-induced endothelial barrier dysfunction in vivo. *Mol Pharmacol.* 2008;74(1):1-8.

97. Satpathy M, Gallagher P, Lizotte-Waniewski M, Srinivas SP. Thrombin-induced phosphorylation of the regulatory light chain of myosin II in cultured bovine corneal endothelial cells. *Exp Eye Res.* 2004;79(4):477-486.

98. McLachlan RW, Yap AS. Not so simple: the complexity of phosphotyrosine signaling at cadherin adhesive contacts. *J Mol Med.* 2007;85(6):545-554.

99. Vestweber D, Winderlich M, Cagna G, Nottebaum AF. Cell adhesion dynamics at endothelial junctions: VE-cadherin as a major player. *Trends Cell Biol.* 2009;19(1):8-15.

100. Gavard J. Breaking the VE-cadherin bonds. *FEBS Lett.* 2009;583(1):1-6.

101. Dudek SM, Garcia JG. Cytoskeletal regulation of pulmonary vascular permeability. *J Appl Physiol.* 2001;91(4):1487-1500.

102. Lum H, Andersen TT, Siflinger-Birnboim A, Tiruppathi C, Goligorsky MS, Fenton JW, 2nd, Malik AB. Thrombin receptor peptide inhibits thrombin-induced increase in endothelial permeability by receptor desensitization. *J Cell Biol.* 1993;120(6):1491-1499.

103. Moore TM, Chetham PM, Kelly JJ, Stevens T. Signal transduction and regulation of lung endothelial cell permeability. Interaction between calcium and cAMP. *Am J Physiol.* 1998;275(2 Pt 1):L203-222.

104. Sandoval R, Malik AB, Minshall RD, Kouklis P, Ellis CA, Tiruppathi C. Ca(2+) signalling and PKCalpha activate increased endothelial permeability by disassembly of VE-cadherin junctions. *J Physiol.* 2001;533(Pt 2):433-445.

105. Lynch JJ, Ferro TJ, Blumenstock FA, Brockenauer AM, Malik AB. Increased endothelial albumin permeability mediated by protein kinase C activation. *J Clin Invest.* 1990;85(6):1991-1998.

106. Schwartz M. Rho signalling at a glance. *J Cell Sci.* 2004;117(Pt 23):5457-5458.

107. Yuan SY, Wu MH, Ustinova EE, Guo M, Tinsley JH, De Lanerolle P, Xu W. Myosin light chain phosphorylation in neutrophil-stimulated coronary microvascular leakage. *Circ Res.* 2002;90(11):1214-1221.

108. Imai-Sasaki R, Kainoh M, Ogawa Y, Ohmori E, Asai Y, Nakadate T. Inhibition by beraprost sodium of thrombin-induced increase in endothelial macromolecular permeability. *Prostaglandins Leukot Essent Fatty Acids.* 1995;53(2):103-108.

109. Mong PY, Wang Q. Activation of Rho kinase isoforms in lung endothelial cells during inflammation. *J Immunol.* 2009;182(4):2385-2394.

110. Idris I, Donnelly R. Protein kinase C beta inhibition: A novel therapeutic strategy for diabetic microangiopathy. *Diab Vasc Dis Res.* 2006;3(3):172-178.

111. Birukova AA, Zagranichnaya T, Alekseeva E, Bokoch GM, Birukov KG. Epac/Rap and PKA are novel mechanisms of ANP-induced Rac-mediated pulmonary endothelial barrier protection. *J Cell Physiol.* 2008;215(3):715-724.

112. Werthmann RC, von Hayn K, Nikolaev VO, Lohse MJ, Bunemann M. Real time monitoring of cAMP levels in living endothelial cells: thrombin transiently inhibits adenylyl cyclase 6. *J Physiol.* 2009.

113. Lorenowicz MJ, Fernandez-Borja M, Kooistra MR, Bos JL, Hordijk PL. PKA and Epac1 regulate endothelial integrity and migration through parallel and independent pathways. *Eur J Cell Biol.* 2008;87(10):779-792.

114. Schüssler M, Fricke U, Nikolov N, Hölzl J. Comparison of the Flavonoids Occurring in Crataegus Species and Inhibition of 3′,5′-Cyclic Adenosine Monophosphate Phosphodiesterase *Planta Med.* 1991;57 S2.

115. Essayan DM. Cyclic nucleotide phosphodiesterases. *J Allergy Clin Immunol.* 2001;108(5):671-680.

116. Bender AT, Beavo JA. Cyclic nucleotide phosphodiesterases: molecular regulation to clinical use. *Pharmacol Rev.* 2006;58(3):488-520.

117. Seybold J, Thomas D, Witzenrath M, Boral S, Hocke AC, Burger A, Hatzelmann A, Tenor H, Schudt C, Krull M, Schutte H, Hippenstiel S, Suttorp N. Tumor necrosis factor-alpha-dependent expression of phosphodiesterase 2: role in endothelial hyperpermeability. *Blood.* 2005;105(9):3569-3576.

118. Kooistra MR, Dube N, Bos JL. Rap1: a key regulator in cell-cell junction formation. *J Cell Sci.* 2007;120(Pt 1):17-22.

119. Holz GG, Kang G, Harbeck M, Roe MW, Chepurny OG. Cell physiology of cAMP sensor Epac. *J Physiol.* 2006;577(Pt 1):5-15.

120. Daly RJ. Cortactin signalling and dynamic actin networks. *Biochem J.* 2004;382(Pt 1):13-25.

121. Surapisitchat J, Jeon KI, Yan C, Beavo JA. Differential regulation of endothelial cell permeability by cGMP via phosphodiesterases 2 and 3. *Circ Res.* 2007;101(8):811-818.

122. Bucci M, Roviezzo F, Posadas I, Yu J, Parente L, Sessa WC, Ignarro LJ, Cirino G. Endothelial nitric oxide synthase activation is critical for vascular leakage during acute inflammation in vivo. *Proc Natl Acad Sci U S A.* 2005;102(3):904-908.

123. Vennat B, Pourrat A, Pourrat H, Gross D, Bastide P, Bastide J. Procyanidins from the roots of Fragaria vesca: characterization and pharmacological approach. *Chem Pharm Bull (Tokyo).* 1988;36(2):828-833.

124. Doutremepuich JD, Barbier A, Lacheretz F. Effect of Endotelon (procyanidolic oligomers) on experimental acute lymphedema of the rat hindlimb. *Lymphology.* 1991;24(3):135-139.

125. Gohel MS, Davies AH. Pharmacological agents in the treatment of venous disease: an update of the available evidence. *Curr Vasc Pharmacol.* 2009;7(3):303-308.

126. Gerstner ER, Duda DG, di Tomaso E, Ryg PA, Loeffler JS, Sorensen AG, Ivy P, Jain RK, Batchelor TT. VEGF inhibitors in the treatment of cerebral edema in patients with brain cancer. *Nat Rev Clin Oncol.* 2009;6(4):229-236.

127. Gerriets T, Walberer M, Ritschel N, Tschernatsch M, Mueller C, Bachmann G, Schoenburg M, Kaps M, Nedelmann M. Edema formation in the hyperacute phase of ischemic stroke. Laboratory investigation. *J Neurosurg.* 2009;111(5):1036-1042.

VIII APPENDIX

1 Abbreviations

8-Bromo-cAMP	8-Bromoadenosine-3´,5´-cyclic monophosphate
AC	adenylate cyclase
AJ	adhesion junction
AP1	activator protein-1
Cell Signaling	Cell Signaling Technology®
CAM	cell adhesion molecule
cAMP	cyclic adenosine 3´,5´-monophosphate
cAMPS-Rp	(R)-Adenosine, cyclic 3´5´-(hydrogenphosphorothioate) triethylammonium salt
CHF	chronic heart failure
DAG	diacylglycerol
DMSO	dimethyl sulfoxide
DTT	dithio-1,4-threitol
EC	endothelial cell
EDTA	ethylenediaminetetraacetic acid
EGTA	ethylene glycol tetraacetic acid
EHP	endothelial hyperpermeability
Epac-1	exchange proteins directly activated by cAMP-1
Epac-cAMP/8-pCPT-2´-O-Me-cAMP	8-(4- Chlorophenylthio)-2´-O-methyladenosine-3`, 5`- cyclic monophosphat
FCS	fetal calf serum
FITC	fluorescein isothiocyanate
FURA-2, AM Ester	Fura-2-pentakis(acetoxymethyl) ester
HEPES	N-(2-hydroxyethyl)piperazine-N'-(2-ethanesulfonic acid)

HMEC	human microvascular epithelial cell
HUVEC	humen umbilian vain endothelial cell
ICAM	intercellular adhesion molecule
IP_3	inositol triphospath
MLC2	myosin light chain 2
MLCK	myosin light chain kinase
MLCP	myosin light chain phosphatase
NF-κB	nuclear factor kappa-light-chain-enhancer of activated B cells
PBS	phosphate-buffered saline
PDE	phosphodiesterase
PIP_2	phasphatidylinositol-4,5-bisphosphate
PKC	protein kinase C
PKA	protein kinase A
PMSF	phenylmethylsulfonylfluorid
phos.	phosphorylated
Rac1	Ras-related C3 botulinum toxin substrate 1
Rap1	Ras-proximate-1
RhoA	Ras homolog gene family, member A
ROC	receptor-operated Ca^{2+} channel
Santa Cruz	Santa Cruz Biotechnology
SOC	store-operated Ca^{2+} channel
STAT-1	signal transducers and activator of transcription protein-1
sub.	substrate
TNFα	tumor necrosis factorα
VASP	vasodilator-stimulated phosphoprotein
VEC	vascular endothelial cadherin

2 Publications

2.1 Original publications

Bubik MF, Bihari P, Willer EA, Jürgenliemk G, Ammer H, Krombach F, Zahler S, Vollmar AM, Fürst R. Activation of barrier protective and attenuation of barrier disruptive pathways: dual impact of WS$^®$ 1442 on vascular endothelial permeability. in preparation.

Furst R, **Bubik MF**, Bihari P, Mayer BA, Khandoga AG, Hoffmann F, Rehberg M, Krombach F, Zahler S, Vollmar AM. Atrial natriuretic peptide protects against histamine-induced endothelial barrier dysfunction in vivo. ***Mol Pharmacol****.* 2008;74(1):1-8.

Furst R, Schroeder T, Eilken HM, **Bubik MF**, Kiemer AK, Zahler S, Vollmar AM. MAPK phosphatase-1 represents a novel anti-inflammatory target of glucocorticoids in the human endothelium. ***FASEB J****.* 2007;21(1):74-80.

Bubik M, Ott M, Mahringer A, Fricker G. Rapid assessment of p-glycoprotein-drug interactions at the blood-brain barrier. ***Anal Biochem****.* 2006;358(1):51-58.

2.2 Oral presentations

<u>**Bubik MF**</u>, Hoffmann F, Mayer BA, Zahler S, Vollmar AM, Fürst R. ANP preserves endothelial barrier function in vivo- first insights into the underlaying mechanisms. 48th Spring Meeting of the Deutsche Gesellschaft für experimentelle und klinische Pharmakologie und Toxikologie, March 13-15, 2007, Mainz, Germany. ***Naunyn Schmiedebergs Arch Pharmacol.*** 2007;375 Suppl 1:65.

<u>Fürst R</u>, Eilken H, Schroeder T, **Bubik MF**, Kiemer AK, Zahler S, Vollmar AM. MKP-1 mediates the anti-inflammatory action of dexamethasone at low concentrations in humen endothelial cells. 48th Spring Meeting of the Deutsche Gesellschaft für experimentelle und klinische Pharmakologie und Toxikologie, April 4-6, 2006, Mainz, Germany. ***Naunyn Schmiedebergs Arch Pharmacol.*** 2006;372 Suppl 1:21.

2.3 Poster presentations

Bubik MF, Bihari P, Jürgenliemk G, Ammer H, Krombach F, Zahler S, Vollmar AM, Fürst R. Dual impact of the Crategus special extract WS[®] 1442 on the endothelial hyperpermeability: inhibition of barrier-destabilizing and activation of barrier stabilizing pathways. 7th International Symposium on Biology on Endothelial Cells, September 2-5, 2009, Vienna, Austria.

Mayer BA, **Bubik MF**, Zahler S, Vollmar AM, Fürst R. ANP protects against endothelial leagage by influencing endothelial cell contraction signaling. 50th Spring Meeting of the Deutsche Gesellschaft für experimentelle und klinische Pharmakologie und Toxikologie, March 10-12, 2009, Mainz, Germany. *Naunyn Schmiedebergs Arch Pharmacol.* 2009;379 Suppl 1:37.

Fürst R, **Bubik MF**, Zahler S, Vollmar AM. A standardized Crataegus extract protects against endothelial hyperpermeability. 7th Joint Meeting of AFERP, ASP,GA,PSE&SIF, August 3-8, 2008, Athens, Greece.

FürstR, **Bubik MF**, Mayer BA, Bihari P, Khandoga AG, Hoffman F, Krombach F, Zahler S, Vollmar AM. Atrial natriuretic peptide protects against histamine-induced impairment of endothelial barrier function. 4th European Meeting on Vascular Biology and Medicine, September 17-20, 2007.

Bubik MF, Zahler S, Vollmar AM, Fürst R. ANP preserves endothelial barrier function in vivo – first insights into the underlaying mechanisms. Annual Meeting of the Gesellschaft für Microzirkulation und Vaskuläre Biologie, October 12-14, 2006, Munich, Germany. *J Vasc Res.*2006;43:563.

Fürst R, Schroeder T, Eiken HM, **Bubik MF**, Kiemer AK, Zahler S, Vollmar AM. MKP-1: novel anti-inflammatory target of glucocorticoids in human endothelial cells. 31st FEBS Congress, June 24-29, 2006 Istambul, Turkey. *FEBSJ.* 2006;273 Suppl 1:328-329.

Bubik MF, Zahler S, Vollmar AM, Fürst R. Atrial natriuretic peptide abrogates TNFα – and histamine-induced changes in VE-cadherin and myosin light chain distribution and phosphorylation. 47th Spring Meeting of the Deutsche Gesellschaft für experimentelle und klinische Pharmakologie und Toxikologie, April 4-6, 2006, Mainz, Germany. *Naunyn Schmiedebergs Arch Pharmacol.* 2006;372 Suppl 1:24.

3 Curriculum vitae

Name	Martin Friedrich Bubik
Geburtsdatum	03. Juni 1977
Geburtsort	Pforzheim
Nationalität	deutsch
Hochschule	seit April 2005 Dissertation zum Dr. rer. nat. in der Arbeitsgruppe von Herr Dr. Robert Fürst am Lehrstuhl Pharmazeutische Biologie von Frau Prof. Dr. Angelika M. Vollmar, Department Pharmazie, Ludwig-Maximilians-Universität München
	Studium der Pharmazie 1999-2003 an der Ruprecht-Karls-Universität Heidelberg, Institut für Pharmazie und Molekulare Biotechnologie
Schule	1988 – 1997: Theodor-Heuss-Gymnasium Mühlacker 1984 – 1988: Schiller-Grundschule Mühlacker
Berufsausbildung	Dezember 2004 Approbation als Apotheker
	Mai-Oktober 2004: Pharmaziepraktikum im Institut für Pharmazie und Molekulare Biotechnologie, Abteilung Pharmazeutische Technologie und Biopharmazie, von Prof. Dr. Gert Fricker der Ruprecht-Karls Universität Heidelberg
	Nov 2003- April 2004 Pharmaziepraktikum bei Herrn Apotheker Dirk Hännig in der Kurfürsten-Apotheke in Heidelberg,

4 Acknowledgements